University of Debrecen, Department of Biophysics and Cell Biology

THE ROLE OF PERSISTENT NICKS AT THE BOUNDARIES OF INTERPHASE CHROMATIN LOOPS AND THEIR POSSIBLE INVOLVEMENT IN PATHOLOGICAL GENE REARRANGEMENTS

Thesis for the degree of doctor of philosophy (Ph.D.)

By:
Lóránt Székvölgyi

Supervisor:
Prof. Dr. Gábor Szabó

DEBRECEN
2006

TABLE OF CONTENTS

1. MAGYAR NYELVŰ ÖSSZEFOGLALÓ 4

2. INTRODUCTION 10

2.1 *Size is indeed a matter: architectural principles of chromatin packaging* 10

2.2 *The nuclear matrix* 14

2.3 *Loop-size chromatin fragmentation and its clinical implications* 19

3. OBJECTIVES 23

4. MATERIALS AND METHODS 24

5. RESULTS 37

5.1 *En masse chromatin fragmentation in healthy, non-apoptotic cells* 37

5.2 *Implementing an experimental strategy for the detection of single-strand discontinuities at the level of individual cells* 39

5.3 *Detection and characterization of free DNA-termini in nuclear halos by in situ nick translation labeling* 42

4.4 *Assessing the intranuclear topography of the revealed ss breaks at a model fragile site, the breakpoint cluster region of MLL gene* 45

5.5 *Assessing the role of common DNA sequence motives in the occurrence of single-strand breaks at MLL bcr* 50

5.6 *Assessing the role of epigenetic factors, including topoisomerase II binding in the occurrence of single-strand breaks at the MLL bcr* 54

5.7 *Implementing a novel screening method for the clinical investigation of epigenetic markers* 58

6. DISCUSSION 62

6.1 *The relationship between higher-order chromatin structure, loop-size DNA fragmentation and breakpoint cluster regions involved in pathological gene rearrangements.* 62

6.1.1 *When are the observed ss breaks generated? Two competing scenarios.* 62

6.1.2 *Visual evidence for the global disassembly of chromatin to loop-size units* 63

6.1.3 *Persistent nicks at the borders of chromatin loop. The role of nucleoskeletal RNA.* 65

6.1.4 *Visual evidence for the disassembly of chromatin to loop-size units at a model fragile site, the MLL bcr* 66

6.1.5 *Nick-forming sequence motives can position ss breaks* 67

6.1.6 *Topoisomerase II can cleave positioned nick-forming sequence motives at the MLL bcr* 70

6.1.7 *Concluding remarks* 71

6.2 *Implementing a novel screening method for the monitoring of epigenetic markers of diagnostic importance* 73

7. SUMMARY 75

8. REFERENCES 77

9. ACKNOWLEDGEMENTS 84

10. PUBLICATIONS 85

11. SUPPLEMENTARIES 88

1. Magyar nyelvű összefoglaló

Egyszál folytonossághiányok szerepe a kromatin hurkok kialakításában és patológiás génátrendezõdésekben

A genom szerveződésében van egy általános alapelv: az örökítőanyag egy limitált térfogatot foglal el, s hossza sokszorosan felülmúlná az őt tartalmazó kompartment dimenzióit, ha nem szerveződne ún. magasabbrendű struktúrákba. Mai tudásunk szerint a magasabbrendű kromatin szerkezet alapja a DNS molekula hurkos-doménekbe történő szerveződése, amely a magstruktúra enigmatikus „nukleáris mátrix" koncepciójával hozható összefüggésbe. A 30-150 kbp méretű DNS régiókat formáló hurkok a kromatin szerkezeti hierarchiájának azon szintjét alkotják, melynek fontos, ám teljességgel feltáratlan funkcionális relevanciája lehet. A hurkok kihorgonyzási pontjai (angolul *scaffold//matrix attachment regions, S/MARs*) gyakran promoterek, replikációs origók, rekombinácós forró pontok közelében találhatóak, s egyre valószínűbb, hogy alapvető szerepet játszanak különféle patológiás gén-átrendeződésekhez / kromoszóma aberrációkhoz vezető folyamatokban. A S/MAR szekvenciák meglepő sajátsága a nagyfokú heterogenitásuk és a konszenzus szekvenciák hiánya; egyedüli kivétel a topoizomeráz II enzim konszenzus szekvenciája, amely az eddig megszekvenált S/MAR-ok 85%-ában jelen van.

A kromatin hurkok közvetlenül megfigyelhetők az un. halo-kísérletek során, és kromatin fragmentációs jelenségek kapcsán. Előbbi esetben sejteket nagy ionerősségű sóoldattal extrahálva ún. halo-preparátumot nyerhetünk, amelyben a sejtmag mátrixhoz rögzülő, illetve abból kibomló kromatin hurkok tömegét figyelhetjük meg. A kromatin hurok-méretű darabokra történő fragmentálódása (hurok-méretű DNS fragmentáció) megfigyelhető mind apoptotikus sejtek, mind normál sejtek esetében - intenzív proteolitikus körülmények között: az ionos detergens és proteáz, valamint kelátor jelenlétében izolált DNS ~50 kbp-os átlagos

méretű, szemben az agaróz-blokkban lizált sejtekből származó DNS megabázisos méretével, amely feltehetően a hurkok rögzítési pontjainál történő törés/hasadás eredménye.

Az akut és poszt-terápiás leukémiák nagy részében a Mixed Lineage Leukemia (MLL) gén mintegy 40 partnergén valamelyikével transzlokálódik. Az MLL töréspont klaszter régiója (breakpoint cluster régiója, bcr) az 5. és 11. exonok közötti 8.3 kb-os szakaszt öleli fel. De novo leukémiákban az MLL BCR az 5.exon és a 8.intron első harmada közötti területen törik leggyakrabban, míg poszt-terápiás leukémiákban a 8. intron második harmada és a 11.exon közötti szakaszon, ezen belül leggyakrabban egy topoizomeráz II konszenzus szekvencia környezetében, a 9. exonban. A bcr a mi szempontunkból az 50 kbp-os fragmentáció töréspontjainak egy reprezentánsa, mely azért is érdekes, mert a leukemogenezis egy sajátos, kísérleti stratégiánk szempontjából lényeges modellje épül arra a tényre, hogy az MLL bcr apoptózisban is tapasztalt preferenciális hasadását olyan kimérikus transzkriptumok megjelenése is követte, melyek kromoszóma transzlokáció bekövetkezésére utaltak.

Munkánk során a teljes kromatin állományon illetve az MLL bcr-en, mint modell rendszeren azt az izgalmas hipotézist vizsgáltuk, amely szerint a hurok-méretű kromatin fragmentációban érintett fragilis helyek egyben a kromoszóma rendellenességek, transzlokációk predilekciós helyei.

<u>Célkitűzések:</u>

1. A magasabbrendű, hurok-szintű kromatinszerkezet kialakításának nem ismerjük a mechanizmusát. Ebben jelentős előrelépést tehetünk, ha sikerül azonosítani azokat a szekvencia motívumokat / karakterisztikus fehérjéket, melyek az általunk régóta vizsgált kromatin fragmentációs jelenség hurok-méretű periodicitását megmagyarázzák.

2. A korai apoptotikus fázisban talált MLL transzlokációkat illegitim repair folyamatokkal magyarázzák, melyek a kurrens értelmezés szerint megmentenék a sejtet a pusztulástól, daganatos transzformáció árán („abortív" apoptózis modell). A töréspontok és a topoizomeráz II kötőhelyek MLL régión belüli finom eloszlásának vizsgálata során azt reméljük megtudni, hogy létezik-e a fragmentációs pontoknak egy jól meghatározott halmaza a kromatinon, melyek az átrendeződések predilekciós helyeiként fungálnak.

3. Különböző típusú rákos megbetegedéseknél számos gén epigenetikus szabályozásában specifikus diszreguláció figyelhető meg. Az MLL hiszton-modifikációinak vizsgálata különösen indokolt azokban az esetekben, amikor a citosztatikus kezelést követően, főleg topoizomeráz II gátlószerek alkalmazása esetén a betegek jelentős százalékában várható második daganatos vagy leukémiás betegség kialakulása. Ezért célul tűztük ki egy új, ChIP-minták kiértékelésére alkalmas áramlási citometriás platform kifejlesztését („*ChIP-on-beads*"), amely a rutin diagnosztikai laboratóriumok számára a real time QPCR egy olcsóbb alternatíváját kínálja a különféle betegségek aetiológiájában szerepet játszó epigenetikai markerek szűrésére és monitorozására.

<u>Kísérleti stratégiák:</u>

Több sejtvonalban és emberi perifériás limfocitákban (PBL) egy új eljárással (field inversion single-cell gelelectrophoresis, *FI-SSGE*) egyedi sejtek szintjén detektáltuk a kromatin hurkok mag-mátrixról történő lecsatolódását illetve a hurok-méretű fragmentációt. Az eredményeket konfokális lézerpásztázó mikroszkópiával (*CLSM*) vizualizáltuk, illetve lézerpászázó citometriával (*LSC*) kvantifikáltuk. A hurok-lehorgonyzási pontokra jellemző DNS-végeket *in situ nick transzlációval* karakterizáltuk. A töréspontok sejtmagon belüli topográfiáját a *halo-*

FISH kísérletekkel lokalizáltuk. *Primer extenzióval* térképeztük a kromoszóma átrendeződéseket bevezető DNS-hasításokat, illetve sejtmag extraktumokkal végzett in vitro assay-kben teszteltük az MLL bcr fragilitását okozó faktorokat. A töréspont klaszterre jellemző hiszton-kódot és az egyik legjellegzetesebb S/MAR-fehérje, a topoizomeráz II enzim szerepét kromatin immunoprecipitációval (*ChIP*), a bcr-en belüli heterogén kromatin szerkezet különféle genotoxikus ágensekre adott válaszát real-time pcr-al (*QPCR*) vizsgáltuk. Az MLL és a szöveti transzglutamináz 2 (TGM2) gén epigenetikus markereit egy új, áramlási citomeria és PCR kombinációján alapuló kvantitatív módszerrel („ChIP-on-beads") vizsgáltuk. Kísérleteinktől azt reméljük, hogy a flow citometriás diagnosztikai laboratóriumok a ChIP-on-beads technikával a daganatos betegségek kezelésére használt kemoterápiás protokollok hatását érzékenyebb, finomabb módon tesztelhetik a jövőben.

Eredmények:

I.

Munkánk során biofizikai és molekuláris sejtbiológiai módszereket alkalmazva elsőként vizualizáltuk és kvantifikáltuk egészséges, nem-apoptotikus sejtekben a teljes kromatin állományt érintő hurok-méretű fragmentációt. Kimutattuk, hogy a kromatin-hurkokat lehorgonyzó sejtmag mátrix preformált nick-klasztereket tartalmaz. Ezen fókuszok *(1)* intenzíven jelölhetőek DNS polimeráz I enzimmel, amely egyöntetű 3'OH-végek jelenlétére utal, *(2)* egyáltalán nem jelölhetőek Klenow enzimmel vagy terminális transzferázzal (TdT), amely kizárja a dupla-szál törések és hosszabb egyszál folytonossághiányok (gap-ek) jelenétét, azonban *(3)* szignifikáns jelölődést kapunk mind Klenow enzimmel illetve TdT-vel, ha a halo preparátumokat előzetesen ribonukleolítikus kezelésnek tesszük ki (RNase A, lúg, Exo III). Az RNáz-kezelés hatására megjelenő Klenow / TdT pozitivítás specifikus RNáz inhibitorral kivédhető. Ezen adatok arra utalnak, hogy a sejtmag mátrix fibrogranuláris

RNS/ribonukleoprotein hálózata kapcsolatban van a kromatin hurkok lehorgonyzási pontjaival, stabilizálva az ott jelen lévő egyszál folytonosság hiányokat. Feltevésünk szerint a nick-RNS/RNP kontaktus létfontosságú ezen nick-ek fenntartásában, mivel így a repair rendszer nem ismeri fel az RNS/RNP-vel maszkírozott DNS-végeket. A nick-fókuszok, strukturális szerepük mellett, kiindulási pontjai lehetnek a különféle fiziológiás folyamatok (pl. apoptózis, rekombináció) és nem fiziológiás stressz-hatások (pl. xenobiotikumok, kemoterápiás szerek) során megfigyelhető – és agaróz-blokkba ágyazott sejtek S1-nukleáz emésztésével is reprodukálható hurok-méretű DNS fragmentációnak.

A Jurkat ill. az ML-1 emberi sejtvonalak közötti egyik lényeges különbség az MLL gén transzlokált volta az utóbbiban. Halo-FISH kísérleteink azt mutatták, hogy Jurkat sejtekben illetve PBL-ben a normál (germline) MLL bcr jellegzetes, diszkrét módon fragmentálódik a halo képződés során. A fragmentáció ~50 kbp-onként manifesztálódik a kromatin hurkok kihorgonyzási pontjain perzisztáló nick-ek mentén. Az MLL gént átrendeződött konfigurációban (tMLL) tartalmazó ML-1 sejtek esetében, ill. centromérikus szonda esetén jelentősen eltérő fragmentációs mintázatot (hurok-struktúrát) kaptunk. A kromatin hurok-méretű fragilitása nem a sejtproliferáció (S-fázis) következménye, viszont szoros korrelációt mutatott a vizsgált régiók *(1)* transzkripciós aktivitásával, *(2)* DNáz szenzitivitásával, illetve *(3)* egyes hiszton-módosításokkal. Kimutattuk, hogy az MLL bcr-en - S/MAR-fehérje kötő kapacitása miatt - speciális DNS-fehérje interakciók alakulhatnak ki. ChIP kísérleteink szerint (*1*) a topoizomeráz II enzim preferenciálisan (aszimmetrikusan) kötődik mind a germline és transzlokált MLL-bcr telomerikus szakaszához, (*2*) az etoposide-kezelés egy fellazult kromatin-szerkezet kialakítása révén (megnövekedett H3K4 metiláció / H3Kcetiláció illetve DNáz szenzitivitás) közvetetten megnöveli a bcr-hez kötődő topo II mennyiségét. Ez az adatsor, és az a tény, hogy az ~50 kbp fragmentum végek konszenzus szekvenciája az MLL breakpoint cluster régió egyik hot-spotja, egy erős topoizomeráz II kötőhely szekvenciájával

jelentős egyezést mutat, alátámasztják azt a lehetőséget, hogy az enzim egyes izoformái, szubpopulációi valamilyen, a hurokszerű periodicitással korreláló kötődést mutathat a kromatin mentén.

Kísérleti eredményeink alapján feltételezzük, hogy RNS-sel maszkírozott egyszál folytonossághiányok, nick-ek határolják a kromatin hurkos-doméneit, és ezen, mindkét szálon a hurkok határánál halmozódó nick-ek mentén ds fragmentáció következik be, amint megszűnik a kromatinba szervezett állapot. Az MLL bcr esetében a topoizomeráz II enzim–nukleáz és ligáz aktivításai révén - pozicionálhatja és hozhatja létre a nick-eket.

II.

Metodikai fejlesztésünk, az általunk „ChIP-on-beads”-nek nevezett áramlási citometriás ChIP kiértékelő módszer - a QPCR technológiához hasonlóan - megbízható képet ad a vizsgált gének epigenetikai állapotáról. Az általunk kidolgozott új módszer segítségével a H4 hiszton acetilációjának, illetve a H3 hiszton metilációjának magas szintjét mutattuk ki az MLL és TGM2 gének promóter régióiban. Ezek a modifikációk szignifikánsan lecsökkentek apoptózis során, ami együtt járt a TGM2 és MLL mRNS-ek kifejeződésének lecsökkenésével. A ChIP-on-beads-nek technika megfelelő készülékkel (pl: Becton Dickinson FACSarray) nagyszámú minta egyidejű vizsgálatára alkalmas, amely reményeink szerint lehetővé teszi a különféle daganatok progressziójára karakterisztikus epigenetikus markerek vizsgálatát a klinikai rutin diagnosztikában.

2. *INTRODUCTION*

***2.1** Size is indeed a matter: architectural principles of chromatin packaging*

The mass of DNA in an unreplicated haploid genome, such as that of a sperm nucleus, is called genome size, or alternatively, C-value, that shows a 40000-fold variation in different eukaryotes, ranging from $5x10^{-3}$ pg to $2x10^{2}$ pg[1]. C-value seems unrelated to the number of protein coding genes (this puzzling lack of relationship is called C-value paradox), but strongly correlates with nuclear volume and cell volume, as well as cell cycle length and minimum generation time[1,2]. Based on these correlations, the 'skeletal DNA' hypothesis postulates that *(1)* the overall bulk of the DNA is able to control the growth rates of different cell types, and *(2)* a major fraction of the genetic material exists as non-genic 'nucleoskeletal DNA' establishing the optimal nuclear volume. Therefore, the C-value of an organism is simply a secondary result of selection for a given nuclear volume, which is in turn a result of the evolutionary compromise between selection for appropriate cell size and developmental rates. Changes in nuclear volumes in different diploid somatic cells are brought about primarily by controlling the degree of folding or unfolding of DNA, basically by *(1)* eliciting changes in the amount of constitutive heterochromatin (interestingly, this type of heterochromatin appears to be missing in organisms in which nuclei do not undergo large volume changes during their life cycle), and *(2)* by regulating the assembly of an 'extra' nuclear matrix through the synthesis of special nucleoskeletal RNA[1,2] (as will be discussed later). It seems reasonable to assume that nuclear volume cannot depend simply on the amount of DNA it contains, implying a role for specific genes controlling these mechanisms. This means that mutations of such genes could cause large changes in nuclear volume, thus they must be subject to selection in order to maintain the characteristic nuclear volumes of

different cells. The question that cells evolve large genomes, either because they need them as a nucleoskeleton, or simply because they can tolerate more useless DNA, is still open.

Regarding the spatial organization of the genetic material, it seems evident that the dimensions of the nucleus ($1.13x10^2$ μm^3 in humans) are vastly exceeded by the exceptionally long DNA molecule (1.8 m in humans), assuming a general packaging mechanism that follows a yet partially identified principle. The eukaryote genome is highly compartmentalized, starting from the "beads on a string array" of nucleosomes to the formation of metaphase chromosomes representing the highest level of compaction (Figure 1); packaging ratio (i.e. the ratio of the DNA double helix length to the actual length of the compartment that contains it) increases by many-fold during this process.

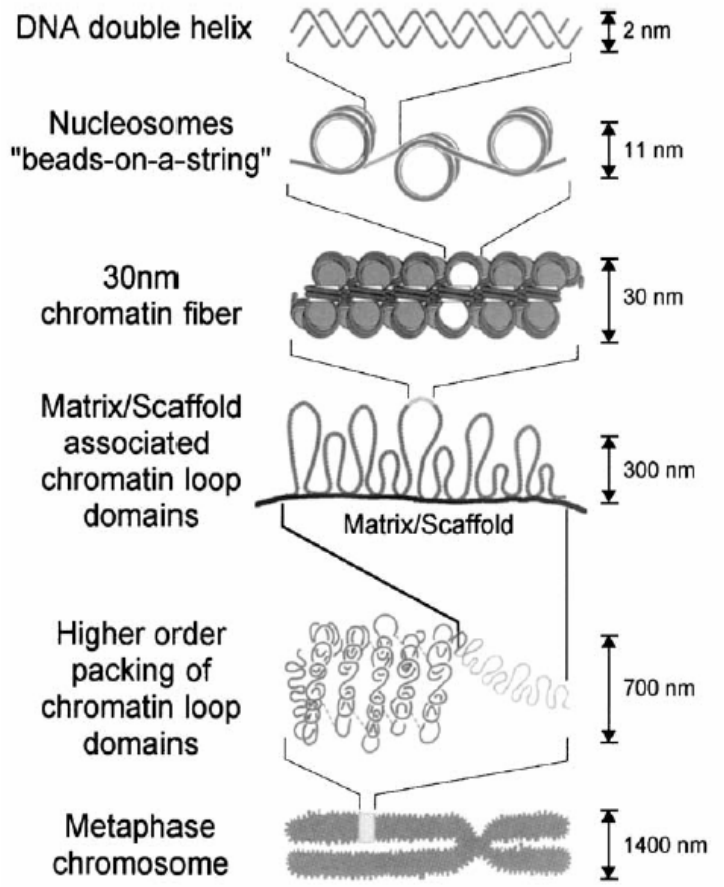

Figure 1: Hierarchical organization of chromatin in the mammalian nucleus (based on ref.[3])

At a certain level of hierarchical DNA packaging, as demonstrated by numerous studies, the 30 nm fibers fold up into repeating ~20-200 kbp loop domains, probably representing the fundamental units of both DNA replication and transcription[4,5]. A number of recent advances in molecular cell biology have contributed to the identification of replication and transcription factories that appear to be composed of series of DNA loops (termed MLCs, i.e. multi-loop chromatin domains)[3,4], as well as to the discovery of chromosome territories (CTs) representing the highest level organization in the interphase nucleus. Current models suggest that CTs are separated by interchromatin domains (ICDs) rich in the nuclear machinery for nucleic acid metabolism (Figure 2.A). In the ICD model, extended segments of transcribed genes are in direct contact with the ICD compartment, as they lie at the surface of CTs or intrachromosomal channels; the ICD space is barely invaded by fine fibers of chromatin loops, suggesting rare interchromosomal interactions.

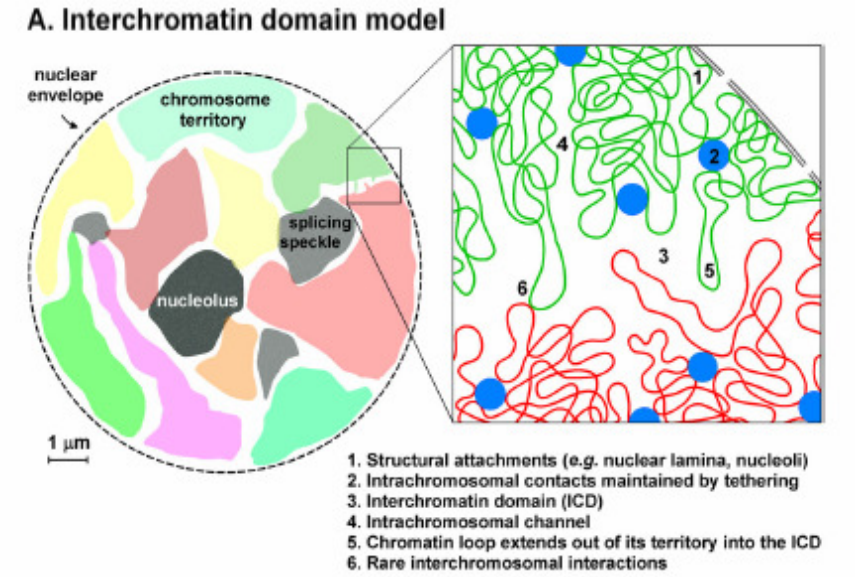

Figure 2: ICD model of chromatin organization in mammalian nuclei
(based on ref.[6])

Unfortunately, this model is not fully consistent with the high frequency of complex chromosomal aberrations, and also ignores the estimated diffusion kinetics of chromatin; measurements on translocation frequencies and chromosome dynamics do not imply

significant physical separation of CTs, rather they suggest the existence of high levels of intermingling between territories.

The discrepancy between theoretical considerations and physical calculations has been circumvented by a novel model of higher order chromosome structure, termed interchromosomal network (ICN) model[6] (Figure 2.B). It postulates that chromatin of different chromosomes is not separated by an ICD compartment, but is allowed to expand into the sorrounding territories. The level of intermingling is profoundly influenced by ongoing transcription that probably stabilizes the associations between particular loci, and these interactions are restricted by structural attachments like the nuclear envelope and other subcompartments. The preferential association of some chromosomes (e.g. 1,2, and 9) suggests co-localization in certain parts of the chromatin, which may be a result of the spatial juxtaposition of CTs. Since chromatin loops extending from a CT can invade neighboring CTs, DNA breaks formed in regions of intermingling are more likely to produce interchromosomal rearrangements.

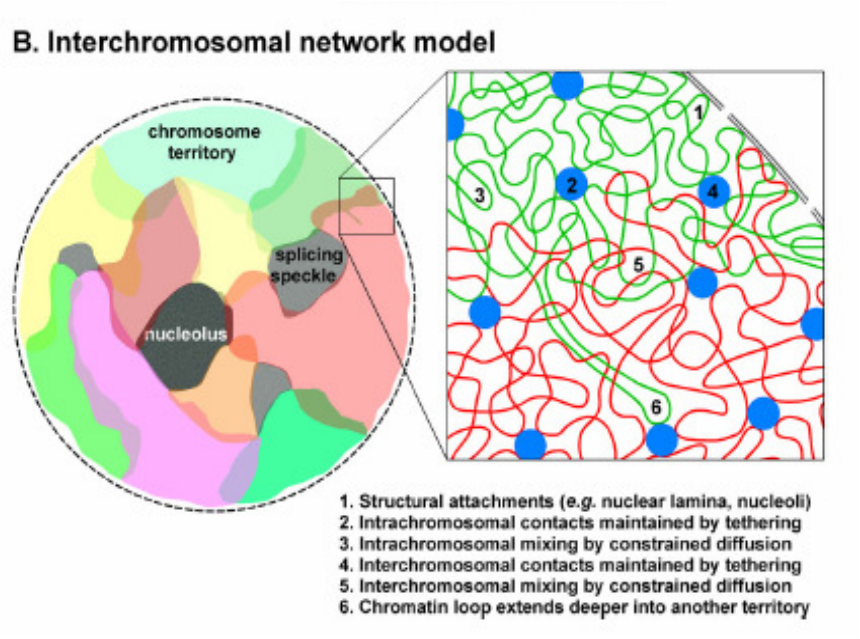

Figure 3: ICN model of chromatin organization in mammalian nuclei
(based on ref [6].)

2.2 *The nuclear matrix*

Research aimed at answering the question how chromatin fibers confined into a highly limited volume are involved in the coordination of biochemical processes and individual gene functions has gained impetus with the discovery of nuclear matrix/scaffold/nucleoskeleton. In 1966, for the first time, Don Fawcett defined the nuclear matrix as a residual non-chromatin framework structure of the cell nucleus readily observed in unextracted cells under the electronmicroscope[7]. From that time on a lot of 'operational' definitions were introduced, which relied on the specific extraction protocols applied for matrix preparation, fueling controversies among biologists. Basically, the field of nuclear matrix research has historically rested on *(1)* the electron microscopic observations of non-chromatin structures in the nuclei of cultured cell and tissues, *(2)* the development of protocols for isolating these non-chromatin components preserving their ultrastructure, *(3)* the observation that chromatin is organized into discrete loops attached at their bases to a non-chromatin structure, *(4)* the discovery of spatially distinct nuclear domains that maintains the main architectural features of the nucleus, including the nuclear lamina with pore complexes, chromosome territories and nucleoli (Figure 4).

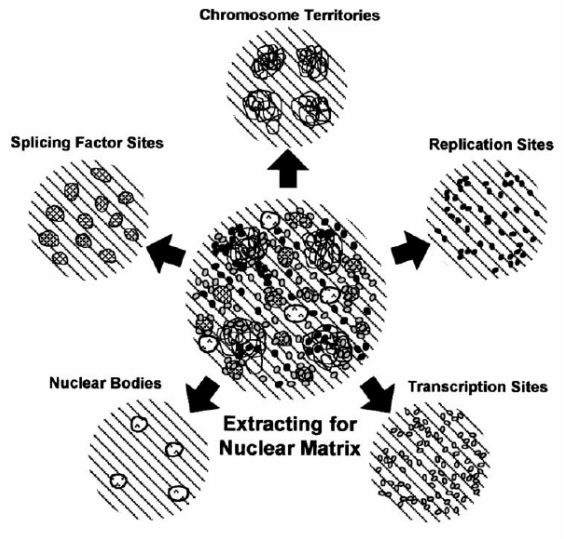

Figure 4: Maintenance of functional domains after extraction for nuclear matrix (based on ref.[3])

Biochemical and detailed ultrastructural studies of the nuclear matrix required the development of techniques to remove the major part of the tenaciously bound, dense and obscuring chromatin while retaining the underlying structure in a nearly native from and composition. Different fractionation protocols have uncovered a network of highly branched filaments, connected to the nuclear lamina and well distributed through the nuclear volume[8] (Figure 5). These data imply that the matrix is a structurally independent entity and its integrity does not depend on typical nucleosomal chromatin organization.

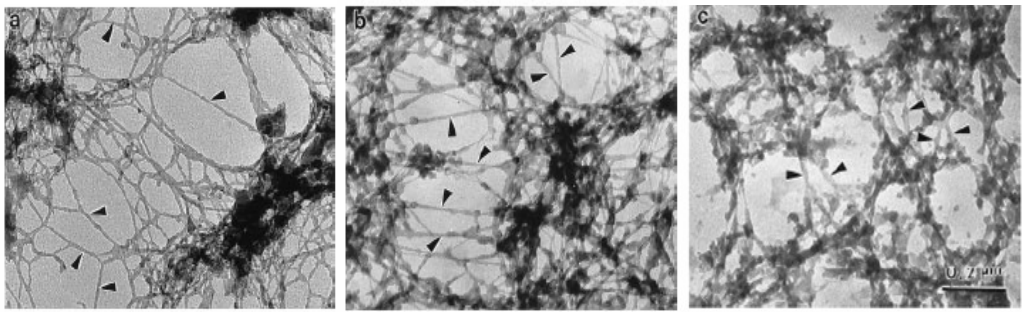

Figure 4: Ultrastructural comparision of nuclear matices prepared by three different methods (based on ref.[8])

The protein composition of the matrix is quite different from that of other cellular or nuclear fractions, as determined by 2D gels typically revealing about 200 major protein spots[9] (for review see ref.[8]). A subset of these matrix proteins seems to be cell-type specific, whereas the expression of others correlates with malignant progression of tumour cells. Antibodies against known nuclear proteins revealed lamins A, B and C, numatrin or B-23, topoisomerase II and hnRNP core proteins. Recent studies have identified the S/MAR specific proteins SATB1 and SAF-A/B, as well as nuclear actin and several actin-associated proteins (as myosin, structural protein 4.1 that binds to nuclear mitotic apparatus protein NuMA, which is also a matrix resident protein), numerous ss-binder proteins, matrins and specific transcriptional

modulators. In the latest studies, special acidic chromosome territory anchor proteins (CTAPs) were identified that were released from RNase-treated nuclear matrices[10]. CTAPs seem to be crutial for the maintenance of chromosome territory organization, although we do not know where and how these molecules assamble into functioning structures in the nucleus.

Based on advanced EM-visualization studies, the revealed fine web of 10-nm matrix filaments appears to be associated with a second layer of nucleic acid containing structure, a fibrogranular RNA / ribonucleoprotein (RNP) network[8,11-15] (Figure 5). Special components of the hnRNAs seem to be tightly associated with the remnants of salt-extracted nuclei, positioned by direct or indirect attachments to the 10-nm filamaments allowing for a considerable plasticity in nuclear architecture and function. Since the bulk of this hnRNA fraction could be eliminated by exogenously added RNases, the structural integrity of the nuclear matrix appears to be dependent on interactions between the RNP- and core-filament networks. A large body of data suggests that this hnRNA-rich internal matrix might be also involved in anchoring the structural / functional units of higher-order chromatin structure, the supercoiled chromatin loop domains.

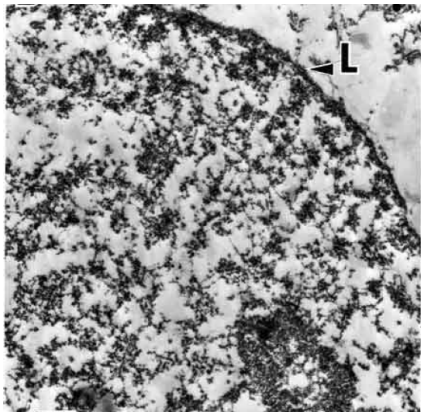

Figure 4: The RNP network of the nucleus is well preserved after removal of chromatin in a nuclear matrix preparation.
RNA was detected by the EDTA-regressive staining method. '*L'* denotes nuclear lamina. (based on ref.[8])

Cockerill and Gerrard have demonstrated for the first time that isolated nuclear matrices contain specific affinity binding sites where DNA remains bound to the remnants of salt-extracted nuclei (called nuclear halos) after extensive nuclease treatment[16]. The number of these sites was estimated to be 50000 per nucleus. The DNA sequence elements retained selectively in the presence of non-specific competitors by the isolated nuclear matrices were termed matrix associated regions (MARs). In an independent study, Laemmli and his co-workers have identified specific DNA scaffolding elements using a weak ionic detergent, lithium diiodosalicylate (LIS) for histone removal, and the captured sequences were termed scaffold attachment regions (SARs)[17,18]. Further studies have suggested that SARs and MARs are identical genomic elements, thus they have been collectively named as S/MARs.

In the *Drosophyla* genome, S/MARs proved to be interspersed at interval of 26-112 kbp that is consistent with the sizes of chromatin loops in flies and mammals[19]. They have a quite heterogenous character lacking any consensus sequences, but certain patterns and common structural motives could be identified using *in silico* and both *in vitro* and *in vivo* techniques. The predictive scheme has revealed *(a)* preferential occurance of stretches of AT-rich sequences and both A_n runs and $(AT)_n$ tracts (including several ATTA and ATTTA motives), *(b)* high frequency of intrinsically curved DNA, *(c)* concentrated sites of topoisomerase II (topo II) consensus sequences[20]. Based on these criteria, S/MAR activity seem to be related to topological features that are not strictly dependent on primary DNA sequence. Chemical probing and 2D gel analyses of S/MAR constructs being under superhelical tension revealed that these elements readily relieve torsional stress-generated mechanical forces assuming stable base-unpared configuration[20-22]. Base unpairing was shown to be initiated at nucleation sites called ‘core unwinding elements’ (CUEs), then extend over wider segments termed ‘base unpairing regions’ (BURs). These nucleation sites have been found to be closely associated with several types of DNA functional elements, e.g. *E. coli ori*C, ARS elements in *yeast* and

Drosophyla origins of replication, transcriptional regulatory regions including human c-myc oncogene, chicken β^A- globin gene, interferon-β gene and yeast FBP1 gene[4,20]. The pronounced base unpaired character of S/MARs along with their propensity to form non-B DNA structures might explain their frequent coincidence with recombination hot spots (see later).

Although S/MARs have been considered principally as domain borders located at the putative ends of chromatin loops, they have been also implicated in a variety of biological functions. These include for instance *(1)* DNA replication: most of the mapped mammalian and avian replication origins co-localize with MARs (involving e.g. human *c-myc* gene or chiken *α*-globin gene); *(2)* transcription: *(a)* S/MARs can act as domain openers in the vicinity of enhancers, *(b)* they can elevate the level of transcription rates in the absence of enhancers (transcriptional augmentation), *(c)* they can stimulate gene expression from heterologous reporter genes when integrated into the genome, *(d)* they are able to limit the effects of enhancers (acting as insulators); *(3)* recombination and repair: S/MARs are possible hotspots of recombination providing landing platform for several repair enzymes, nucleases and topoisomerases (for review see ref.[20]).

Recently, several investigatos have addressed the question whether S/MAR elements, besides structuring the human genome, might also give rise to the extreme instability of certain loci[6,22-33]. S/MARs have gained special attention because these regions often seem to be involved in pathological gene rearrangements[6,22,32,34-39]. This assumption is based on the observed co-localization of recombination breakpoints with sites of DNA cleavage involving the excision of chromatin loops at S/MARs (during e.g. the initial stages of apoptosis, as will be discussed). DNA rearrangements seem to occur non-randomly along the length of the chromosomes, and at least some of the hotspots coincide with common fragile sites of chromosomal loci. The latter regions are charachterized by recurrent breaks or gaps enriched

at peaks of enhanced DNA flexibility. Based on a large body of biophysical and biochemical data, the general view holds that these DNA lesions must be recognized and healed by efficient repair mechanisms, othervise the cell dies. The presence of unrepaired discontinuities in the DNA would seem puzzling, partly because of the widely accepted model of continuous chromosomal DNA molecules suggesting that DNA breaks are incompatible with life. But is that indeed the case?

2.3 *Loop-size chromatin fragmentation and its clinical implications*

Indicative of the loop arrangement of higher-order chromatin organization, various chromatin fragmentation phenomena have been observed that involve the preferential cleavage of DNA, most likely at the bases of the loops, to ~20-200 kbp fragments. The phenomenon seems particularly important because *(a)* it reflects regularities in the organization of interphase chromosomes, and *(b)* it appears to be interrelated with questions concerning e.g. apoptosis, genome instability and chemotherapy-associated gene rearrangements[40-45].

Apoptosis is characterized by the degradation of DNA into a specific pattern of high and low molecular weight fragments; unequivocal explanation as to the mechanism of DNA degradation has yet to emerge. High molecular weight (HMW) DNA fragmentation involes the release of chromatin loops through the cleavage of DNA domains at S/MARs, whereas smaller fragments (the DNA ladder) arise from endonucleolytic activity at the linker regions[40,43]. 2D alkaline gel-electrophoretic analyses have demonstrated the occurance of frequent single-strand cuts in the initial steps of HMW fragmentation[39,46], implicating chromatin-bound and diffusible nucleases (e.g. CAD, DNaseY, DNase I, DNase II, endonuclease G,) as well as topoisomerase II in eliciting these cleavages[39,47-52]. Until recenty, the executional phase of apoptosis has been perceived as an irreversible point with no turning

back, committing the cells to die. Several recent observations seem to contradict these findings, offering a new model of carcinogenesis alluded to as 'abortive apoptosis'[53,54]. This model proposes a mechanism whereby a special family of proteins, known as IAP's (Inhibitor of Apoptosis Proteins) specifically blocks the activated forms of caspase 3, a critical component of apoptosis execution. Cells arrest in the phase of HMW DNA fragmentation that may lead to incorrect DNA repair with rearrangements, and consequent cell recovery. This failure in the cell death program can leave cells with potentially tumorigenic DNA lesions causing serious clinical consequences. Candidate examples of a disease process related to the failed execution of apoptosis are the therapy related leukemia's such as Acute Lymphoid Leukemia (ALL) and Acute Myeloid Leukemia (AML). These diseases are linked to treatments of primary cancers utilizing inhibitors of topoisomerase II. The nonintercalating epipodophyllotoxin etoposide (VP16) has been effectively applied in the therapy of various neoplastic diseases, including testicular cancer, lymphomas, acute leukemia, lung small cell carcinoma, but neither the mechanism of cytotoxicity, nor the means of tumor cell resistance are completely understood. In view of the fact that etoposide stabilizes topoisomerase II-DNA complexes *in vivo*, the elicited single and double strand (ss and ds) breaks are generally thought to be instrumental in drug toxicity. Since cells proceed to die even after the drug has been removed and the breaks have been repaired[55-58] the formation of ss/ds breaks seems to precede and initiate further pathological changes. The primary molecular alterations in leukemogenesis involving topo II activity have been intensively studied in a confined, 8.3 kbp-long breakpoint cluster region (bcr) within the *M*ixed *L*ineage *L*eukemia (*MLL*) gene. MLL codes for a transcription factor involved in development, and is rearranged in the majority of childhood acute leukemias and posttherapeutic leukemias[28,30,34,42,43,59-65]. Translocation breakoints seem to be concentrated around a topo II consensus sequence in the telomeric half of the bcr, co-localising with a DNase hypersensitive site. This bcr is also a

predilection point for DNA cleavages early on in apoptosis, linking an error-prone repair of these breaks to pathological gene rearrangements[35,36,66]. The connection between etoposide toxicity, DNA breaks and the regulatory machinery involved in the control of chromatin structure at MLL bcr is generally recognized, but not clearly understood.

In the early '90s, our group discovered a new type of chromatin fragmentation that took place in isolated nuclei of healthy, proliferating eukaryotic cells upon treatment with ionic detergents[67]. The *en masse* disintegration of chromatin into regular, ~50 kbp fragments seemed unique in a sense that it was manifested in the absence of apoptosis and it involved almost the total nuclear DNA[68]. Several earlier observations are reminiscent of these findings. Weintraub described a chromatin particle migrating as a discrete 20-40 kb entity on a standard agarose gel[69]. Kokileva observed a spontaneous, progressive degradation of rat liver DNA in isolated nuclei from loop-size (>30 kb on standard agarose gels) to nucleosomal fragments[70,71]. Tchurikov described a spontaneous, non-random, disintegration of Drosophila, human and plant chromatin in pulse field gel-electrophoretic experiments[72]. Based on the fact that fragmentation can be avoided if agarose-embedded cells are exposed to the lysing solutions, mechanical factors are generally considered as its major cause. Remarkably, the high molecular weight DNA obtained in this procedure immediately turns into loop-size fragments when the agarose plugs are melted up to 60-95 ^{o}C, or upon exposure to S1 nuclease, as shown for different mammalian cells as well as yeast cultures[68,73,74]. These latter phenomena may be interpreted to suggest that single-stranded discontinuities, probably nicks, are present in the lysed nuclei that are prevented from becoming manifest double-strand breaks when enclosed in an agarose matrix. Analysis of cloned breakpoint sequences revealed certain regularities suggestive of specific mechanisms that may account for the apparently non-random nature of fragmentation[75]. It was also notable that one of the sequence motives

shared by several ~50 kb breakpoints was also present in the topoisomerase II binding consensus within the breakpoint cluster region of the MLL gene.

The above findings remind of the apoptotic HMW fragmentation; however, they involve normal, non-apoptotic cells. Thus it is possible that the disassembly of chromatin into loop-size units upon protein denaturing treatments in the case of healthy, non-apoptotic cells represents a normal cellular mechanism the apoptotic HMW DNA fragmentation is superimposed on. Our concept, anticipating preformed ss DNA discontinuities in the chromosomes at loop-size intervals is distinguished from the prevailing view contemplating HMW chromatin fragmentation merely as a prelude to cell death. We hypothesize that the ss breaks present at every ~50 kbp throughout the entire genome (according to the above data and to those discussed in this thesis) might explain the frequent involvement of loop anchorage sites in pathological gene rearrangements. Consequently, the elucidation of mechanism involved in these phenomena will be of great value to understand the link beween etoposide-evoked anomalies of DNA integrity in apoptosis and the molecular machinery organizing higher-order chromatin structure.

3. OBJECTIVES

The four *major goals* of this study have been as follows**:**

1. We wished to detect possible single-stranded regions as predilection points of ~50 kbp fragmentation at the level of individual cells, implementing a novel experimental strategy based on a combination of cell-biophysical and molecular biological approaches.

2. We wished to characterize *in situ* the chemical nature of the revealed DNA-termini as well as their possible interaction with nuclear matrix components, with a special emphasis on the intranuclear topography of the breakpoints.

3. We wished to establish an *in vitro* and *in vivo* experimental system to better understand the primary molecular steps of leukemogenesis that may involve topo II activity. As a model, we have studied a prototypic fragile site, the breakpoint cluster region of MLL gene.

4. Having recognized the role of epigenetic regulation in the above phenomena, we attempted to develop a novel screening method with high-throughput potentialities for the clinical investigation of epigenetic markers.

4. MATERIALS AND METHODS

Cells: Jurkat, ML-1, HL-60, Hela, NIH 3T3, DC3F and DC3FOH cells used in this study were cultured in standard conditions. Peripheral blood lymphocytes (PBLs) were freshly prepared using magnetic beads (Dynal) according to the manufacturer's recommendations.

Isolation of genomic DNA from mammalian cells: Isolation of genomic DNA was carried out as follows: cells were washed twice in PBS then lysed in lysis-buffer (50 mM Tris-Cl pH 8, 10 mM EDTA, 100 mM NaCl, 1 % SDS, 0.5 mg/ml proteinase K) at 55 °C for 12 hours. SDS/EDTA/Proteinase K lysates were directly applied for FIGE, or phenol/chloroform extracted DNA was proceeded by linear amplification analysis.

Neutral and denaturing field inversion gel-electrophoresis (FIGE): 1 % agarose gels were prepared in 1×TAE (40 mM Tris-acetate, 1 mM EDTA). Neutral field inversion gel-electrophoresis was carried out at 6 V/cm, in 1×TAE, applying an MJ Research PPI 200 Power Inverter, in a cold room. Running parameters were set to maximize resolution in the 50-400 kb range. After gel-electrophoresis, gels were stained with 0.5 μg/ml ethidium bromide (EBr). Denaturing field inversion gelelectrophoresis was carried out as follows: agarose plugs containing intact human chromosomes were equilibrated in 1×TAE containing 8 M urea, for 2 hours, then cut into 2 equal parts. Heat denaturation was performed at 60°C, 80°C or 90°C for 5 or 15 minutes. The denatured DNA in these samples stay single-stranded (ss) during electrophoresis in 1×TAE containing 1 M urea, used as the electrophoresis buffer. To prepare the urea-agarose gels, urea was added (at 1 M final concentration) to the 1 % agarose solution prepared in 1×TAE, when it cooled below 60°C. After electrophoresis, gels

were washed in 1×TAE for 2 hours, then in 100 mM NaCl for 2 hours, to renature DNA. Gels were stained with 0.5 µg/ml EBr for 30 minutes.

In vitro cleavage assays of the MLL bcr: High quality nuclear extracts were prepared with the nuclear extract kit of Activemotif, according to the manufacturer's instructions. Cleavage assays were carried out as follows: 2-3 µg pMEP4-MLL plasmid (from Peter Aplan, NIH, Bethesda, USA) was incubated in 20 µl buffer A (150 mM KCl, 15 mM Tris-Cl pH 7.4, 2 mM DTT, 10 mM $MgCl_2$) supplemented with 5 µl nuclear extract (and 40 µM etoposide (Sigma), where indicated), at 37 °C for 20 min. Proteins were removed by digestion with 200 µg/ml proteinase K (from MBI Fermentas) in the presence of 1 % Sarkosyl (Sigma), at 55 °C for 1h. Cleavage products were phenol/chloroform extracted, ethanol precipitated and dissolved in 20 µl TE, then run on an 1% agarose gel in the presence of EBr or amplified by linear extension. In some experiments buffer A was omitted and the nuclear extract alone was added to the DNA samples. Size-fractionated nuclear extracts were generated by Superose gel chromatography (Amersham Pharmacia) following the manufacturer's recommendations; fractions were eluted in 500 µl buffer A, than tested for cleavage activity. For S1-nuclease sensitivity assays, 2 µg of pMEP4-MLL plasmid was cleaved in a volume of 100 µl by 2-25-100 U of S1-nuclease at 17 °C for 1 hour. Cleavage products were proteinase K treated, phenol/chloroform extracted, ethanol precipitated and resuspended in 20 µl TE, then run on a 0.5 % agarose gel or amplified by linear extension. Topoisomerase II-depleted nuclear extracts were made by *in vitro* immunoprecipitation with polyclonal antibodies against topo IIα (18511α) and topo IIβ (18513β) raised in rabbits. 10 µl of anti-human topoisomerase II polyclonal antibody was added to the mixture of 5 µl nuclear extract and 40 µl buffer A, and gently rotated for 3 hours on ice. Blocked protein A Sepharose beads (Upstate) were used to

remove topoisomerase II-antibody complexes; after centrifugation, the supernatant was incubated with the pMEP4-MLL plasmid and amplified cleavage products were analyzed on a sequencing gel.

Linear amplification of the cleavage products: Linear amplification was based on the method published by Salus and Jost[76] with minor modifications. Briefly, the reaction was carried out in a volume of 100 µl in the presence of 0.5 µg pMEP4-MLL plasmid DNA treated as described above, or 25 µg BamH I digested genomic DNA. Linear PCR was carried out in samples containing 3 mM $MgCl_2$, 2.5 mM of each dNTP, 25 pmole sense or antisense primer (tgaatctcccgcaatgtcca and cttgaagggctcacaacagacttgg, respectively), 1 µl of deoxycytidine 5'-[α-^{32}P] triphosphate (3000 Ci/mmol, IZINTA Trading Co., Hungary), 3 U of Taq-polymerase (MBI Fermentas). After 30 cycles, the reaction products were phenol/chloroform extracted, ethanol precipitated and resuspended in 10 µl of 50 mM NaOH/0.5 M EDTA/4 M urea, 0.02 % xylene cyanol). Sequence ladders were generated with the fmol® DNA Cycle Sequencing System (Promega); 4 fmole of the PCR product was used as a template. The sequencing gels contained 8 % polyacrilamide/7 M urea. The samples were heated at 95 °C for 5 minutes immediately before loading and sequencing ladders were run alongside the amplified cleavage products. The results were evaluated on a phosphorimager (Biorad).

Nuclear halo preparation: Exponentially growing Jurkat and ML-1 cells, or freshly prepared peripheral blood lymphocytes (PBLs) were embedded in 1 % LMP-agarose and pipetted onto the surface of agarose-precoated glass slides. Where indicated, Jurkat and ML-1 cells treated with 40 µM etoposide for 6 hours were used to investigate apoptotic DNA fragmentation. The samples were treated with a series of different lysis buffers for 6 minutes on ice (buffer A: 2 M NaCl, 10 mM Tris-Cl pH 8, 50 mM EDTA, 0.5 % Triton X-100, 10 % DMSO; buffer B:

the same as buffer A, but with 0.5 M NaCl; buffer C: 2 M NaCl, 10 mM Tris-Cl pH 8, 50 mM EDTA, 0.2 % Sarkosyl, 0.5 % Triton X-100, 10 % DMSO; buffer D: the same as buffer C, but with 0.5 M NaCl). In certain experiments alkaline lysing conditions (pH 12), expected to preclude any enzymatic activity, were applied. Where indicated, the nuclear halos were fixed in 2 % formaldehyde for 10 minutes. All solutions contained protease inhibitors (Protease inhibitor cocktail, Sigma Aldrich). Loop-size DNA fragmentation was visualized by the comet assay, with the samples run in field inversion mode (FIGE-comet). FIGE of the nuclear halos and of isolated DNA was performed using an MJ Research PPI 200 power inverter; after running, the samples were neutralized in 1 M Tris-Cl pH 8 / 10 mM EDTA for 5 minutes, then dehydrated in an ascending series of ethanol for 2 minutes each at 4 °C, finally in methanol and acetone for 15 minutes each at -20 °C. Running parameters were set to maximize resolution in the ~50-400 kbp range. In the experiment shown in Figure 1.D., the nuclear halos and FIGE-comets were scraped off from the surface of the glass-slides and following β-agarase digestion, the DNA was isolated by phenol-chloroform extraction and analyzed by FIGE on a 1 % agarose gel, prepared in 1xTAE.

Preparation of chromatin fibers: Stretched DNA fibers were prepared exactly by the method described by Parra[77]. Briefly, Individual Jurkat cells or PBLs (100-3000 / slide) in 5 µl of PBS were placed at one and of a glass slide, air-dried and immediately lysed with a solution of 0.5 % SDS / 50 mM EDTA / 200 mM Tris (pH 7.4) for 5 minutes at room temperature. The slide was tilted to allow the drop of sample to run downwards by hydrodynamic forces, resulting in a DNA stream extending down the slide. The DNA stream was air dried and (1) in situ nick translated with DNA polymerase one, then fixed with methanol / acetone, or (2) first fixed in methanol /acetone, then in situ nick translated. The two methods gave comparable results.

Laser scanning cytometry (LSC): FIGE-comets were quantitatively evaluated by image analysis applying an iCys laser scanning cytometer and an iCyte 2.6 software (CompuCyte, USA). Cyber Gold stained samples were excited with the 488-nm argon-ion laser line of the equipment and the fluorescence emission was detected in the green channel applying a 530±15-nm band pass filter. Two different intensity level contour thresholds were set up for the green fluorescence. The first was set up to detect low level fluorescence intensity for whole comets. The other contour threshold using a virtual channel was set up to recognize only the higher intensity nuclear locations for comet heads. Both the comet head and whole comet fluorescence intensity integrals and image locations were recorded. These primary data were transported into a Microsoft Excel sheet (Microsoft Corp. USA) and tail moment calculations were completed with the software. Tail moment is defined as a product of the distance between the head and tail mass centers and the relative amount of DNA in the tail compared with the total DNA in each comet, according to the following equation: TM = d x FLtail / (FLhead + FLtail), where FLhead is the DNA fluorescence in the comet head, FLtail is the DNA fluorescence in the comet tail, and d is the distance between the centers of mass of the head and the tail images. The unit of T is length[78,79].

Characterization of the DNA-termini by *in situ* nick translation: The presence of endogenous nicks in the nuclear halos was studied by situ nick labeling performed with DNA polymerase I, Klenow enzyme and terminal transferase, respectively. All reagents were purchased from Fermentas. Immediately after halo-preparation, the slides were washed in 100 ml of ice cold 0.5xTE for 5 minutes, and then 200 ul of labeling mix A (1x Pol I / Klenow buffer, 50 uM biotin-11-dUTP, 50 uM 3dNTP, 5 U DNA polymerase I / Klenow fragment) or mix B (1xTdT buffer, 150 uM biotin-11-dUTP, 5 U TdT) was added to each slide, respectively, and incubated under coverslips for 1-10 minutes at 20 °C. The reactions were stopped by washing

in 100 ml of ice-cold TE for 10 minutes, and then dehydrated and fixed as described above. Biotin-11-dUTP incorporation was detected by monoclonal anti-biotin antibodies (Sigma), and the signals were enhanced by an AlexaFluor 488 labeled anti-biotin signal amplification kit (Molecular Probes).

Microscopy and digital image processing: Full field images were made with a 7.1 million pixels Olympus C-7070 WideZoom professional digital compact camera mounted on an Olympus CX31 microscope with 4X, 10X, and 40X achromat objectives, 50W Hg lamp light source from a reflected light fluorescence attachment and mirror units for blue and green fluorescence excitation. CLSM images were made by an LSM510 confocal laser scanning microscopy system. SybrGold stained samples were excitated by the 488 Argon ion laser line, and emission was detected in single track mode, through the 515-540 band pass filter in the green fluorescence channel, applying 1.5 µm pinhole. Fluorescence signals of AlexaFluor 488-labeled samples were detected as described above, except that multi-track mode was used to simultaneously detect propidium iodide fluorescence through the 515-545 nm band pass filter of the red channel. Images were processed as follows: the size of chromatin fragments was estimated by dividing the length of diploid genome ($6x10^9$ bp) by the number of fragments generated in alkaline FIGE or by the number of nick-translated spots. These numbers were determined by dividing the total (background corrected) fluorescence signal (PI stained DNA after FIGE or AlexaFluor 488 fluorescence of nick-translated spots) by the mean intensity of spots. Full field fluorescence images were processed using SCIL Image (TNO, Delft, The Netherlands). Binary masks to identify individual spots were created by thresholding the fluorescence images after background subtraction using the rolling ball algorithm. Lower threshold values were determined as average fluorescence from cell-free areas of the image; small objects originating from background noise were removed using

another binary mask after Gauss filtering; spots were void of holes as confirmed by a dilation-erosion cycle. The size-distribution histogram of unit spots was generated and its median determined; the average fluorescence of median sized spots was taken as the mean intensity of individual spots which was of the same magnitude, within 20% error, as the median of spot fluorescence intensity distribution. Image processing was done by Dr. György Vereb.

FISH analysis of nuclear halos and FIGE-comets: The DNA of nuclear halos and FIGE-comets were visualized by Sybr Gold (Molecular Probes), propidium iodide (Sigma) and DAPI (Vector Laboratoratories, Inc., USA), respectively. Fluorescence in situ hybridization was performed on nuclear halo and FIGE-comet slides prepared in mild lysis conditions (nuclear halo buffer A or buffer B), to completely preserve matrix and chromosome territory organization. To study loop-size DNA fragmentation at the MLL bcr, the LSI MLL Dual Color, break apart rearrangement probe (Vysis Inc., USA), spanning a contiguous 540 kbp genomic region of 11q23, including the breakpoint cluster region of the MLL gene, was used. The LSI MLL probe consists of a 350 kbp centromeric flank of the MLL bcr labeled with SpectrumGreen, and a 190 kbp telomeric flank of the 8.3 kbp MLL bcr labeled with SpectrumOrange, sonicated to an average fragment size of 600 bp. The chromosome 8 specific probe was generously supplied by the Resource for Molecular Cytogenetics (University of California Cancer Center, San Francisco, CA, USA) and labeled by biotin via nick translation according to the protocol of the supplier (ROCHE Diagnostics GmbH, Applied Sciences, Germany). The chromosome 15 painting probe was purchased from Appligene and was used according to the manufacturer's recommendations. The slides were denatured in 2 M NaOH (2 min, at room temperature), dehydrated in an ascending series of ethanol (70%, 85%, 100%; 2 min each), and air dried. DNA probes and cellular DNA were denatured at 73°C for 5 min, and the probe solution was dropped on the cells. Overnight

hybridizations were performed at 37 °C in a hybridization oven. Post-hybridization washing steps were done according to the manufacturer's instructions. Samples were scored for the number of fluorescent signals per cell using a fluorescent microscope (OPTON, Oberkochen, Germany) equipped with selective filters for the detection of FITC, SpectrumGreen, SpectrumOrange and DAPI. Three colour images were captured using a digital imaging analysis system (ISIS Metasystem GmbH, Altlussheim, Germany). FISH was done in collaboration with Dr. Margit Balázs and Zsuzsa Rákosy.

Chromatin immunoprecipitation: All reagents used contained protease inhibitors (Protease inhibitor cocktail, Sigma Aldrich). ChIP was performed according to the method published by Kuo and Allis[80] with modifications: Jurkat cells were cultured in standard conditions, and where indicated, they were treated for 3 hours with 40 µM etoposide (Sigma) to induce apoptosis. Cells were fixed with 1 % formaldehyde for 10 minutes at room temperature, and fixation was stopped by the addition of glycine to a final concentration of 150 mM. For the isolation of nuclei, cells were washed twice in ice-cold PBS, and incubated for 10 minutes in buffer N (5 mM Pipes pH 8, 85 mM KCl, 0.5 % NP-40) on ice. After centrifugation at 3000 g at 4 °C for 10 minutes, the pelleted nuclei were resuspended in sonication buffer (1 % SDS, 10 mM EDTA, 50 mM Tris-HCl pH 8), incubated on ice for 10 minutes, then sonicated to an average fragment size of 200 bp. Cell debris were removed by centrifugation at 10000 g at 4 °C, for 20 minutes; aliquots of soluble chromatin were frozen in liquid nitrogen and stored at -80 °C. Before immunoprecipitation, 0.1 ml of the chromatin solution was diluted 10-fold in buffer IP (0.01 % SDS, 1.1 % Triton X-100, 1.2 mM EDTA, 20 mM Tris pH 8, 167 mM NaCl), and the samples were precleared with 40 µl of blocked protein A Sepharose beads (Upstate, catalog no. 16-157). Immunoprecipitation was carried out overnight on a rotating plate at 4 °C with antibodies (Upstate) against modified histones: anti-acetyl H4, 2 µg/IP, catalog no. 06-866, and anti-

dimethyl H3 Lys 4, 5 µg/IP, catalog no. 07-030. Complexes were collected using 40 µl of blocked protein A Sepharose, and an aliquot of the 'no antibody' control sample was preserved to determine the amount of amplified DNA obtained without immunoprecipiation ('input' DNA). Subsequently, the Sepharose beads were pelleted and washed twice with each of the following buffers: buffer A (0.1 % SDS, 1 % Triton X-100, 2 mM EDTA, 20 mM Tris-HCl, 150 mM NaCl; pH 8), buffer B (0.1 % SDS, 1 % Triton-X 100, 2 mM EDTA, 20 mM Tris-HCl, 500 mM NaCl; pH 8), buffer C (0.25 M LiCl, 1 % NP 40, 1 % sodium deoxycholate,1 mM EDTA, 10 mM Tris-HCl; pH 8), and TE (10 mM Tris-HC, l mM EDTA; pH 8, 1). Cross-links were reversed by heat-treatment at 65 °C for 6 hours, then samples were treated with 0.2 mg/ml Dnase-free RNase (from Sigma Aldrich) for 30 minutes at 37 °C. Proteins were digested by 0.5 mg/ml proteinase K in the presence of 0.1 % SDS for 3 hours at 50 °C and DNA was purified on PCR clean-up columns (Qiagen). Samples were eluted in 50 µl of TE and stored at -20 °C. The level of histone acetylation and methylation were determined by *a)* the ChIP-on-beads technique, *b)* real time quantitative PCR. Both in the case of 'no antibody' (nAb) controls and 'Ab' samples, the number of copies were expressed as a percentage of input DNA.

Supplementary figure 1: the position of FISH probe and PCR amplicons used in halo-FISH studies and ChIP / QPCR experiments

Schematic representation of the MLL breakpoint cluster region. ***Small boxes***: exons; ***B***: Bam H1 cleavage sites flanking the 8.3 kbp MLL bcr; ***CEN***: centromeric (5') flank of MLL-bcr; ***TEL***: telomeric (3') flank; ***cen*** and ***tel***: the position of amplicons spanning the 5'- and 3'-MLL flanks, respectively, studied in real time QPCR and ChIP studies; ***green*** and ***red lines***: dual-colour break-apart rearrangement FISH probe spanning the MLL-bcr.

PCR and real time quantitative PCR (QPCR): PCR reactions were carried out in reaction volume of 25 µl. Primers designed for *(a)* the breakpoint cluster region of the MLL gene: fw5'-3' AGTCTGTTGTGAGCCCTTCCA, rev5'-3' CGACGACAACACCAATTTTCC, probe5'-3' Fam-AAGTTTTGTTTAGAGGAGAACGAGCGCCCT-Tamra (termed 'telomeric assay'), fw5'-3'-TGCAGGCACTTTGAACATCCT, probe5'-3 Fam-AGCACTCTCT CCAATGGCAATAGTTCTAAGCAA-Tamra,' rev5'-3' CTGATCCTGTGGACTCCA TCTG (termed 'centromeric assay'), and *(b)* for the promoter region of the human TGM2 gene investigated in ChIP-on-beads studies: fw 5'*Fam*-GAGACCCTCCAAGTGCGAC-3', rev 5'*Biotin*-CCAAAGCGGGCTATAAGTTAGC-3'. Standard reaction conditions were applied (2,5 mM dNTP, 0,4 µM of forward and reverse primers, 1.5 mM $MgCl_2$, 2 U Taq polymerase, 2 µl of ChIP-DNA) with a two-step cycling profile: 1x 95 °C:1 minute; 24x 95 °C: 12 sec, 55 °C: 30 sec; 1x 60 °C: 7 minutes. In the ChIP-on-beads studies, *Fam*/*biotin* labeled products were purified on PCR clean-up columns, and then analyzed by either agarose gel-electrophoresis, or by flow cytometry, capturing them on streptavidin-conjugated microbeads (see below). The PCR reactions were stopped in the linear phase as validated by real time QPCR measurements, that were performed by the same but unlabeled oligonucleotides, in conjunction with a TaqMan probe of 5'-3' Fam-CCGCCTCGGCAGTG CCA-Tamra. All reactions were performed in a volume of 22 µl according to the manufacturer's instructions. Measurements were done in triplicates, and the relative number of amplicons was determined by the $2^{-\Delta Ct}$ quantification method. The MLL and TGM2 mRNA levels were measured by reverse transcriptase real time QPCR as described. Total RNA was extracted by Trizol reagent (Invitrogen) from control and etoposide-treated Jurkat and ML-1 cells as decribed[81]. The mRNA copy numbers were normalized to cyclophilin transcript levels.

Measurement of DNase I sensitivity: Nuclei were prepared from Jurkat and ML-1 cells resuspended in SSCP (0.15 M NaCl, 0.015 M cacodylic acid), by lysing them in ice-cold SSCP + 0.25 % NP-40. Five volumes of ice cold Hepes-buffer (0.17 M KCl, 10 mM Hepes, 3 mM $MgCl_2$) was added, and the samples were centrifuged. Nuclei were recovered in Hepes-buffer and divided into several aliquots, which were treated with different concentrations of DNase I (Promega) for 10 minutes at room temperature. Digestion was stopped by incubation of the nuclei resuspended in lysis-buffer (50 mM Tris-Cl pH 8, 10 mM EDTA, 100 mM NaCl, 1 % SDS, 0.5 mg/ml proteinase K) at 55 °C for 16 hours. DNA was isolated by phenol-chloroform extraction and ethanol precipitation, dissolved in TE buffer, digested with BamH1 and re-extracted as above. The number of intact MLL-copies in each sample was determined by real time QPCR and normalized to the control without DNase digestion.

Flow cytometry:

Cell cycle measurements: normal and etoposide-treated Jurkat and ML-1 cells were fixed in ice-cold 70 % ethanol at -20 °C, overnight. After fixation, cells were resuspended in PBS, and treated with 100 µg/ml RNase A for 30 minutes at room temperature. DNA was stained with propidium-iodide at a final concentration of 50 µg/ml. Measurements were carried out on a Becton-Dickinson FACScan flow cytometer (Mountain View, CA, USA): the samples were run at *high speed*, the laser power was set to 15 mW and the fluorescence signals were detected through the FL2 channel, in logarithmic mode. The results were evaluated by the BDIS CELLQUEST 3.3 (Becton-Dickinson) software and the indicated conditions were applied for FISH and ChIP analyses (see Suppl. Fig. 5.B.). In some FISH experiments, S-phase cells were selectively labelled by a 1 hour pulse of BrdU. Washing steps and FISH analysis were carried out as described[82]. The BrdU-foci were detected by mouse-anti-BrdU

and goat-anti-mouse-FITC antibodies (Vector Laboratoratories, Inc., USA), used at a dilution of 1:50 and 1:500, respectively. Incubations and subsequent washes were done as described.

Measurements of epigenetic changes by ChIP-on-beads method: immunoprecipitated DNA samples (input, nAb, Ac H4/Met H3 K4, respectively) were tagged with 5'-*Fam/biotin* by PCR. 5 µl of tagged ChIP-DNA was added to 10,000 streptavidin-coated, plain beads (purchased from Polyscience AG, Switzerland) in 50 µl PBS. These samples were incubated for 20 minutes at room temperature, and then washed in 1 ml PBS. Flow cytometry was performed as described above, except that fluorescent signals were collected thorugh the FL-1 channel.

Supplementary table 1: main properties of polymerases used in the study

Applied enzyme	*3'-5' exonuclease*	*5'-3' exonuclease*	*Strand displacement*
DNA polymerase I, E.coli	++	+	-
Klenow fragment	++	-	++
Terminal Deoxynucleotidyl Transferase (TdT)	-	-	Not applicable: attaches nucleotides to the 3'-OH groups of ss or ds DNA

Supplementary table 2: main properties of nucleases used in the study

Applied enzyme	*Substrate*	*Mode of action*	*Polarity of cleavage*	*Reaction products*
Deoxyribonuclease I (DNaseI)	ssDNA, dsDNA, DNA in RNA-DNA hybrids	endonuclease	-	5'-dNMPs, 5'-oligonucleotides
Exonuclease III, E.coli	dsDNA (with nicks, blunt ends, 5'-overhangs)	exonuclease	3'-5'	5'-dNMPs, ssDNA
	Apurinic / apyrimidinic DNA	AP endonuclease	5' to an abasic site	DNA with nick 5' to AP sites
	RNA in RNA-DNA hybrids	RNase H (exonuclease)	3'-5'	NMPs
	DNA with 3' phosphorilated ends	3'-phosphatase	-	DNA with 3'-OH ends
S1 nuclease	ssRNA, ssDNA, nicks in dsDNA	Degradation of ss nucleic acids	-	5'-NMP, 5'-dNMP, 5'-oligonucleotides
Ribonuclease A (RNase A)	ssRNA	Cleaves the phosphodiester bond between 3'-C or 3'-U and 5'-OH residues	-	3'-CMP, 3'-UMP, oligonucleotides with terminal 3'-CMP or 3'-UMP

5. RESULTS

***5.1** En masse loop-size chromatin fragmentation in healthy, non-apoptotic cells*

Routine procedures of DNA preparation involving extensive protein denaturing treatments (SDS/proteinase K/EDTA) of live cells or nuclei usually yield lysates that contain genomic DNA fragmented to loop-size molecules (Figure 5.). The average fragment size obtained in this procedure is surprisingly narrow, concentrated around ~50 kbp and involves almost the total genomic DNA. The phenomenon can also be observed in formaldehyde-fixed nuclei, as well as upon rapid alkaline lysis of live cells (Figure 5, panel 3) which is expected to preclude any residual enzymatic activities (e.g. topo II, a typical chromatin bound enzyme). These data confirmed the earlier observations reported by our group[67,68,83], and also extended these to a cell line with altered topoisomerase II status.

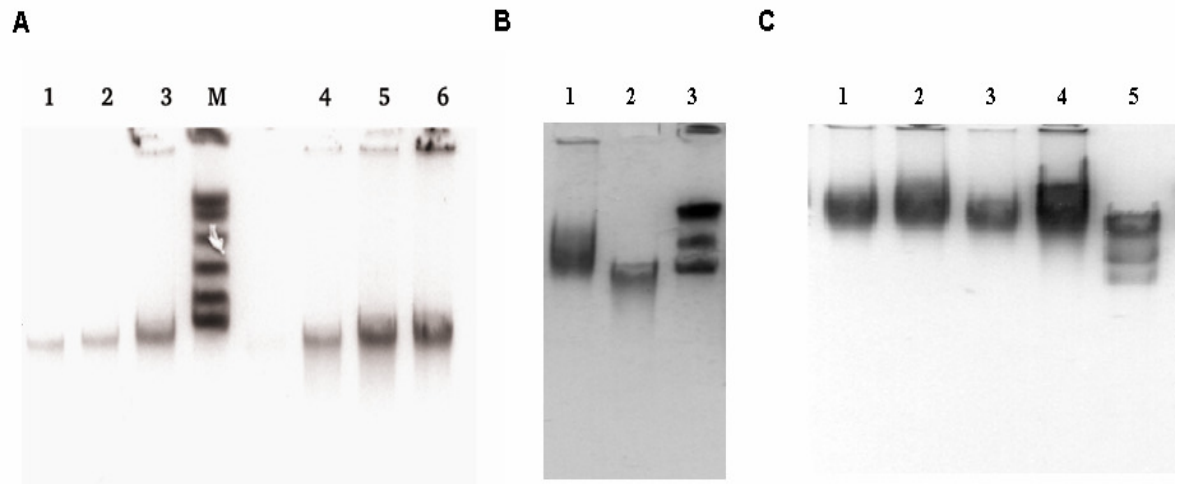

Figure 5: Loop-size chromatin fragmentation observed in normal, non-apoptotic cells. *En masse* loop-size fragmentation of chromatin derived from healthy mammalian cells detected by FIGE. ***(A)** Lanes* **1-2-3**: SDS/EDTA/PK lysates of normal Jurkat, HL-60, NIH3T3 cells, respectively. *Lanes* **4-5-6**: the same as in *lanes 1-2-3*, but lysates were made from isolated nuclei; M: pulse marker; last lane denotes 50 kbp ***(B)*** SDS/EDTA/PK lysates of ***(1)*** normal DC3F and ***(2)*** topoisomerase II-deficient DC3FOH cells. ***(3):*** pulse marker; last lane denotes 50 kbp ***(C)*** SDS/EDTA/PK lysates of normal PBLs ***(1)***, nuclei prepared from PBLs ***(2)*,** nuclei prepared form PBLs, lysed in alkaline conditions ***(3)*,** PBLs, lysed in alkaline conditions ***(4)***. ***(5):*** pulse marker; first lane denotes 50 kbp.

Since fragmentation can be avoided when cells are embedded into agarose plugs prior to lysis, mechanical factors rather than nucleolytic activities are generally believed to play the primary role in these phenomena. Based on this observation, random breakage of the long DNA molecules when prepared without embedding into agarose plugs would be expected. However, the following observations run counter this view: chromosome-long double-stranded DNA turns into loop-size fragments when agarose-encapsulated samples are heat-denatured in the presence 8 M urea, or upon exposure to single-strand specific S1 nuclease (Figures 6 and 7.).

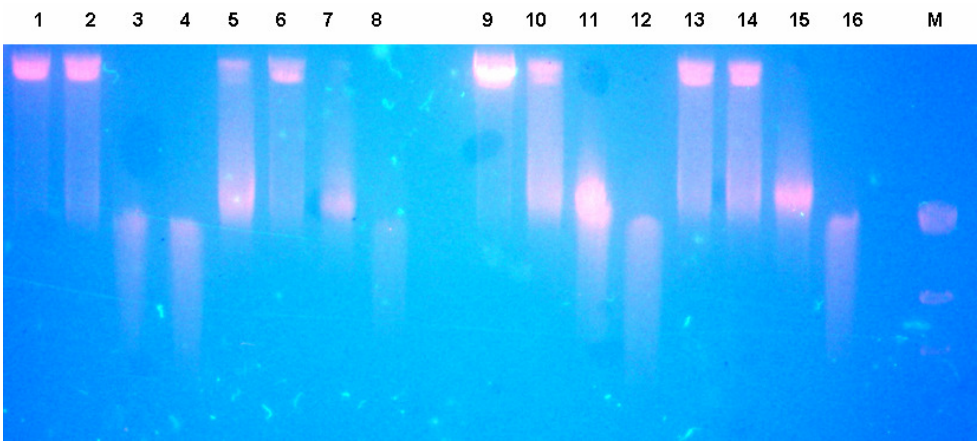

Figure 6: FIGE analysis of S1 nuclease digested, agarose-embedded lysed human cells. *Lane* **1:** control (undigested) Jurkat cell lysate. *Lanes* **2-3-4:** Jurkat cell lysates digested with 20-200-2000 U/ml S1 nuclease for 3 hours at 20 °C, respectively. *Lane* **5-6-7-8:** Jurkat cell lysates digested with 2000 U/ml S1 nuclease for 1-0.5-2-6 hours at 20 °C, respectively. *Lane* **5-12:** the same as 1-4 except that ML-1 cells were used. *Lane* **13-16:** the same as 5-8 except that ML-1 cells were used. *Lane* **17:** λ-phage DNA.

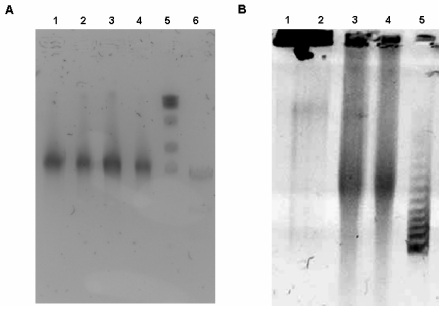

Figure 7: ***(A)*** **Field inversion gelelectrophoresis of S1 nuclease treated, agarose-embedded human cell lysates**. *Lane 1*: S1 nuclease digested human PBLs; *Lane 2*: S1 nuclease digested lysates of human HL-60 cells. *Lane 3*: S1 nuclease digested lysates of human Jurkat cells; *Lane 4:* S1 nuclease digested lysates of human ML-1 cells*; Lane 5:* pulse marker; last lane denotes 50 kbps. *Lane 6*: λ-phage DNA. ***(B)*** **Denaturing field inversion gelelectrophoresis of agarose-embedded human cell lysates.** Single-stranded DNA samples were run in the presence of 8 M urea. *Lane 1-2*: control, i.e. dsDNA of agarose-embedded Jurkat and ML-1 cells, respectively. *Lane 2-3*: denatured (ss) DNA of Jurkat and ML-1 cells. *Lane 5*: ss pulse marker**.**

These data can be interpreted to suggest that single-stranded discontinuities are present in the lysed nuclei that are prevented from becoming manifest double-strand breaks when enclosed in an agarose matrix. Characterization of possible single-stranded regions as predilection points of ~50 kbp fragmentation might also prove useful in understanding if/how apoptotic HMW fragmentation might give rise to gene rearrangements.

5.2 *Implementing an experimental strategy for the detection of single-strand discontinuities at the level of individual cells*

In an attempt to confirm the above results obtained by mass biochemical approaches, we have implemented a novel technique we name field inversion single-cell gel-electrophoresis (FI-SSGE) that is suitable for the simultaneous visualization of chromatin loops and loop-size DNA fragmentation at the level of single cells. The technique is an adaptation of the conventional comet assay[78,79], and it is novel in the sense that the applied periodically inverted electric field helps resolve large DNA molecules (Figure 8.). Neutral FIGE of high-salt extracted nuclei is expected to reveal double-strand breaks; by contrast, alkaline FIGE of nuclear halos will expose single-stranded regions in the chromatin structure (Figure 9.). The number of breaks is directly proportional to the tail moment distributions of the FIGE-comets, which can be quantificated by laser scanning cytometry as described in 'materials and methods'. The results can be plotted as probability distribution histograms showing the distribution of tail moments in a cell population, or in two-dimensional distributions of two simultaneously measured parameters, i.e. in dot plot format where each dot represents a cell (Figure 10.).

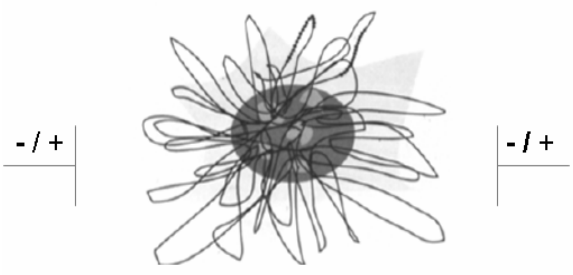

Figure 8: Scheme showing the principle of FI-SSGE analysis. Nulcear halos are obtained by salt extraction of live cells in various conditions (e.g. neutral, alkaline, 2 M NaCl-extraction removing both H1 and nucleosomal histones, 0.5 M NaCl-extraction that removes only H1 histones) are subjected to periodically inverted electric field that is able to resolve loop-size DNA. FI-SSGE is performed in either alkaline, or neutral conditions, resulting in the electrophoresis of denatured ss or native ds DNA molecules, respectively.

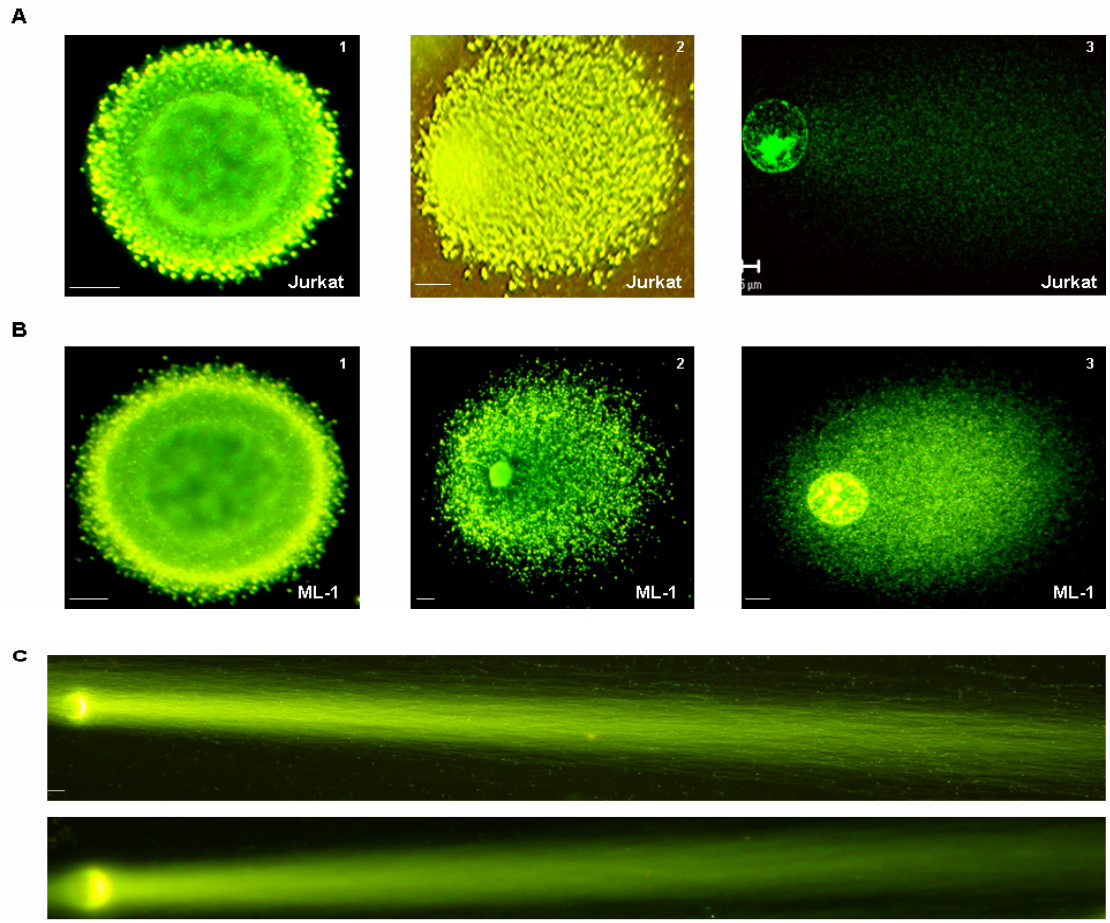

Figure 9: ***A.*** **FIGE-comet analysis of high-salt extracted nuclei.** Nuclear halos of healthy Jurkat cells, before (*left*) and after *alkaline FIGE* (*middle* and *right*); ***B.*** the same as *A.* except that ML-1 cells were studied. Fluorescent microscopic full field images (upper panel: left, middle, and all images in the lower panel) and scanning confocal images (upper panel: right) are shown. The average DNA content of the individual granules, estimated from the ratio of the average fluorescence intensity of median-sized spots to the total fluorescence of FIGE-comets, is ~50 kbp, accurately coinciding with the size of chromatin loops as observed in the fragmentation experiments. Scale: 5 µm. ***C.*** *Neutral FIGE*-comet of high-salt extracted nuclei. The DNA of Jurkat cell nuclear halos unfolds to parallel stretches of long fibres. Scale: 5 µm.

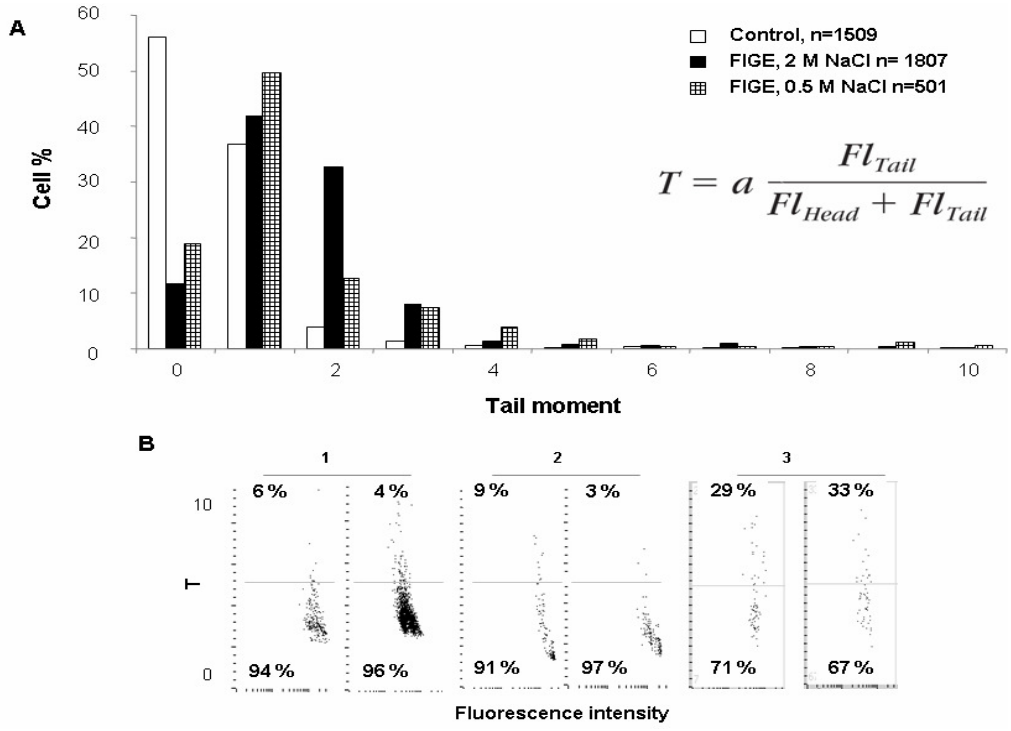

Figure 10: Analyses of alkaline FIGE-comet tail moments by laser scanning cytometry (LSC) at different experimental conditions. *(Upper panel)* Tail moment distribution histograms of alkaline-FIGE comets compared to that of nuclear halos, prepared in two different conditions; 'n' and 'm' denote cell numbers *(Lower panel)* Pairwise comparison of tail moments of FIGE-comets upon alkaline (B.1., *left*) or neutral lysis (B.1., *right*); 2 M NaCl-extraction (B.2., *left*) or 0.5 M NaCl-extraction (B.2., *right*); applying proteinase K pretreatment (B.3., *left*), or without proteinase K (B.3., *right*). X-axis: fluorescence intensity (in arbitrary units) corresponding to DNA content; Y-axis: tail moment distributions.

Upon alkaline FIGE, the nuclear halos of healthy, non-apoptotic Jurkat and ML-1 cells become completely disassembled to granules (Figure 9.A and B.). Each granule contains ~50 kbp DNA, as determined by quantitative image analysis (see Materials and Methods) and electrophoresis of the DNA isolated from the slides (Figure 11.). Alkaline FI-SSGE of nuclear halos prepared in different lysis conditions gave identical results, with minor differences in the tail moment distributions (Figure 10.). Similar granules were seen in the case of several proliferating or resting human cell lines (Jurkat, ML-1, HL60, HeLa, PBL), in S. *cerevisiae* protoplasts (not shown). The size of DNA derived from the nuclear halos and FIGE-comets are similar (~50 kbp; lanes 1-2 of Figure 11.), and also indistinguishable from that of the S1 nuclease-treated (double-stranded, ds), or urea-denatured

(ss) chromatin samples (Figures 7.). The particles containing the DNA loops were revealed only in alkaline electrophoretic conditions; neutral FIGE resulted in the unfolding of chromosomal DNA into parallel stretches of long fibers (compare Figure 10.A and C.). The above data collectively suggest that regularly spaced single-strand discontinuities rather than simply base-unpaired secondary structures (see details later) may be involved in delimiting interphase chromatin loops.

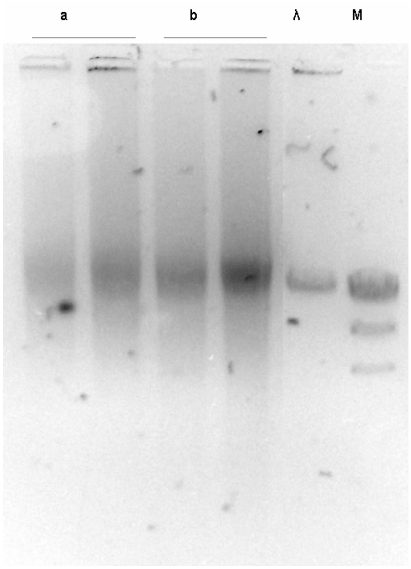

Figure 11: Field inversion gelelectrophoresis (FIGE) of the DNA isolated from nuclear halos and alkaline FIGE-comets shown in Figure 9. *Lane 1*: DNA isolated from nuclear halos. *Lane 2*: DNA isolated from alkaline FIGE-comets. *Lane 3*: λ phage DNA; *lane 4*: pulse marker, first line denotes 50 kbp.

5.3 *Detection and characterization of free DNA-termini in nuclear halos by in situ nick translation labeling*

The DNA-termini at the revealed ss discontinuities were characterized by in situ nick labeling performed with DNA polymerase I, Klenow enzyme, and terminal transferase (TdT). As shown in Figures 12 and 13, the breaks could be efficiently labeled by DNA polymerase I, indicative of uniform ends with free 3' OH.

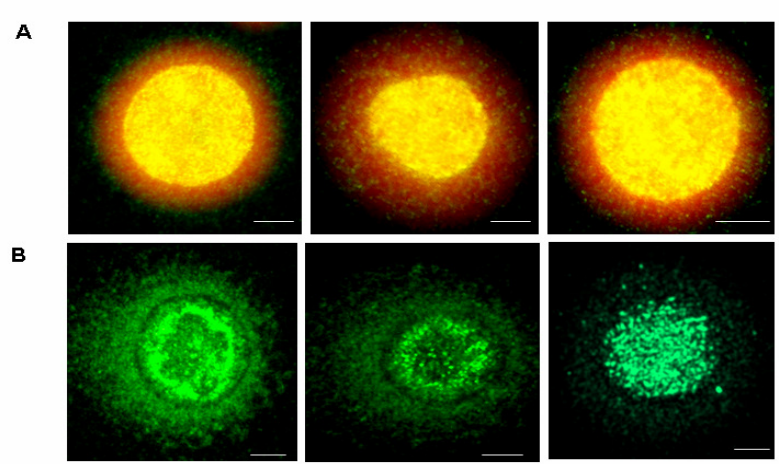

Figure 12: Characterization of DNA breaks present in nuclear halos by *in situ* nick translation. Samples were prepared in neutral lysis conditions. *Upper panel*: full field images; *red*: DNA (PI), *yellow:* nick translated regions (overlapping with the red signals). *Lower panel:* CLSM images of biotin-dUTP labeled nick translated regions, detected by indirect immunfluorescence.

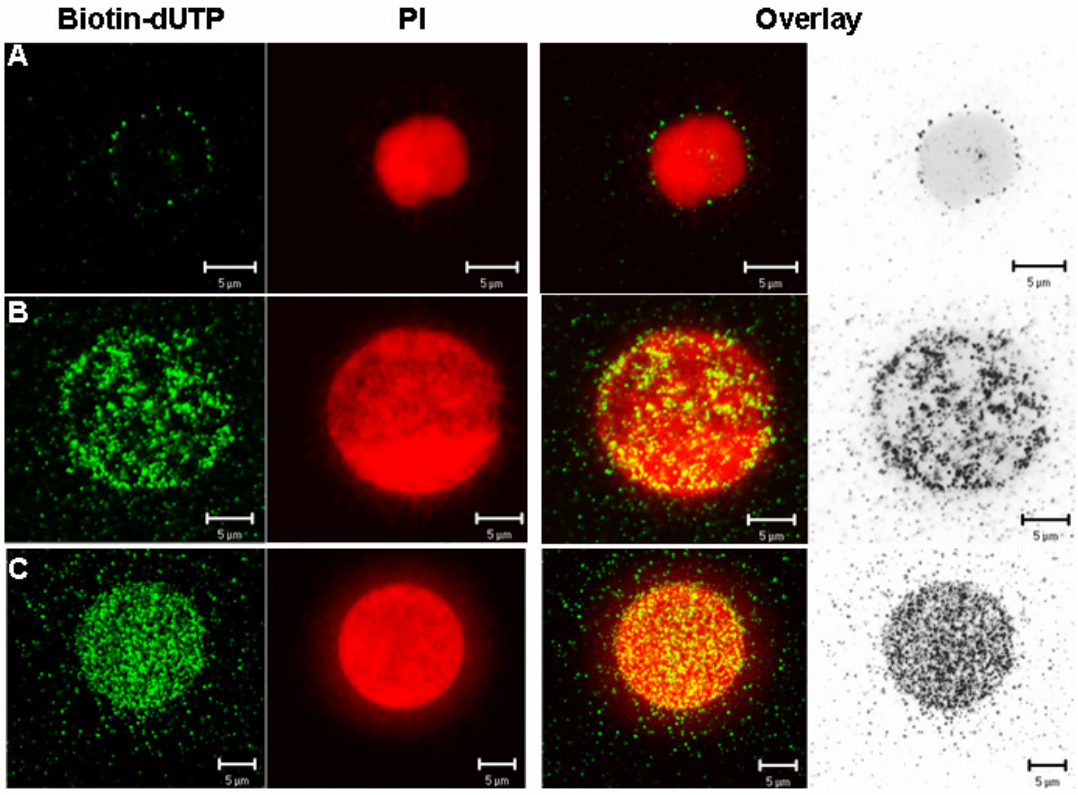

Figure 13: *In situ* nick translation of nuclear halos with DNA polymerase I. *red*: DNA (PI), *green:* incorporated biotin-dUTPs, *yellow:* nick-translated regions overlapping with red signals.*Lanes A-B-C:* 1-5-10 minute biotin-dUTP pulses, respectively.

The degree of spatial regularity of incorporation was assessed in stretched chromatin fibers (Figure 14.). In these samples, nick-translated regions alternate with completely nick-free zones along the continuous DNA threads, implying their non-random distribution.

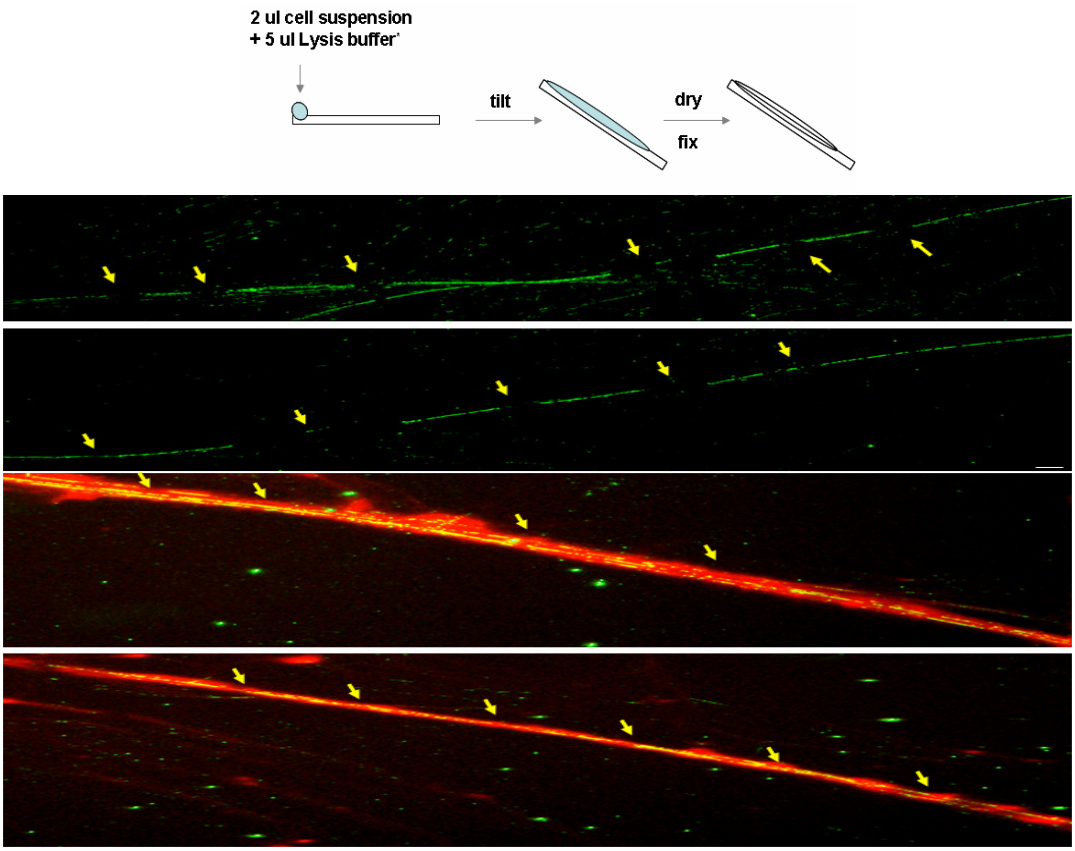

Figure 14: Charachterization of free DNA-termini in stretched chromatin fibers by in situ nick translation with DNA polymerase I. Full field fluorescent microscopic images, magnification: 400x. *Green:* incorporated biotin-dUTPs, *red*: DNA (PI), *yellow:* nick translated regions overlapping with red signals. Detection: by indirect immunfluorescence as described in 'material and methods'. Arrows point to sites of nick-free regions.

Neither TdT, nor Klenow enzyme could efficiently label the nuclear halos (Figures 15, 16.), arguing against the presence of longer single-stranded gaps and double stranded breaks. Remarkably, both enzymes could intensively incorporate biotin-dUTP if the samples were previously exposed to exonuclease III (Exo III), RNase A or alkali (Figure 15, 16.). The number of nick-translated spots, determined by image analysis, was comparable to the number of disassembled granules seen after alkaline FIGE (Figure 9.). In the presence of specific RNase inhibitor the effect of RNase A was

completely precluded (Figure 15.H.), providing direct evidence for the involvement of RNA in blocking nick labeling.

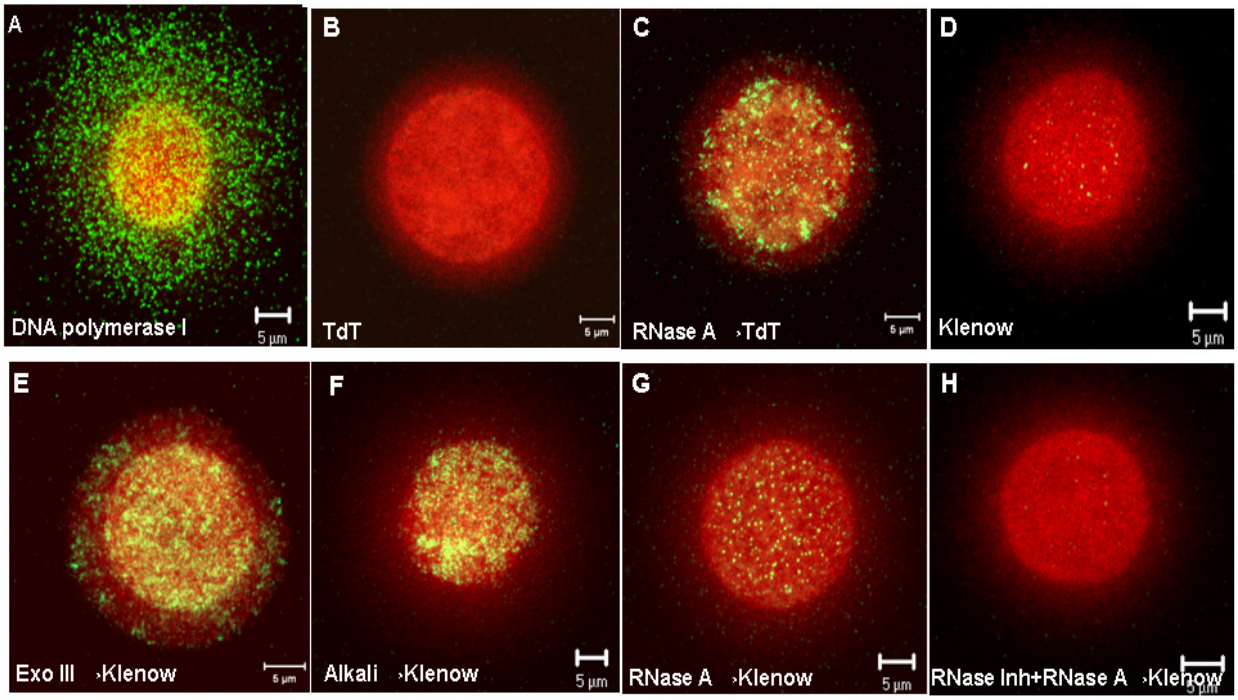

Figure 15: Characterization of DNA breaks present in nuclear halos by *in situ* nick translation. *Green*: nick translated regions; *Red*: DNA (PI). *A.* Breaks in the nuclear halos can be efficiently labeled by DNA polymerase I. *B.* Breaks in the nuclear halos are barely labeled by TdT. *C*. Nuclear halos pretreated with RNase A can be efficienty labeled by TdT. *D*. Breaks in the nuclear halos are barely labeled by Klenow fragment. *E.* Nuclear halos pretreated with Exonuclease III can be efficiently labeled by Klenow fragment. *F.* Nuclear halos prepared under alkaline conditions can be efficiently labeled by Klenow fragment. *G.* Nuclear halos pretreated with RNase A can be efficiently labeled by Klenow fragment. *H.* Placenta RNase inhibitor prevents the effect of RNase A on the labeling of nuclear halos by Klenow fragment. For RNase A treatments 2 µg/ml enzyme concentration was used, for 15 minutes at room temperature.

5.4 *Assessing the intranuclear topography of the revealed ss breaks at a model fragile site, the breakpoint cluster region of MLL gene.*

To study the role of particular DNA regions in the observed phenomena, FISH experiments were performed on nuclear halos and alkaline FIGE-comets, focusing on the breakpoint cluster region (bcr) of the Mixed Lineage Leukemia gene.

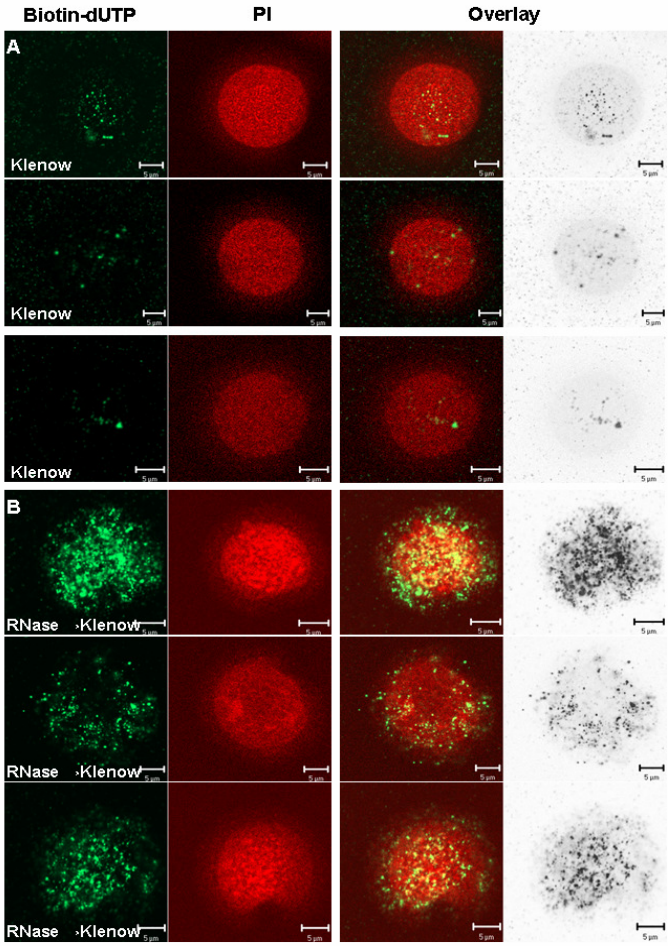

Figure 16: In situ nick translation of nuclear halos with Klenow enzyme. *red*: DNA (PI), *green:* incorporated biotin-dUTPs, *yellow:* nick translated regions overlapping with the red signals. **Upper three panels:** 10 minute biotin-dUTP pulse. **Lower three panels:** the same as above except that samples were pretreated with 200 µg/µl RNase A for 15 minutes at room temperature

In Jurkat cells and peripheral blood lymphocytes (PBLs) harboring germline MLL (gMLL), the halo-FISH signals consistently appeared in two forms: as tightly condensed spots (Figures 17.A.2. and B.1.), similar to the interphase-FISH signals obtained in the case of intact nuclei (Figure 17.A.1), or strings of fluorescent speckles (Figure 17.A.2.). The majority of halos contained one compact and one dispersed form (52.5 %, n=120) as shown in Figure 17.A.2. In the alkaline FIGE-comets, the FISH signals were fragmented to several discrete, distant spots in the case of both Jurkat cells and PBLs (Figure 17.A.3 and B.2.); whereas neutral FIGE has lead to compact signals (Figure 17.E.). In

alkaline FIGE-comets the FISH signals become dispersed also in the case of a chromosome painting probe (Figure 17, panel H), excluding probe specific artifacts.

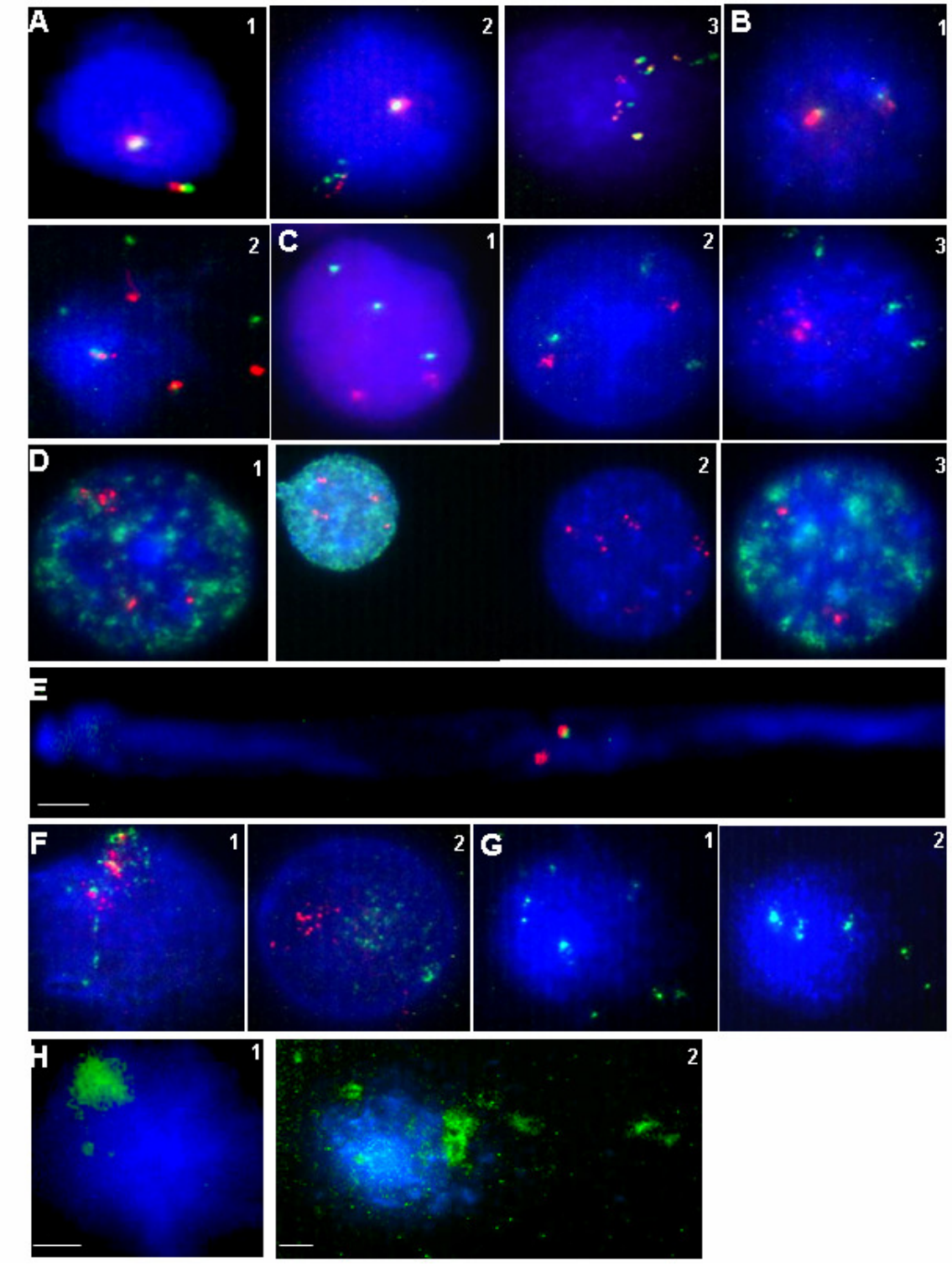

Figure 17: Disintegration of chromatin at the MLL bcr as studied by halo-FISH. *Green*: centromeric MLL flank; *Red*: telomeric MLL flank; *Blue*: DNA stained by DAPI. Scale: 5 µm. **A. *1*:**

Interphase-FISH performed on Jurkat cells harbouring germline MLL (gMLL); ***2*:** Halo-FISH performed on Jurkat nuclear halos; ***3*:** Halo-FISH performed on Jurkat alkaline FIGE-comets. **B. *1*:** Halo-FISH performed on the nuclear halos of resting peripheral blood lymphocytes (PBLs); ***2:*** Halo-FISH performed on the alkaline FIGE-comets of resting PBLs. **C. *1*:** Interphase-FISH performed on ML-1 cells harbouring rearranged MLL (tMLL, t(11;6) reciprocal translocation between MLL and AF6 genes). ***2*:** Halo-FISH performed on ML-1 nuclear halos; *3*: Halo-FISH performed on ML-1 alkaline FIGE-comets. **D.** Simultaneous analysis of 5-bromodeoxyuridine incorporation and loop-size DNA fragmentation in proliferating Jurkat and ML-1 cells. *Green*: BrdU-foci; *Red*: MLL FISH signals**. *1-2*:** Halo-FISH performed on the nuclear halos of BrdU-pulsed Jurkat cells; ***3*:** Halo-FISH performed on the nuclear halos of BrdU-pulsed ML-1 cells. **E.** Halo-FISH analysis of neutral FIGE-comets prepared from Jurkat cells. *Green*: centromeric MLL flank; *Red*: telomeric MLL flank; Scale: 10 µm. **F. *1*:** Halo-FISH performed on the nuclear halos of apoptotic Jurkat cells; **2:** Halo-FISH performed on the nuclear halos of apoptotic ML-1 cells. Apoptosis was induced by etoposide-treatment and monitored by flow cytometry (see also Figure 24.). **G.** Halo-FISH analysis of alkaline FIGE-comets at chromosome 8 centromeres in Jurkat cells. *Green*: centromere 8 specific FISH probe. **H.** Halo-FISH analysis of chromosome territories before ***(1)*** and after ***(2)*** alkaline FIGE of nuclear halos prepared from Jurkat cells. *Green*: chromosome 15 painting probe.

The average fragment size obtained by dividing the length of the region recognized by the dual-color FISH probe with the observed average fragment number (10.18 +/- 0.39 (SEM)) was 106 kbp (n=200), a value compatible with the loop-size. In ML-1 cells harboring rearranged MLL (tMLL), the majority of the signals (80 %, n=120) were in most nuclear halos and FIGE-comets retained as condensed spots (compare Figure 17.C. with 17.A. and 17.B.), suggesting the the incidence of nicks may be dependent at least partly on chromosomal contex. In line with this notion, centromeric DNA at chromosome 8 also exhibited a distinct pattern of fragmentation (Figure 17.G.1-2.) with an average fragment size of 330 kbp (n=150), which is consistent with the estimated loop periodicity of centromeres[84,85].

FISH-analyses of the MLL-bcr carried out in etoposide-treated Jurkat and ML-1 cells showed a markedly different picture of fragmentation, with numerous fine speckles (Figure 17.F.) corresponding to the oligonucleosomal DNA cleavages detected in these samples by agarose gelelectrophoresis and flow cytometry (Figure 18.). There was no difference in the fragmentation pattern of FISH signals between non-cycling PBLs and cycling Jurkat cells, and between BrdU-positive (S-phase) and BrdU-negative cells (Figure 17.D.1-3.), ruling out transient nicks related to Okazaki fragment processing from the realm of possible explanations.

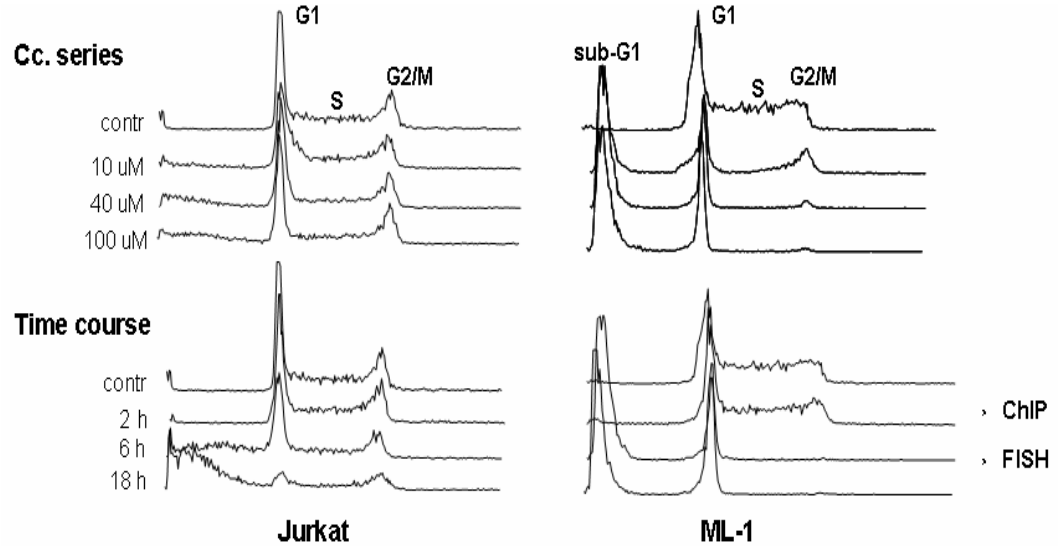

Figure 18: Flow cytometric analysis of DNA distribution in etoposide-treated Jurkat and ML-1 cells. Samples investigated by halo-FISH and chromatin immunoprecipitation (see below) are indicated.

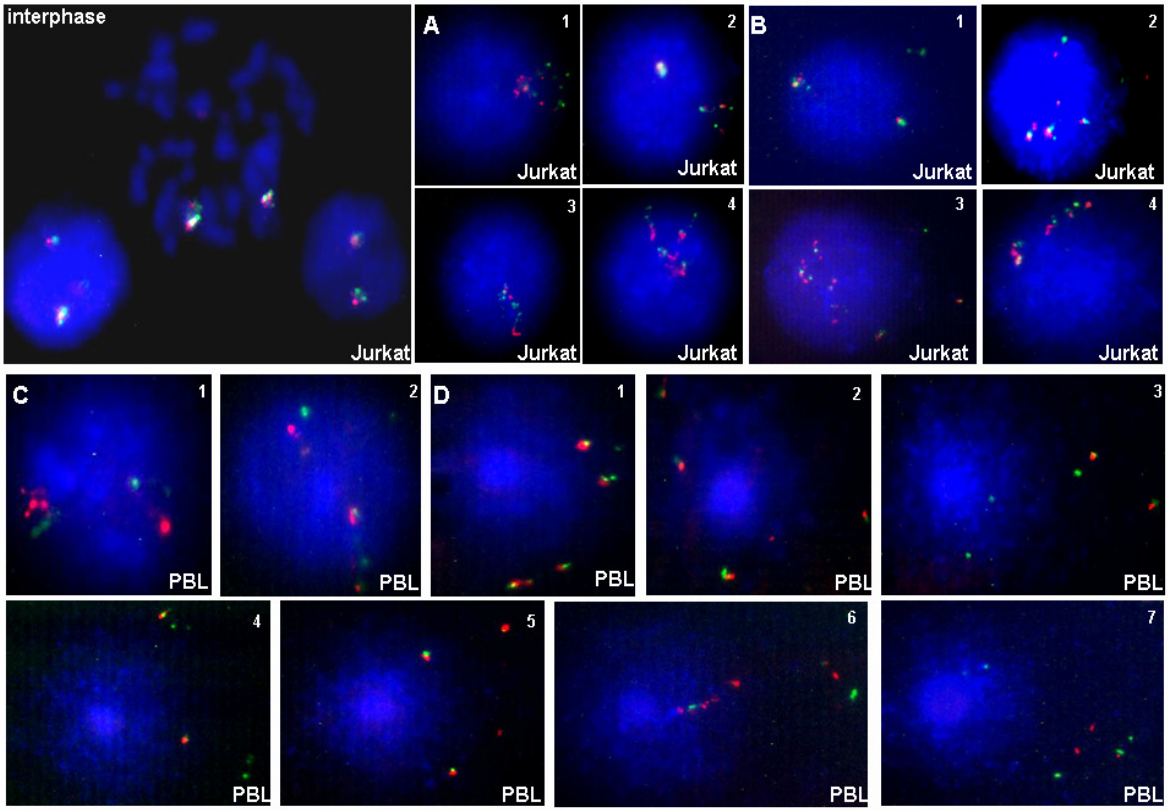

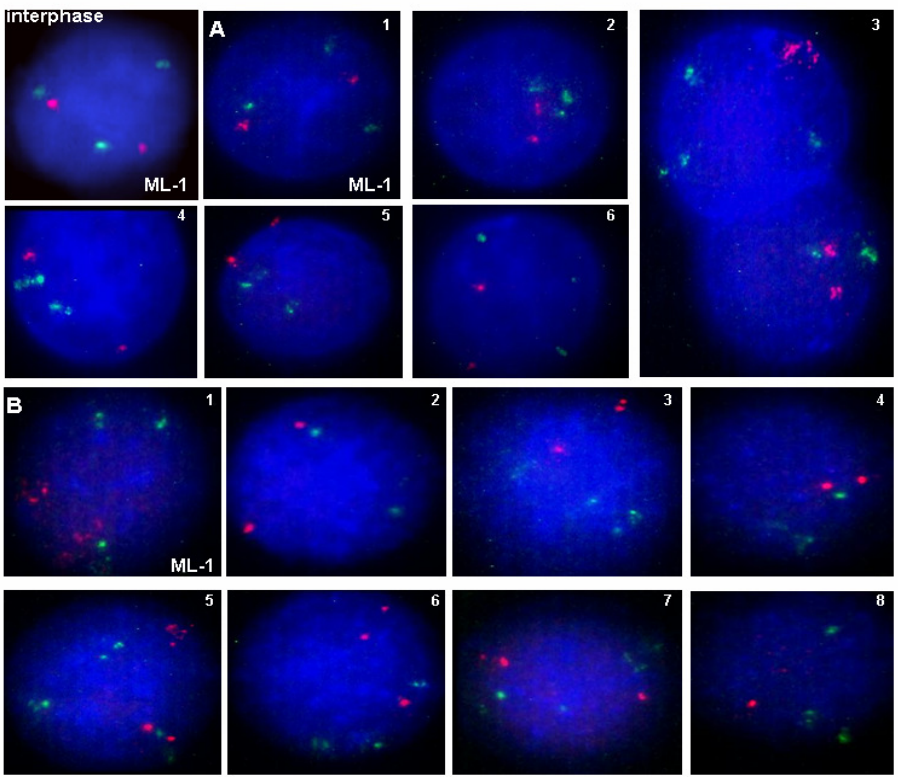

Supplementary Figure 1: Further examples are shown for the disintegration of chromatin at germline and rearranged MLL, as studied by halo-FISH. *Green*: centromeric MLL flank; *Red*: telomeric MLL flank; *Blue*: DNA stained by DAPI. Jurkat cells, PBLs, ML-1 cells are indicated.

5.5 *Assessing the role of common DNA sequence motives in the occurrence of single-strand breaks at the MLL bcr.*

We suggest that the results of in situ nick labeling and halo-FISH studies are best explained by the presence of regularly spaced single-stranded breaks in the DNA. However, the role of nick-forming sequences at special secondary structures (hairpins, bubbles, cruciforms) cannot be ruled out, since these motives may predispose particular DNA regions for enzymatic nicking upon cell lysis. These sequence elements were investigated by *(a)* incubation of the MLL-bcr containing plasmid DNA or PCR-amplified linear MLL bcr segments with nuclear extracts, monitoring DNA cleavages on agarose gels and also by primer extension linear amplification; and by *(b)* primer extension linear amplification performed on genomic DNA prepared from healthy, non-apoptotic cells.

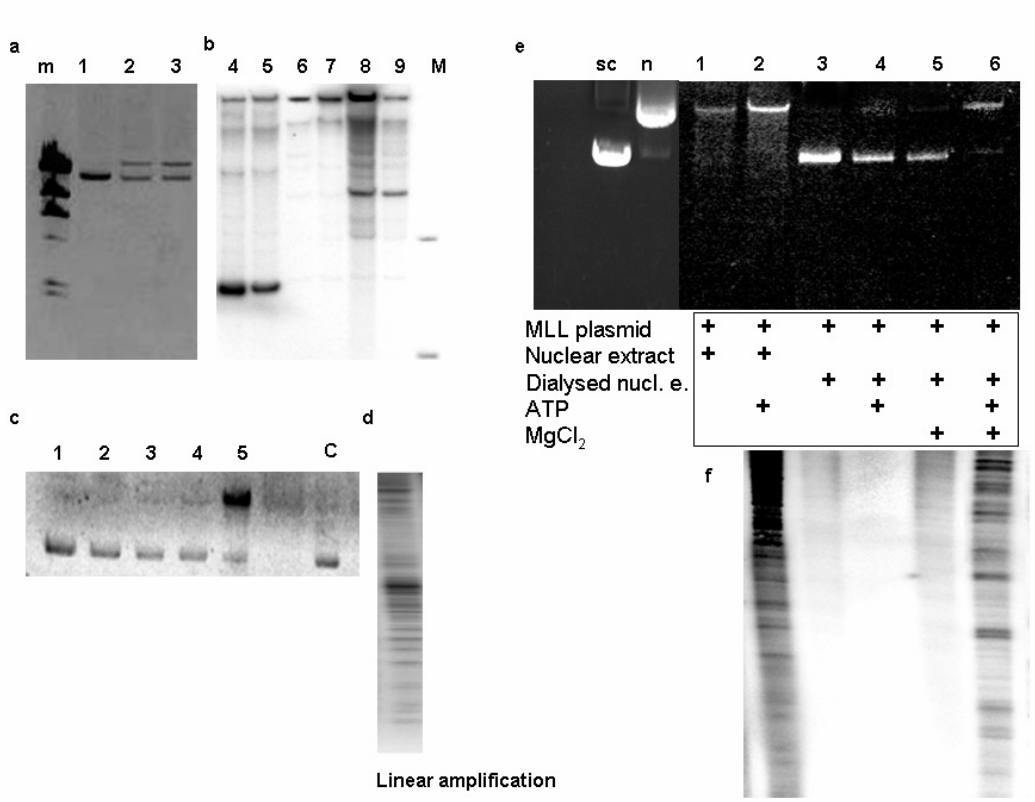

Figure 19: *In vitro* cleavage of pMEP4-MLL plasmid with nuclear extracts. ***(Upper panel)*** flowchart of the procedure. ***(Lower panel) a:*** *In vitro* cleavage of the pMEP4-MLL plasmid with nuclear extracts. *Lane 1*: control plasmid; *lane 2:* plasmid + nuclear extract; *lane 3:* plasmid + nuclear extract + 40 µM etoposide. ***b*:** Linear amplification of the *in vitro* cleavage products from 'a'. *Lane 4:* sense strand, plasmid + nuclear extract*; lane 5*: sense strand, plasmid + nuclear extract + 40 µM etoposide; *lane 6:* sense strand, untreated plasmid; *lane 7*: antisense strand, untreated plasmid; *lane 8*: antisense strand, plasmid + nuclear extract; lane 9: antisense strand, plasmid + nuclear extract + 40 µM etoposide. *M:* marker (500 bp and 200 bp). ***c:*** *In vitro* cleavage of MLL-bcr with size fractionated nuclear extracts. *Lanes 1-2-3-4:* pMEP4-MLL plasmid cleaved with different, <200 kDa fractions; *lane 5:* plasmid cleaved with the 200-300 kDa fraction; *C:* untreated plasmid. ***d:*** Linear amplification of MLL-bcr cleaved *in vitro* with the >200 kDa size fraction. ***e:*** *In vitro* cleavage of MLL-bcr with ATP- and/or Mg^{++}-depleted nuclear extracts. *Sc*: supercoiled plasmid; n: nicked circular plasmid. ***f***: Linear amplification of the *in vitro* cleavage products from *'e'*.

As shown in Figures 19 and 20, MLL bcr appears to carry special structures of preferential vulnerability when intact plasmid DNA or its PCR-amplified linear segment is exposed to nuclear extracts *in vitro*, and when DNA isolated from cells (i.e. exposed to nuclear milieu *in vivo*) is analysed. Linear amplifications using specific primers that span a high-affinity matrix associated region in MLL bcr revealed cleavage sites that seem to be distributed in a non-random manner. Cleavage activity is included in a large >200 kDa protein complex (Figure 19. d) and requires Mg^{++}

and ATP (Figure 19. e, f). In the absence of these cofactors, or when exposed to fractions from outside the high molecular weight range, the superhelical structure of the plasmid is maintained.

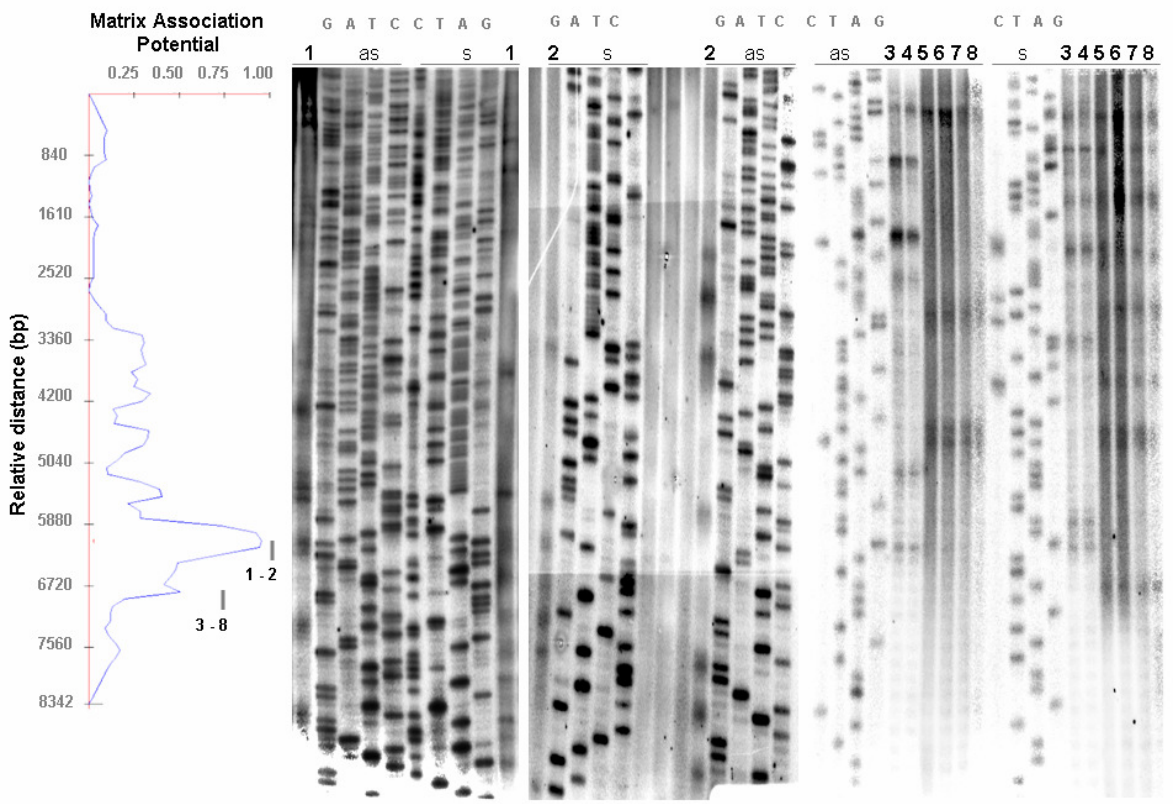

Figure 20: Detection of single-strand breaks in MLL bcr by primer extension mapping. *Left*: matrix association potential of MLL bcr, analyzed by the MAR-Wiz algorithm.*Right*: linear amplification analysis of ss breaks in the indicated high scoring region. ***Lane 1-antisense strand:*** MLL-bcr cleaved *in vitro;* T: 7174., G: 7183., A: 7189., AG: 7191-7192., T: 7205; ***lane 1-sense strand:*** MLL-bcr cleaved *in vitro;* G: 6310., C: 6314., G: 6330., C: 6339*;* ***lane 2-sense strand:*** ~50 kb DNA isolated from Jurkat cells (G) 6304, 6330; (C) 6313; (T) 6317, 6329; ***lane 2- antisense strand:*** ~50 kb DNA isolated from Jurkat cells (G) 7147, 7165, 7188, 7193, 7205; ***lanes 3-4:*** MLL PCR-amplimer cleaved with topo II enzyme; ***lanes 5-6-7-8:*** MLL bcr cleaved *in vitro*

Furthermore, exposure of MLL bcr-carrying plasmid DNA to purified topoisomerase II (Figure 20.) or S1 nuclease (Figure 21.) elicit cleavages at the nucleotide positions of nick-formation observed on human genomic DNA isolated from various mammalian cells without any treatment or after exposure to etoposide (Figure 20). The coincidance of S1 cleavage sites at certain nucleotide positions with the nicks observed in plasmid and genomic DNA is noteable (Table I.). These data are in line with the possibility that certain sequence elements can be preferentially involved in the *en masse* disassembly of chromatin to loop-size fragments.

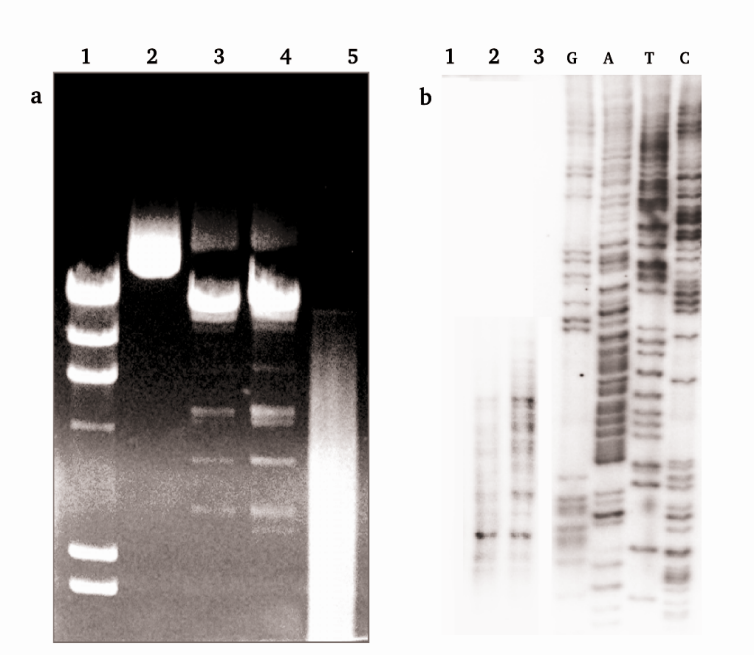

Figure 21: ***a:*** **Cleavage of the pMEP4-MLL plasmid with S1-nuclease.** *Lane 1:* λ Hind III; *lane 2:* untreated pMEP4-MLL plasmid; *lane 3:* plasmid + 25 U S1 nuclease; *lane 4:* plasmid + 100 U S1 nuclease; *Lane 5:* plasmid + 0.4 U DNase I + 25 U S1 nuclease. ***b:*** **Linear amplification of the cleavage products of S1-nuclease treated pMEP4-MLL plasmid.** Breaks have been detected in an Alu-sequence (G: 6329; A: 6334; 6351; 6359; 6363). Lane *1:* untreated plasmid; *lane 2:* pMEP4-MLL plasmid + 25 U S1; *lane 3:* pMEP4-MLL plasmid + 100 U S1.

Table I: Summary of linear amplification data

	6310 G	6315 A	6324 C	6330 G	6352 C	7147 G	7155 A
~50 kb DNA from HL-60 cells	+	+	+	+	+	+	+
~50 kb DNA from K 562 cells	+	-	-	+	-	+	+
MLL-bcr cleaved with HL-60 nuclear extract	+	+	+	+	?	+	+
MLL-bcr cleaved with K 562 nuclear extract	+	+	-	+	+	+	+
MLL-bcr cleaved with S1-nuclease	?	?	-	+	+	?	?

discrete fragment observed; (-) discrete fragment not observed; (?): not detected

5.6 *Assessing the role of epigenetic factors, including topoisomerase II binding in the occurrence of single-strand breaks at the MLL bcr.*

The results of the above in vitro cleavage studies suggest that a divalent cation and ATP dependent enzymatic activity present in the nuclear extracts is crucial in the initiation of nicks at specific nucleotide positions, leading to the circular form of the plasmid. One possible candidate could be topoisomerase II which preferencially binds to matrix associated regions *in vitro* and *in vivo*, requires Mg^{++} and ATP and has been shown to function as part of a large protein complex (toposome). The fact that MLL bcr comprises seven topo II consensus sequences and also the results of our cleavage experiments with topo II-immunoprecipitated nuclear extracts (see Figure 19. A.) suggest that a major factor involved in MLL-bcr breakage *in vitro* may indeed be topo II or a protein complex co-immunoprecipitated with topo II. Figure 19 (panels B and C) shows an in vitro immunoprecipitation analysis performed with anti-topoisomerase II-antibodies on MLL-bcr carrying plasmids that were incubated with either nuclear extracts or purified topoisomerase II. The results suggest that in the presence of nuclear extracts the telomeric portion of MLL-bcr has a significantly higher affinity for topo II, than its centromeric flank ($p<0.01$; the etoposide-treatment did not cause significant change). By contrast, when purified enzyme was added alone to the plasmid samples, each halves bound similar amount of topo II. These observations and the strikingly different fragmentation patterns of germline and rearranged MLL (revealed in halo-FISH studies) promted us to study the epigenetic features of these regions, including topo II binding. In vivo chromatin immunoprecipitation studies have been performed both in control and etoposide-treated Jurkat and ML-1 cells. As demonstrated in Figures 22-23, gMLL and tMLL showed markedly different histone modification characteristics *(a)* in their different chromosomal positions (compare Jurkat and ML-1 cells), *(b)* between control and etoposide-treated samples, *(c)* between the telomeric and centromeric flanks of both gMLL and tMLL.

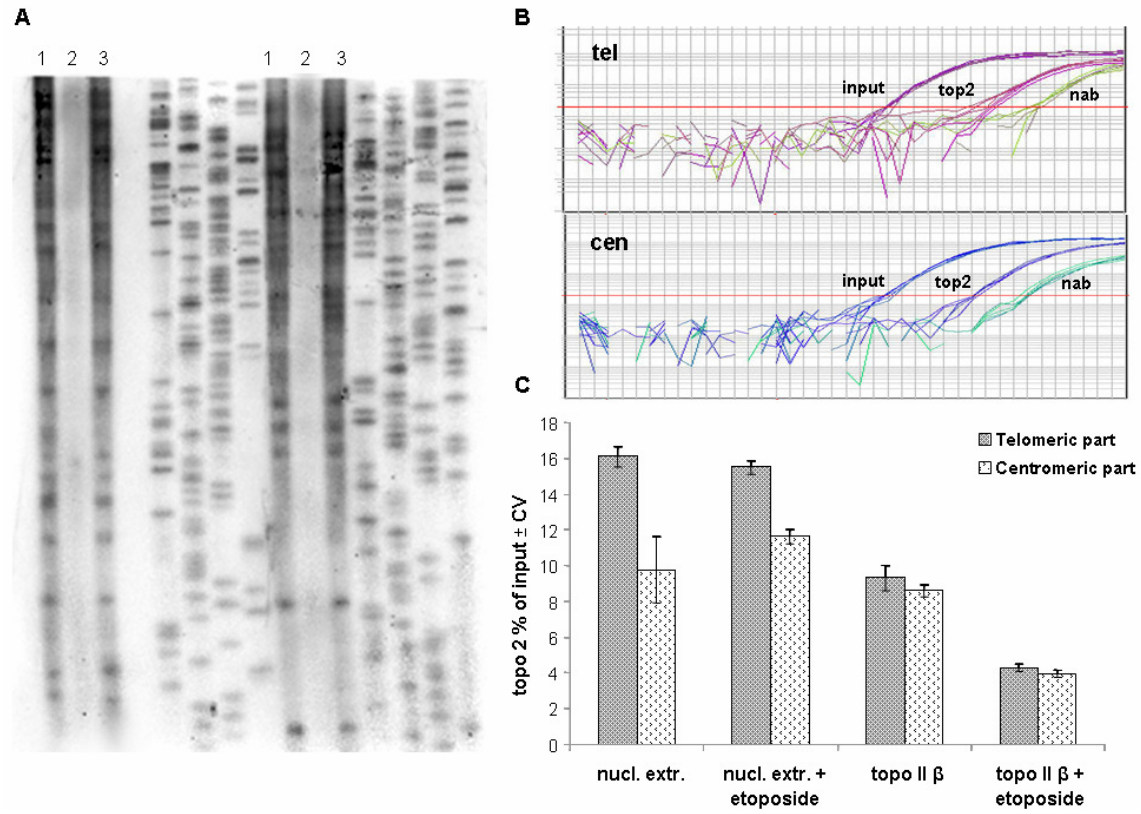

Figure 22: Investigation by linear amplification and in vitro chromatin immunoprecitiptation of the possible role of topoisomerase II in eliciting cleavages at MLL bcr. ***(A):*** Linear amplification of MLL-bcr cleaved *in vitro* with complete (*lanes* ***1,4***), topo II-depleted (*lanes* ***2,5***) and topo2-supplemented (*lanes* ***3,6***) nuclear extracts. *Lanes* ***1-2-3*** and ***4-5-6****:* sense and antisense strands, respectively, with sequence ladders alongside (GATC). In the samples shown in *lanes* 3 and 6, MLL-bcr was cleaved with topo2/α enzyme added to the topo2-depleted nuclear extract. ***(B):*** Kinetic PCR curves of in vitro immunoprecipitated, nuclear extract- or purified topo II-treated MLL plasmid, performed with anti-topo II Ab. ***(C):*** ChIP yields are expressed as a percentage of 'input' samples. Backgrounds (i.e. the 'no Ab % of inputs') were subtracted.

To rule out the possibility that these differences were due to the direct effect of etoposide treatment on transcription and cell cycle, MLL mRNA expression and cell cycle progression were monitored by rtQPCR and flow cytometry: as Figures 18 and 22 show, no significant changes were revealed. In normal cells, topo II-binding was significant in the telomeric MLL-flanks, similarly to the in vitro ChIP results shown in Figure 20. After etoposide-treatment gMLL bound more topo II in both MLL-flanks (compare samples denoted by 'control' and 'eto'), but tMLL showed reduced topo II levels on

the telomeric flanks and considerably higher amounts at the centromeric MLL flanks. Furthermore, tMLL exhibited a significantly lower DNase-sensitivity than gMLL suggestive of a compact chromatin structure at tMLL and an open chromatin configuration at gMLL. These data collectively imply that in different chromosomal regions the incidence of nicks may also be determined at the epigenetic level, not only by DNA sequence.

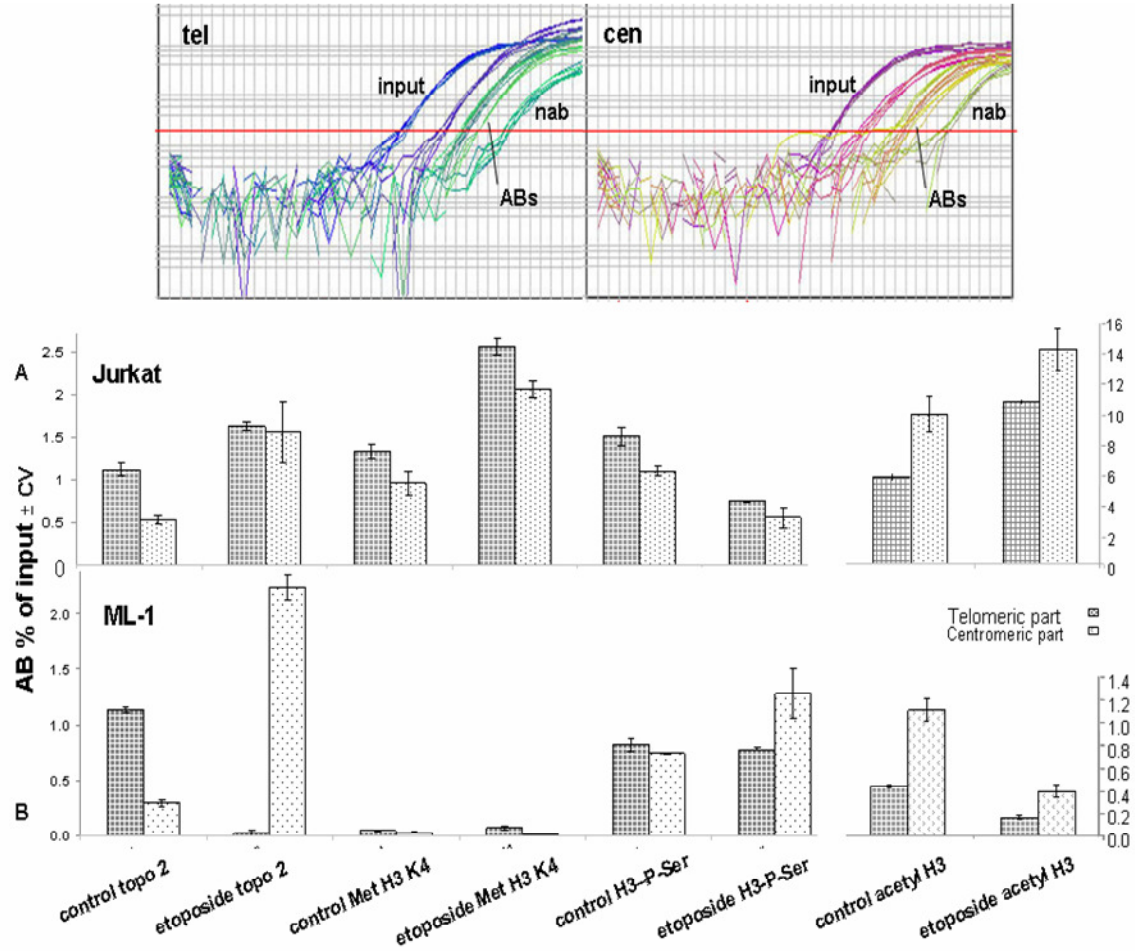

Figure 23: Investigation of histone modifications and in situ bound topoisomerase II levels at MLL bcr, detected by chromatin immunoprecipitation (ChIP) in normal and etoposide-treated Jurkat and ML-1 cells. Jurkat cells possess germline MLL at 11q23; ML-1 cells have rearranged MLL, translocated to 6q27. Telomeric and centromeric MLL bcr flanks are indicated *(Upper panel):* Kinetic PCR curves. *(Lower panel):* immunoprecipitated MLL bcr fragments expressed as the percentage of 'input' samples. Backgrounds (i.e. the 'no Ab % of inputs') are subtracted. Note that the scale is different on the right side of the Figure.

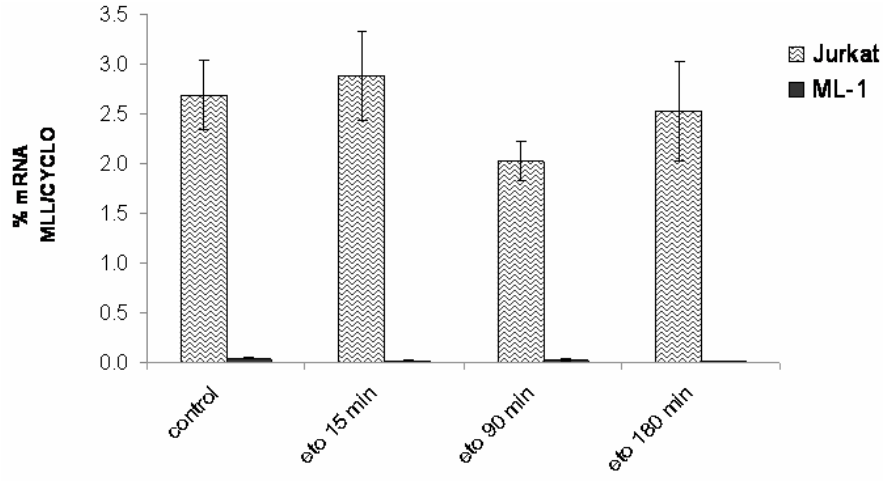

Figure 24: Reverse transcriptase real time QPCR analysis of MLL gene expression in normal and etoposide-treated Jurkat and ML-1 cells. MLL mRNA levels were normalized to cyclophilin transcript levels.

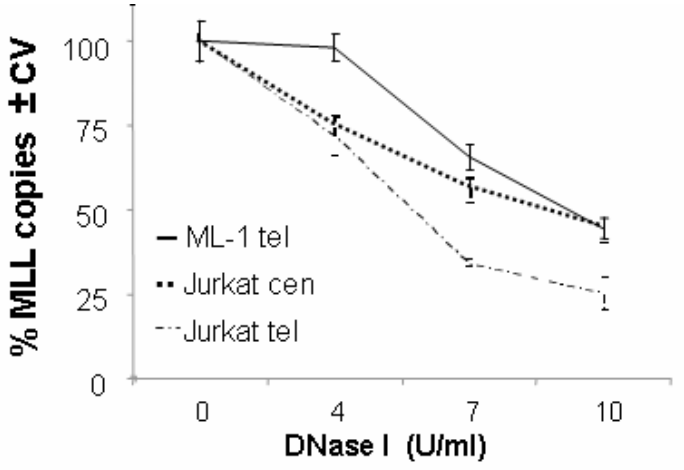

Figure 25: Measurement of DNase I-sensitivity at MLL bcr by real time QPCR. *(bold line)*: Jurkat cells harbouring germline MLL (gMLL) at 11q23, telomeric flank; *(dotted line)*: ML-1 cells harbouring rearranged MLL (tMLL) at 6q27, telomeric part; *(dashed line)*: Jurkat cells harbouring germline MLL (gMLL) at 11q23, centromeric flank.

5.7 *Implementing a novel screening method for the clinical investigation of epigenetic markers.*

In view of the special significance of epigenetic context in the incidence of nicks predisposing perhaps for pathological gene rearrangements, we have developed a flow-cytometry based screening method for the evaluation of ChIP results, named 'ChIP-on-beads'. The technique is based on the capture of the products of a conventional PCR run to low cycle numbers, on microbeads. It can be easily implemented in a routine flow-cytometric clinical labortory without special expertise in real time QPCR.

We have investigated the cellular levels of H4 acetylation and H3 lysine 4 methylation of the tails of histones at the promoter of the TGM2 gene, to test wheter these covalent modifications can be detected using a flow-cytometric platform. We have shown earlier that flow-cytometry, by virtue of its sensitivity, allows the quantitative evaluation of conventional PCR reactions at much lower cycle numbers, well within the linear range of amplification, compared to the conventional agarose gel-electrophoretic/densitometric measurements. By analyzing ChIP samples using the latter approach, at least 35 cycles of amplification was required to even visualize the PCR products of the 'Ab' and 'nAb' samples (not shown). The 'input' sample already reached the plateu phase at this cycle number, and the usually slight difference between the 'nAb' and 'Ab' samples were diminished. These constraints make interpretation difficult, calling for the more reliable and sensitive flow-cytometric analysis that makes measurements possible within the linear phase of amplification.

To optimize the signal-to-noise ratio of the measurement, we made a dilution series from the ChIP samples and amplified them by PCR. Small aliquots of the amplification products were bound to streptavidin-conjugated microbeads and quantified by flow-cytometry. The distribution means were used to calculate the fraction of DNA copy numbers in the ChIP samples relative to the input DNA, as shown in panel A of Figure 26.

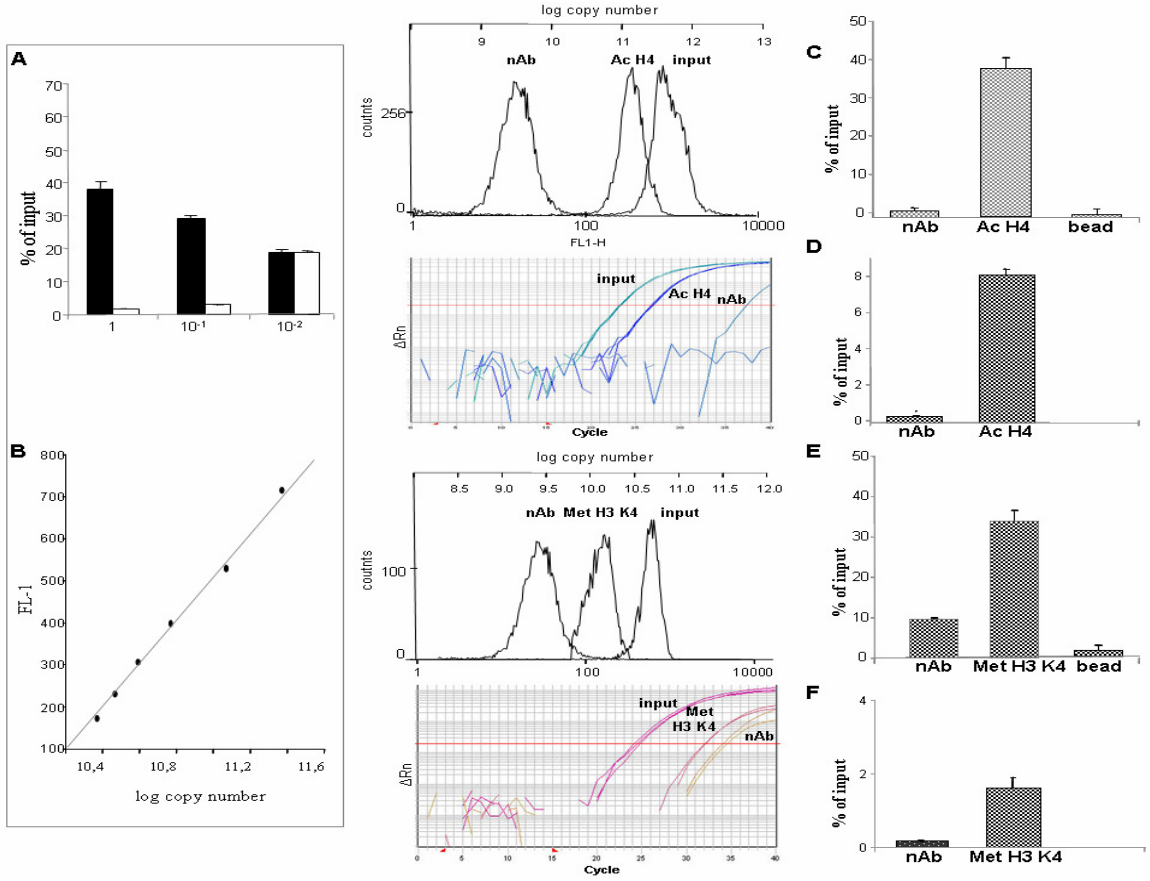

Figure 26: ChIP-on-beads analysis of the promoter of the TGM2 gene, targeting polyacetylated H4 (Ac H4) and lysine 4 methylated H3 histones (Met H3 K4).
(A) Titration of 'input', 'antibody' (Ab) and 'no antibody' (nAb) ChIP samples for TGM2 copy numbers (10-fold dilutions). The PCR amplified products were captured on streptavidin-coated microbeads, and measured by flow-cytometry. The '% of input' values (i.e. the mean fluorescence intensity of 'Ab' and 'nAb' samples normalized to the 'input' mean fluorescence intensity) are plotted. The bars indicate the coefficient of variation (CV, SD values normalized to input means). ***(B)*** Calibration curve (FL-1 vs. log copy number), based on a dilution series of known quantities of *Fam/biotin*-tagged PCR products. TGM2 copy numbers of ChIP-PCR samples were determined by reference to this standard curve. ***(C)*** *Left panel*: Fluorescence distribution histograms of the amplified ChIP DNA samples captured on streptavidin-conjugated microbeads, analyzed by flow-cytometry. *Right panel:* Mean FL-1 values of the 'antibody' (Ac H4), 'no antibody' (nAb) and 'bead only' (bead) fluorescence distribution histograms normalized to the input mean FL-1. The bars indicate the coefficient of variation (CV). ***(D)*** *Left panel*: Kinetic curves obtained for the same ChIP DNA samples in parallel QPCR experiments. The threshold cycle (Ct) is denoted by a vertical line dissecting the PCR curve. *Right panel:* Evaluation of the QPCR data. Mean Ct values of the 'Ab' and 'nAb' samples were normalized to the mean input Ct. Bars: CV. ***(E)*** *Left panel*: Fluorescence distribution histograms of the amplified ChIP DNA samples captured on streptavidin-conjugated microbeads, analyzed by flow-cytometry. *Right panel:* Mean FL-1 values of the 'antibody' (Met H3 K4), 'no antibody' (nAb) and 'bead only' (bead) fluorescence distribution histograms normalized to the input mean FL-1. The bars indicate the coefficient of variation (CV). ***(F)*** *Left panel*: Kinetic curves obtained for the same ChIP DNA samples as in *(E)* in parallel QPCR experiments. The threshold cycle (Ct) is denoted by a vertical line dissecting the PCR curve. *Right panel:* Evaluation of the QPCR data. Mean Ct values of the 'Ab' and 'nAb' samples were normalized to the mean input Ct. Bars: CV.

High levels of histone modification were found at 1-10-fold dilutions, with a reduction of this specific yield to background levels at higher (>100-fold) dilutions; therefore we have performed all the subsequent measurements with undiluted samples, providing the highest efficiency of detection. Panel B demonstrates that the fluorescence intensity of the microbeads increases linearly with the quantity of the fluoresceinated PCR products added, and allows the expression of ChIP-PCR yields as absolute copy numbers. The chromatin in the promoter region of the TGM2 gene is markedly acetylated (via Ac H4 modifications) and methylated (on H3 K4), as shown in panels C and E, respectively; our data were compared to the results of parallel QPCR measurements (panels D and F). The QPCR approach, evaluated by the threshold cycle method ($2^{-\Delta Ct}$ quantification, [86]), also indicated high levels of these modifications.

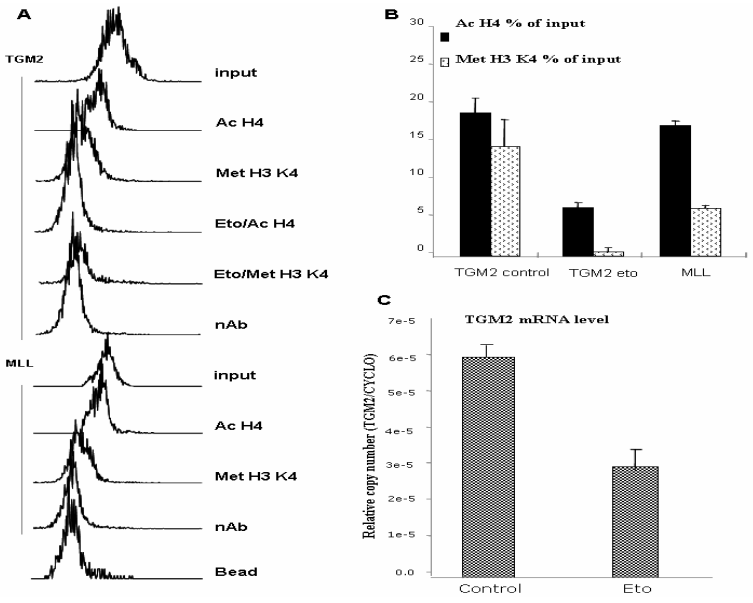

Figure 27: ChIP-on-beads analysis of Ac H4 and Met H3 K4 histone modifications at the TGM2 gene promoter in healthy and apoptotic Jurkat cells. Apoptosis was induced by etoposide-treatment (Eto). ***(A)*** Fluorescence distribution histograms of the PCR amplified ChIP samples captured on streptavidin-conjugated microbeads and analyzed by flow-cytometry. ***(B)*** The level of modified histones is expressed as '% of input' values, based on the means of distribution and after subtracting the backbround (i.e. the 'nAb % of input' values). ***(C)*** Relative decrease of the TGM2 expression level upon etoposide treatment, measured by QPCR. TGM2 mRNA copy numbers were normalized to cyclophilin transcript levels. The bars indicate the coefficient of variation (CV).

The ~4-fold lower extent of both histone acetylation and methylation obtained by QPCR corresponds to only ~2 rounds of PCR, and does not affect the conclusion that this region contains acetylated and methylated histones, since Ab/input ratios above 0.2 % are generally considered to be positive. The presence of the TaqMan probe can influence the amplification efficiency, and may account for this difference. Thus, the promoter region of the type 2 transglutaminase gene in Jurkat cells exhibits histone modifications characteristic of active genes, according to both the flow-cytometric and real time QPCR readout of ChIP experiments, and these observations can be regarded as significant both in the biological and methodological sense alike.

Next, we studied whether changes in the level of the above histone modifications upon physiological processes can be detected by ChIP-on-beads. Apoptosis, readily elicited in these cells by etoposide, was followed by flow-cytometric and gel-electrophoretic analysis of DNA fragmentation (Figure 18.). We compared control and early-apoptotic Jurkat cells for changes in the level of Ac H4 and Met H3 K4 of the TGM2 promoter (see Figure 27., panel A and B.), and observed a significant decrease in both histone modifications, suggestive of the closure of chromatin structure early upon apoptosis. Consequently, TGM2 transcriptional repression was confirmed by parallel reverse transcriptase QPCR measurements, showing a significant reduction in TGM2 expression upon exposure to etoposide. In comparison, high values of identical histone modifications were obtained at exon 9 of the MLL gene (used as positive control) in accordance with its known histone-code profile that we also confirmed by QPCR (data not shown); in contrast, the β-globin gene (used as negative control) gave < 0,1 % Ab/input ratios (not shown).

Based on the above presented data, we can conclude that the ChIP-on-beads method described here gives a reliable picture of the epigenetic status of the genes investigated, compatible with the results of parallel QPCR measurements.

6. DISCUSSION

6.1 *The relationship between higher-order chromatin structure, loop-size DNA fragmentation and breakpoint cluster regions involved in pathological gene rearrangements.*

Still little is known about the signals marking the boundaries of chromatin loops beyond the nuclease hypersensitivity of the chromatin at these sites, the possible involvement of S/MAR elements and their ribonucleoprotein mediated anchorage to a putative nuclear matrix. Here we have shown, confirming at the single-cell level and extending earlier observations of our group that the chromatin of normal, non-apoptotic cells disassembles into *(1)* ~50 kbp double-stranded fragments if exposed to single-strand specific S1 nuclease, or *(2)* ~50 kbp single-stranded fragments upon urea- or alkali denaturation (Figures 6-10). In the absence of these treatments, in salt-extracted nuclear halos, nick-translatable single-stranded regions have been detected in association with these fragments, for the first time. Based on these data we suggest that stably maintained single-strand (ss) discontinuities are present all over the genome, positioned at loop-size intervals. These are probably clusters of non-coincident nicks, masked by RNA containing molecular complexes, as discussed in detail below. An alternative possibility involving nick-prone, base-unpaired secondary structures will also be discussed.

6.1.1 *When are the observed ss breaks generated? Two competing scenarios.*

The revealed ss breaks may have been generated during cell-lysis, or may have preexisted *in vivo*, probably in a masked manner. In the first case, one can assume nuclease hypersensitive sites marking loop-size regions cleaved rapidly upon cell-lysis. Several chromatin bound nucleases (e.g. DNaseY, CAD) or perhaps more likely, matrix-bound topoisomerase II could be implicated in such

instantaneous cleavage. Protein denaturing treatments performed in cell suspensions (i.e. without agarose encapsulation prior to lysis) may lead to the release of any of these enzymes from a DNA+matrix-associated state. At that point the DNA would fall apart. The release of torsional energy accumulated in the matrix-bound DNA could be a significant factor in this as well as in the other possible mechanism discussed below.

In this second scenario, preexisting ss discontinuities could define the borders of chromatin loops in live cells, being revealed at the moment of urea / alkali denaturation or S1 nuclease digestion; this hypothesis assumes the presence of either stable (static) ss breaks at fixed positions, dynamic ss breaks with constant periodicity at changing positions, or clusters of potential ss break sites, with the individual breaks subject to regulation. Our recent and previous data support this scenario, because *(1)* rapid alkaline lysis at pH 12 (precluding any enzymatic activity) gave rise to similar breaks (Figure and ref. 22) and *(2)* similar ss breaks were observed in fixed cells[83] (in agreement with our own data on HCHO-fixed halos; data not shown). Two recent observations seem to be in line with this model: *(1)* Legault at al have detected a significant basal level of non-random nicks/gaps in the chromain, comparable in numbers to what accounts for the *en masse* chromatin fragmentation phenomenon seen in our systems; *(2)* permanent nicks have been observed at the S. *pombe* mat1 locus, functioning as a novel type of imprint. Similarly to our conclusion, these authors also propose the presence of a significant amount of free DNA-termini, compatible with cell viability, and suggest structural and epigenetic roles to these DNA discontinuities.

6.1.2 *Visual evidence for the global disassembly of chromatin to loop-size units*

In this work, a global disintegration of the DNA into discrete particles has been demonstrated by FI-SSGE for the first time. The appearance of these DNA-particles is independent from the type of applied detergent (non-ionic detergent Triton X-100, ionic detergent Sarkosyl, and their

combination), whether the halos were prefixed using 2% HCHO (data not shown) and if proteinase K pre-digestion of the nuclear halos was applied: all gave rise to very similar tail moment distributions, with similar percentage of fragmented DNA and a preferential involvement of nuclei with G1/G0 DNA content. There are, however, two critical factors the observed phenomenon strongly depends on: the applied ionic strength and the alkaline conditions of FIGE (alkaline FI-SSGE). When NaCl was omitted from the extraction-buffer (or added to < 5 mM concentration), disintegration could not be observed after alkaline FI-SSGE (data not shown). This effect reminds us of Weintraub's early observation of the release of discrete supranucleosome particles that were estimated to contain 20-40 kbp DNA, upon mild nuclease digestion of the chromatin. The integrity of these "a" particles was highly salt-dependent, being no longer discernible at low-ionic strength (< 5 mM NaCl) and becoming more discrete at high-inonic strength (> 150 mM NaCl). The salt concentration used in these experiments is in the same range over which higher-order chromatin structures fold or unfold under the influence of H1 histones. This unanticipated behaviour of the supranucleosome structures was readily reversible, suggesting that even though "a" particles unfold at low salt concentration, they do not dissociate; thus the 20-40 kbp DNA fragments contained in individual particles remain held together, presumably by H1 and H5 histones. In our system, the removal of H1 hisones (by extraction with 500 mM NaCl) seemed to be critical for detecting the DNA-granules after alkaline FI-SSGE. The absence of nucleosomal histones (removed by 2 M NaCl extraction) has not affected the tail moment distributions (Figure 10), implying that H1 may play a special role in stabilizing the predilection sites of loop-size chromatin fragmentation. Our in situ nick-translation studies also support this assumption (see below).

The second critical factor in our system is the application of alkaline conditions of FIGE. Granules containing the DNA loops were revealed only in alkaline electrophoretic conditions; neutral FI-SSGE of nuclear halos resulted in the appearance of stretches of uninterrupted DNA fibers (compare Figure 9.A and C). Upon alkaline or urea-denaturation, unfolding of chromosomes at staggered (non-

coincident) nicks can take place (Figure 9.A, B and 7.B.), and the DNA can also be cleaved at nicks by S1 nuclease (Figure 7.A.). The approximately identical, ~50 kbp size of ss and ds fragments (as confirmed by the identical migration of denatured S1-digested and non-digested DNA samples (see Figure 7. A and B., in line with unpublished observations in our group) argues for the close positioning of nicks on the complementary DNA strands. Their staggered arrangement could preserve ds continuity in the individual chromosomes, explaining the results of neutral FI-SSGE. Because of the facts that *(1)* alkaline FIGE conditions are required for chromatin disassembly (Figure 9.), *(2)* neutral FIGE conditions cannot reproduce the observed disintegration phenomenon even if nuclear halos have been lysed in alkaline (pH 12) buffer before neutral FI-SSGE, *(3)* loop-size fragmentation occurs also when nuclear halos are fixed and cross-linked with formaldehyde before alkaline FI-SSGE (data not shown), *(4)* DNA molecules re-isolated from nuclear halos and alkaline FIGE-comets are similar in size (each ~50 kbp; see Figure 11.), the revealed discontinuities must be preformed and positioned at ~50 kbp intervals throughout the entire genome. In our system, alkaline labile sites do not appear to be involved in DNA breakage as the same pattern of chromatin fragmentation has been obtained both by urea-denaturation and S1 nuclease digestion.

6.1.3 *Persistent nicks at the borders of chromatin loop. The role of nucleoskeletal RNA.*

The intensive labeling of nuclear halos by DNA polymerase I directly confirmed the above model and is suggestive of uniform 3'OH character of the revealed free ends. The lack of TdT- and Klenow labeling argue against the possibility that ds breaks and/or longer single-stranded gaps are present in the nuclear halos (Figure 11-16.). The finding that ribonucleolytic treatments (RNase A, alkali) of the nuclear halos elicit a remarkable augmentation of TdT- and Klenow labeling suggests *(a)* the involvement of RNA in masking the discontinuities, and *(b)* a link between the matrix associated hnRNA/RNP network and loop-size chromatin fragmentation phenomena. By its RNase H activity,

Exo III can degrade the RNA strands in RNA-DNA hybrids, and it can also create gaps by its 3'-5' exonuclease activity. The enhancement of nick labeling by Klenow (after Exo III treatment) can be the result of both Exo III activities. However, RNase A alone has been able to produce the same effect, and its specific inhibition by pancreas RNase inhibitor completely prevented this enhancement (Figure 15.). The observed Klenow / TdT positivity could not have been initiated by Exo III in the absence of nicks in the halos. Neither Klenow, nor the template independent DNA polymerase TdT could incorporate biotin-dUTP without RNase A pretreatment of the nuclear halos, suggesting that the accessibility of nicks (with free 3' OH groups) must be hindered by RNA intimately associated with the DNA. Thus, the revealed DNA ends appear to be masked or blocked by RNA associated with ss discontinuities that delimit the borders of chromatin loops. In view of the fact that matrix hnRNA/ribonucleoprotein is involved in anchoring the chromatin loops to the nuclear matrix, we speculate that there may be a link between these two roles of RNA: anchoring the bases of the loops and masking the ss discontinuities here.

6.1.4 *Visual evidence for the disassembly of chromatin to loop-size units at a model fragile site, the MLL bcr*

The results of our halo-FISH experiments are consistent with the above concept of higher-order chromatin structure. As demonstrated on nuclear halos and FIGE-comets, the disintegration of chromatin at specific sites (MLL, centromere 8) depends on the same factors as global disintegration of chromatin, mentioned above (alkaline FI-SSGE, >500 mM NaCl concentration), resulting in the disassembly of this region into loop-size fragments (the average fragment length obtained for the MLL-specific and centromere-specific probes were 106 kbp and 330 kbp, respectively). Neutral FI-SSGE, maintaining ds continuity, resulted in compact MLL signals. The ss breaks do not seem to be interrelated with apoptotic DNA fragmentation, Okazaki fragment processing (replicative DNA synthesis). On the other hand, the marked difference between the fragmentation patterns of germline

and rearranged MLL in the halo-FISH experiments seems to correlate with *(a)* the transcriptional state of the MLL gene that is expressed in Jurkat cells and PBLs, but not in ML-1 cells (compare Figure and gene expression data available at http://genome.ucsc.edu/), *(b)* the overall transcriptional activity of the regions, as well as *(c)* the gene density in 11q23 and 6q27 regions (Table 2). Furthermore, tMLL exhibited a significantly lower DNase-sensitivity than gMLL (Figure 22.), and the same sequences showed markedly different histone modification characteristics (Figure 21.) in their different chromosomal positions, both in control and etoposide-treated cells. The high levels of H3K-acetylation and H3K4-methylation at gMLL also indicate transcriptionally active, relaxed chromatin structure, suggesting that the incidence of ss breaks is highly dependent on chromosomal context.

Table 2

	11q23.1-11q24.1 (111,100-120,800)	6q26-6q27 (161,000-170,400)	Chr 11	Chr 6
Number of genes	**165**	**68**	**1944**	**1777**
Number of transcripts	**30326**	**6639**	**325942**	**291896**
Number of CpG island	**1197**	**1626**	**14375**	**16217**
Number of repeats	**14627**	**10527**	**192059**	**227243**

Source: http://www.ncbi.nlm.nih.gov/mapview/maps (Mapviewer)

6.1.5 Nick-forming sequence motives can position ss breaks

Our results are consistent with the concept that regularly spaced nicks are present throughout the interphase chromatin. However, the (closely related) possibility that sequences at special secondary DNA structures (hairpins, bubbles, cruciforms) undergo instantaneous nicking upon cell-lysis, can hardly be excluded. Breakpoint junctions of human constitutional translocations, e.g. t(1;22), t(4;22), t(11;22), t(7;22), were found to coincide with cruciform structures, suggesting that their single-strandedness can predispose specific loci to genomic rearrangements[87-89]. Non-B DNA configurations that are formed at these sequences are expected to increase the probability of the

formation of single-strand lesions which can lead to recombinational processes and genomic instability. The t(14;18) translocation involving the Ig heavy chain locus and the *BCL-2* gene is one of the most common rearrangement in human cancer. The *BCL-2* breakpoints are not located at a specific nucleotide position, rather dispersed over a 150 bp region. This major breakpoint region has been shown to have a stable single-stranded character which is recognized by the RAG nuclease complex responsible for *BCL-2* translocation.

The possibility of the existence of such nick-prone (nick-forming) motives was investigated by primer extension amplification, performed in vitro on MLL bcr carrying plasmids or purified ~50 kbp ds DNA molecules. Primer extension data have demonstrated non-coincident nicks on the two strands of genomic DNA at MLL bcr (Figures 17, 18.). Some of the stop sites of the linear PCR reaction were confined to an ALU sequence within MLL bcr (between nucleotides 6072-6358), some others are juxtaposed with another ALU (between nucleotides 7155-7345). ALU sequences tend to form hairpin structures in physiological conditions (based on conformational predictions performed by *DNAfold*, data not shown) and have been implicated in the recombinogenic events leading to different chromosomal aberrations, including t(4;11), t(9;11), t(11;22), t(9;22), MLL dup(11)q23, t(14;18)[90]. Stretches of DNA with special conformational characteristics, prevalent in repetitive elements, and particularly the common 26 bp core sequence in ALUs containing a pentanucleotide motif homologous to the prokaryotic *chi* hotspot, have been proposed to play a role in pathological gene rearrangements[91]. Repetitive elements, especially ALU, are also overrepresented among the breakpoint sequences involved in the ~50 kbp fragmentation of chromatin derived from normal cells[75]. The two ALU repeats flank the DNase I hypersensitive site (mapped between nucleotides 6700 and 7087) that co-localizes with a topoisomerase II binding site. The letter sequence is suspected to play a role in MLL translocations associated with the majority of infant leukemias [42,64]. At least some of the affected children had no prior exposure of anticancer drugs. This fact raises the question of how DNA strand breaks that trigger genetic aberrations are initiated in drug-naive

patients. Several lines of evidence suggest that DNA lesions (nicks, AP sites, mismatches) may induce alterations in the structure of chromatin that stimulate topo II-mediated scission. It was shown that cleavage stimulation induced by a single nick was similar or greater than that generated by therapeutic concentration of the drug. These results indicate that chromosomal translocations present in primary infant leukemias may be triggered by the action of such DNA lesions (e.g. site specific nicks, hairpins or ribonucleotide-linkers) acting as endogenous topo II poisons.

Our cleavage reactions performed on PCR-generated MLL bcr fragments have shown that although linear DNA templates lacking superhelical tension are relatively resistant to S1-nuclease, they are sensitive to nuclear extract exposure (Figures 17-19.). This discrepancy can be explained if we assume that a DNA fragment alone is not able to form specific secondary structures, but nuclear extracts including MAR-binding proteins (e.g. SAF-A/B, SATB1, PARP, XRCC4, Lig4) can facilitate or induce the formation hairpins and cruciformes, and these can be efficiently attacked by certain enzymes (e.g. topoisomerase II) also contained in the extracts. Although certain cleavage sites coincided in linear- and superhelical MLL-bcr templates, the intensity of the bands differed significantly. These results indicate that nick-forming sequences are much more sensitive to nuclear extract or S1 mediated cleavage when inserted into supercoiled plasmids. The co-incidence of nicks in genomic DNA with *(1)* those detected in nuclear extract-exposed plasmid DNA, as well as with *(2)* S1-sensitive sites on plasmid DNA support the notion that ss discontinmuities can form in a sequence specific manner, at defined nucleotide positions, in physiological nuclear milieu as well, i.e. in live cells. Abasic sites or other types of *in vivo* DNA damages are neither expected to occur in plasmid DNA, nor would they co-localize with nicks present in genomic DNA (Table 1.). The above data imply that special nick-forming secondary DNA structures can mark certain sequence elements for nicking *in vivo*, however, they don't reveal the molecular mechanism of the proposed *in vivo* nick formation that could eventually occur only upon cell lysis, or pre-exist in the cell, generated and maintained by unknown mechanisms.

6.1.6 Topoisomerase II can cleave positioned nick-forming sequence motives at the MLL bcr

Our size fractionation and in vitro ChIP data (Figures 19, 22, 23.) implicate topo II as a possible a candidate enzyme for specifically recognizing and cleaving nick-forming sequences; this possibility seems to be in accordance with several earlier and recent observations. Froelich at al. demonstrated that nucleic acid molecules with the potential to form secondary structures are efficient substrates for topoisomerase II-mediated DNA cleavage[92]. In marked contrast to sites of double-strand scission, site specificity within the hairpin was not influenced by DNA sequence. Wang at al. showed that the cleavage activity of human topo II isoforms was several-fold stimulated if a ribonucleotide rather than a deoxyribonucleotide was present in one strand of the DNA substrate[93,94]. The cleavage-enhancing effect of these covalently bound ribonucleotides shared many similarities to the positional effect exerted by either hairpins or abasic sites, suggesting a general influence of DNA imperfections on topo II activity. Ju at al. have reported that the activation of gene expression by nuclear receptors and other classes of DNA binding transcription factors requires topo II-dependent double-strand break formation[95]. These discontinuities create the signals that result in the activation of PARP-1 enzymatic function and a nucleosome specific H1 histone-HMG B exchange, probably serving as a general mechanism for the regulated initiation of gene transcription upon ligand-dependent stimulation.

In our experiments *(1)* topoisomerase II treatment of MLL plasmid DNA reproduced some of the nicks revealed by S1 digestion and the same nicks have been observed on genomic DNA, *(2)* the >170 kDa size fraction of nuclear extracts that exhibited the nicking activity probably represents a protein complex involving topoisomerase II. These data incriminate this enzyme as the active, nicking component in both nuclear extracts and chromatin. Distant, topoisomerase II-generated nicks have been suggested to initiate the molecular events leading to MLL rearrangements in childhood leukemias [30,96].

From the ChIP results performed with anti-topo II antibody we can conclude that *(1)* topo II preferentially recognizes and associates with MLL-bcr *in vitro, (2)* the telomeric half of MLL-bcr (in which primer extension mapping has detected several nicks) binds topo II with a significantly higher probability than its centromeric half. The striking difference in the amount of bound-topo II between centromeric and telomeric MLL bcr flanks could be observed *in vivo* as well (Figures 23.), and this feature may account for the preferential association of translocation breakpoints with the telomeric half in secondary leukaemias. It is also notable that germline MLL bcr showed a markedly different DNase-sensitivity in centromeric and telomeric flanks, in agreement with published Southern blot data. These data imply that in different chromosomal regions the incidence of nicks may be conrolled at the epigenetic level. Our ChIP studies support the notion that chromatin structure, not DNA sequence specificity, is the primary determinant of topo II sites of action *in vivo*. Topoisomerase II apparently more effectively gains access to open chromatin regions (compare ChIP data with the DNase sensitivity profiles shown Figures 20 and 22, 23.), making these sites more susceptible to DNA cleavages and gene rearrangements. Whether the topoisomerase II activity described in the case of MLL bcr has any relevance to the genome-wide formation and maintenance of nicks demonstrated herein remains to be a subject of further studies.

6.1.7 *Concluding remarks*

Data described here fit a model of higher-order chromatin structure where nicks or nick-forming sequences are present in the DNA at loop-size intervals, arranged on the two DNA strands in an alternating, staggered fashion. These nicks may be true discontinuities pre-existing in the live cell, or may be nick-prone secondary structures ready to be nicked upon cell lysis. In either case, the conditions for the nick formation observed in the experimental situation appears to be subject to regulation. These conditions could involve mechanisms affecting topoisomerase II action at these

sites (at least in the case of MLL). Since RNA containing molecular complexes appear to be associated with these sites, we speculate that these putative structures are linked with the nuclear matrix, and mask / maintain these discontinuities *in vivo* (see the model below).

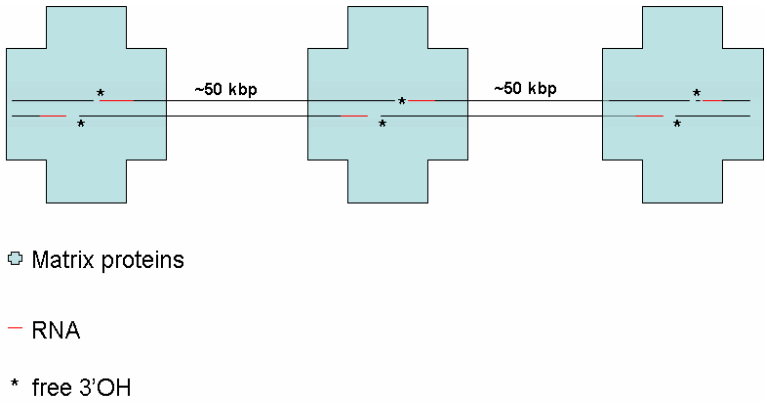

Since the incidence of the observed nicks correlates with the transcriptional activity of the studied chromosomal regions and also appears to be influenced by local epigenetic context, their occurrence might be related to the regulation of transcription generated changes of superhelicity in individual chromatin loops. It is also tempting to speculate that the ss discontinuities present or rapidly formed upon cell lysis at every ~50 kbp throughout the entire genome might explain the frequent involvement of loop anchorage sites in chromosomal translocations and other human malignancies. The disassembly of mammalian genomes to granules containing ~50 kbp DNA could be reproduced using S. *cerevisiae* protoplasts, implying that the ss discontinuities/cleavage-prone sites delimiting interphase chromatin loops are a characteristic feature of all eukaryotes.

6.2 *Implementing a novel screening method for the monitoring of epigenetic markers of diagnostic importance*

Having recognized the role of epigenetic regulation in the incidence of nicks, we attempted to develop a new screening method for the clinical investigation of epigenetic markers. We anticipate that epigenetic analysis will enter routine diagnostic practice whenever monitoring such markers can help predict clinical behavior. Several genes dysregulated at the level of their epigenetic control were shown to associate with different kinds of cancer, highlighting the role of the 'language' of covalent modifications in tumorigenesis [97,98]. For instance, based on the patterns of modifications, two disease subtypes with different risks of tumor recurrence have been characterized in prostate cancer patients, independently from tumor stage, preoperative prostate-specific antigen levels and capsule invasion [99]. When large sets of samples are to be assessed, alternative high through-put platforms for the accurate evaluation of the ChIP results are of general interest. Flow-cytometric analysis has opened a new chapter in the field of quantitative measurement of molecules also in cell-free solutions, after anchoring them to microbeads [100,101], appropriately addressed when used in a multiplex format. In view of the fact that most routine techniques can be adapted to flow-cytometry which exceeds conventional methods in sensitivity and reproducibility, this approach can provide a universal platform for almost any kind of lab purposes [102].

Data presented here have demonstrated that if combined, flow-cytometry and conventional PCR offer a powerful tool in the quantitative analysis of ChIP results. We have found high levels of Ac H4 and Met H3 K4 histone modifications at the TGM2 gene core promoter. These levels significantly decreased upon apoptosis and this was accompanied by the down-regulation of TGM2 mRNA expression, suggesting that this enzyme does not contribute to the early manifestations of apoptosis in Jurkat cells. The flow-cytometric assay we nick-named ChIP-on-beads, can be implemented without specific expertise in quantitative PCR, and it is readily applied in a high-throughput format. We envisage the utility of this novel platform primarily in clinical screening efforts addressing one, or a few, epigenetic markers in many samples simultaneously. The same

samples could be simultaneously run in a FACSarray instrument using fluorescent primers matching its optical channels. It may be the method of choice when large numbers of samples are to be screened, depending on cost and time considerations, availability of instrumentation and expertise. We expect that the epigenetic silencing of tumor suppressor genes will soon become a frequent target of such studies, since these mechanisms may be as important as the mutations inactivating the same genes. Whether real time QPCR, or the ChIP-on-beads will be selected as the method of choice for such screening projects, will be determined by the particular task undertaken, and the capabilities of the clinical labs. We believe that our simple and relatively inexpensive method can help bring the analysis of protein-DNA interactions within reach for routine laboratories, especially those involved in clinical diagnostics.

7. SUMMARY

Although the higher-order structure of eukaryotic chromosomes has been the focus of considerable attention, little is known about the signals that mark the boundaries of interphase chromatin loops. The chromatin fragmentation phenomenon described herein seems particularly important because *(a)* it reflects regularities in the organization of higher order chromatin structure, *(b)* it appears to be interrelated with questions concerning genome instability, apoptosis and chemotherapy-associated gene rearrangements. Applying biophysical and molecular biological techniques (e.g. CLSM, LSC, flow cytometry, halo-FISH, FIGE-SSGE, ChIP), we have visualized the global disassembly of the chromatin of healthy, non-apoptotic human cells into particles apparently containing the DNA-loops, for the first time. Data we have obtained provide evidence for the existence of preformed single-strand discontinuities all over the entire genome, which appear to be arranged on the two DNA strands in an alternating, staggered fashion, positioned at loop-size intervals. The chemical nature of the DNA-termini have been characterized by in situ nick labeling, revealing uniform ends with 3'OH groups, tightly protected by structures sensitive to ribonucleolytic treatments. Our results suggest an association between the nicks present at the bases of chromatin loops and the nuclear matrix attached architectural hnRNA-network.

To study the role of particular DNA regions in the observed phenomena, we extended our studies on the breakpoint cluster region (bcr) of the *M*ixed *L*ineage *L*eukemia (MLL) gene that is frequently rearranged in childhood and posttherapeutic leukemias. The sequence specificity of nick accumulation, the possible function of nick froming sequence motives as well as the role of topoisomerase II have been investigated by linear primer extension footprinting and chromatin immunoprecipitation (ChIP). The results demonstrate the involvement of the above enzyme in the generation / maintenance of nicks at non-random positions. As studied by halo-FISH and ChIP, the disintegration of the chromatin at MLL bcr was dependent on local epigenetic and broader chromosomal context, with marked differences between germline and rearranged MLL. The high

level of H3K-acetylation and H3K4-methylation at gMLL indicates transcriptionally active, relaxed chromatin structure, suggesting that the incidence of ss-breaks is highly dependent on chromosomal context. We hypothesize that the ss discontinuities present at every ~50 kbp throughout the genome might explain the frequent involvement of loop anchorage sites in chromosomal translocations.

In view of the special significance of epigenetic context in the incidence of nicks - probably predisposing for pathological gene rearrangements, we have also developed a novel high-throughput screening method for the evaluation of ChIP results, applicable in a clinical set-up, combining biophysical and molecular biological know-how.

8. REFERENCES

1. Cavalier-Smith,T. Nuclear volume control by nucleoskeletal DNA, selection for cell volume and cell growth rate, and the solution of the DNA C-value paradox. *J. Cell Sci.* **34**, 247-278 (1978).

2. Cavalier-Smith,T. Origins of the machinery of recombination and sex. *Heredity* **88**, 125-141 (2002).

3. Berezney,R. Regulating the mammalian genome: the role of nuclear architecture. *Adv. Enzyme Regul.* **42**, 39-52 (2002).

4. Berezney,R., Malyavantham,K.S., Pliss,A., Bhattacharya,S. & Acharya,R. Spatio-temporal dynamics of genomic organization and function in the mammalian cell nucleus. *Adv. Enzyme Regul.* **45**, 17-26 (2005).

5. Jackson,D.A., Dickinson,P. & Cook,P.R. The size of chromatin loops in HeLa cells. *EMBO J.* **9**, 567-571 (1990).

6. Branco,M.R. & Pombo,A. Intermingling of chromosome territories in interphase suggests role in translocations and transcription-dependent associations. *PLoS Biol.* **4**, e138 (2006).

7. Fawcett,D.W. On the occurrence of a fibrous lamina on the inner aspect of the nuclear envelope in certain cells of vertebrates. *Am. J. Anat.* **119**, 129-145 (1966).

8. Nickerson,J. Experimental observations of a nuclear matrix. *J. Cell Sci.* **114**, 463-474 (2001).

9. Nakayasu,H. & Berezney,R. Nuclear matrins: identification of the major nuclear matrix proteins. *Proc. Natl. Acad. Sci. U. S. A* **88**, 10312-10316 (1991).

10. Ma,H., Siegel,A.J. & Berezney,R. Association of chromosome territories with the nuclear matrix. Disruption of human chromosome territories correlates with the release of a subset of nuclear matrix proteins. *J. Cell Biol.* **146**, 531-542 (1999).

11. Barboro,P. *et al.* Unraveling the organization of the internal nuclear matrix: RNA-dependent anchoring of NuMA to a lamin scaffold. *Exp. Cell Res.* **279**, 202-218 (2002).

12. Barboro,P. *et al.* An intranuclear frame for chromatin compartmentalization and higher-order folding. *J. Cell Biochem.* **88**, 113-120 (2003).

13. Fey,E.G., Krochmalnic,G. & Penman,S. The nonchromatin substructures of the nucleus: the ribonucleoprotein (RNP)-containing and RNP-depleted matrices analyzed by sequential fractionation and resinless section electron microscopy. *J. Cell Biol.* **102**, 1654-1665 (1986).

14. Herman,R., Weymouth,L. & Penman,S. Heterogeneous nuclear RNA-protein fibers in chromatin-depleted nuclei. *J. Cell Biol.* **78**, 663-674 (1978).

15. Muller,M., Spiess,E. & Werner,D. Fragmentation of 'nuclear matrix' on a mica target. *Eur. J. Cell Biol.* **31**, 158-166 (1983).

16. Cockerill,P.N. & Garrard,W.T. Chromosomal loop anchorage of the kappa immunoglobulin gene occurs next to the enhancer in a region containing topoisomerase II sites. *Cell* **44**, 273-282 (1986).

17. Mirkovitch,J., Mirault,M.E. & Laemmli,U.K. Organization of the higher-order chromatin loop: specific DNA attachment sites on nuclear scaffold. *Cell* **39**, 223-232 (1984).

18. Mirkovitch,J., Gasser,S.M. & Laemmli,U.K. Scaffold attachment of DNA loops in metaphase chromosomes. *J. Mol. Biol.* **200**, 101-109 (1988).

19. Mirkovitch,J., Spierer,P. & Laemmli,U.K. Genes and loops in 320,000 base-pairs of the Drosophila melanogaster chromosome. *J. Mol. Biol.* **190**, 255-258 (1986).

20. Bode,J., Benham,C., Knopp,A. & Mielke,C. Transcriptional augmentation: modulation of gene expression by scaffold/matrix-attached regions (S/MAR elements). *Crit Rev. Eukaryot. Gene Expr.* **10**, 73-90 (2000).

21. Bode,J. *et al.* Biological significance of unwinding capability of nuclear matrix-associating DNAs. *Science* **255**, 195-197 (1992).

22. Bode,J. *et al.* Fatal connections: when DNA ends meet on the nuclear matrix. *J. Cell Biochem. Suppl* **Suppl 35**, 3-22 (2000).

23. Burden,D.A. *et al.* Topoisomerase II.etoposide interactions direct the formation of drug-induced enzyme-DNA cleavage complexes. *J. Biol. Chem.* **271**, 29238-29244 (1996).

24. D'Arrigo,C. *et al.* DNA supercoiling in apoptotic chromatin. *Biochem. Biophys. Res. Commun.* **309**, 540-546 (2003).

25. Dardalhon,M., de Massy,B., Nicolas,A. & Averbeck,D. Mitotic recombination and localized DNA double-strand breaks are induced after 8-methoxypsoralen and UVA irradiation in Saccharomyces cerevisiae. *Curr. Genet.* **34**, 30-42 (1998).

26. Debrauwere,H., Loeillet,S., Lin,W., Lopes,J. & Nicolas,A. Links between replication and recombination in Saccharomyces cerevisiae: a hypersensitive requirement for homologous recombination in the absence of Rad27 activity. *Proc. Natl. Acad. Sci. U. S. A* **98**, 8263-8269 (2001).

27. Felix,C.A., Lange,B.J., Hosler,M.R., Fertala,J. & Bjornsti,M.A. Chromosome band 11q23 translocation breakpoints are DNA topoisomerase II cleavage sites. *Cancer Res.* **55**, 4287-4292 (1995).

28. Felix,C.A. Leukemias related to treatment with DNA topoisomerase II inhibitors. *Med. Pediatr. Oncol.* **36**, 525-535 (2001).

29. Filipski,J., Leblanc,J., Youdale,T., Sikorska,M. & Walker,P.R. Periodicity of DNA folding in higher order chromatin structures. *EMBO J* **9**, 1319-1327 (1990).

30. Gilliland,D.G., Jordan,C.T. & Felix,C.A. The molecular basis of leukemia. *Hematology. (Am. Soc. Hematol. Educ. Program.)* 80-97 (2004).

31. Gromova,I.I., Nielsen,O.F. & Razin,S.V. Long-range fragmentation of the eukaryotic genome by exogenous and endogenous nucleases proceeds in a specific fashion via preferential DNA cleavage at matrix attachment sites. *J. Biol. Chem.* **270**, 18685-18690 (1995).

32. Iarovaia,O.V., Shkumatov,P. & Razin,S.V. Breakpoint cluster regions of the AML-1 and ETO genes contain MAR elements and are preferentially associated with the nuclear matrix in proliferating HEL cells. *J. Cell Sci.* **117**, 4583-4590 (2004).

33. Iarovaia,O.V., Bystritskiy,A., Ravcheev,D., Hancock,R. & Razin,S.V. Visualization of individual DNA loops and a map of loop domains in the human dystrophin gene. *Nucleic Acids Res.* **32**, 2079-2086 (2004).

34. Aplan,P.D., Chervinsky,D.S., Stanulla,M. & Burhans,W.C. Site-specific DNA cleavage within the MLL breakpoint cluster region induced by topoisomerase II inhibitors. *Blood* **87**, 2649-2658 (1996).

35. Betti,C.J., Villalobos,M.J., Diaz,M.O. & Vaughan,A.T. Apoptotic triggers initiate translocations within the MLL gene involving the nonhomologous end joining repair system. *Cancer Res.* **61**, 4550-4555 (2001).

36. Betti,C.J., Villalobos,M.J., Diaz,M.O. & Vaughan,A.T. Apoptotic stimuli initiate MLL-AF9 translocations that are transcribed in cells capable of division. *Cancer Res.* **63**, 1377-1381 (2003).

37. Iarovaia,O., Hancock,R., Lagarkova,M., Miassod,R. & Razin,S.V. Mapping of genomic DNA loop organization in a 500-kilobase region of the Drosophila X chromosome by the topoisomerase II-mediated DNA loop excision protocol. *Mol. Cell Biol.* **16**, 302-308 (1996).

38. Khodarev,N.N., Sokolova,I.A. & Vaughan,A.T. Association between DNA cleavage during apoptosis and regions of chromatin replication. *J. Cell Biochem.* **70**, 604-615 (1998).

39. Lagarkova,M.A., Iarovaia,O.V. & Razin,S.V. Large-scale fragmentation of mammalian DNA in the course of apoptosis proceeds via excision of chromosomal DNA loops and their oligomers. *J Biol. Chem.* **270**, 20239-20241 (1995).

40. Oberhammer,F. *et al.* Apoptotic death in epithelial cells: cleavage of DNA to 300 and/or 50 kb fragments prior to or in the absence of internucleosomal fragmentation. *EMBO J* **12**, 3679-3684 (1993).

41. Solovyan,V.T., Bezvenyuk,Z.A., Salminen,A., Austin,C.A. & Courtney,M.J. The role of topoisomerase II in the excision of DNA loop domains during apoptosis. *J. Biol. Chem.* **277**, 21458-21467 (2002).

42. Stanulla,M., Wang,J., Chervinsky,D.S., Thandla,S. & Aplan,P.D. DNA cleavage within the MLL breakpoint cluster region is a specific event which occurs as part of higher-order chromatin fragmentation during the initial stages of apoptosis. *Mol. Cell Biol.* **17**, 4070-4079 (1997).

43. Strissel,P.L. *et al.* Scaffold-associated regions in the human type I interferon gene cluster on the short arm of chromosome 9. *Genomics* **47**, 217-229 (1998).

44. Zhang,Y. *et al.* Genomic DNA breakpoints in AML1/RUNX1 and ETO cluster with topoisomerase II DNA cleavage and DNase I hypersensitive sites in t(8;21) leukemia. *Proc. Natl. Acad. Sci. U. S. A* **99**, 3070-3075 (2002).

45. Zhang,Y. & Rowley,J.D. Chromatin structural elements and chromosomal translocations in leukemia. *DNA Repair (Amst)* (2006).

46. Peitsch,M.C., Muller,C. & Tschopp,J. DNA fragmentation during apoptosis is caused by frequent single-strand cuts. *Nucleic Acids Res.* **21**, 4206-4209 (1993).

47. Nagata,S. Apoptotic DNA fragmentation. *Exp. Cell Res.* **256**, 12-18 (2000).

48. Nagata,S., Nagase,H., Kawane,K., Mukae,N. & Fukuyama,H. Degradation of chromosomal DNA during apoptosis. *Cell Death Differ.* **10**, 108-116 (2003).

49. Nagata,T. *et al.* The regulation of DNAse activities in subcellular compartments of activated thymocytes. *Immunology* **105**, 399-406 (2002).

50. Razin,S.V., Petrov,A., Hair,A. & Vassetzky,Y.S. Chromatin domains and territories: flexibly rigid. *Crit Rev. Eukaryot. Gene Expr.* **14**, 79-88 (2004).

51. Sullivan,B.A. & Karpen,G.H. Centromeric chromatin exhibits a histone modification pattern that is distinct from both euchromatin and heterochromatin. *Nat. Struct. Mol. Biol.* **11**, 1076-1083 (2004).

52. Vassetzky,Y.S., Hair,A. & Razin,S.V. Rearrangement of chromatin domains in cancer and development. *J. Cell Biochem. Suppl* **Suppl 35**, 54-60 (2000).

53. Khodarev,N.N., Sokolova,I.A. & Vaughan,A.T. Abortive apoptosis as an initiator of chromosomal translocations. *Med. Hypotheses* **52**, 373-376 (1999).

54. Vaughan,A.T., Betti,C.J. & Villalobos,M.J. Surviving apoptosis. *Apoptosis.* **7**, 173-177 (2002).

55. Kaufmann,S.H. Induction of endonucleolytic DNA cleavage in human acute myelogenous leukemia cells by etoposide, camptothecin, and other cytotoxic anticancer drugs: a cautionary note. *Cancer Res.* **49**, 5870-5878 (1989).

56. Kaufmann,S.H. Antagonism between camptothecin and topoisomerase II-directed chemotherapeutic agents in a human leukemia cell line. *Cancer Res.* **51**, 1129-1136 (1991).

57. Kaufmann,S.H., Desnoyers,S., Ottaviano,Y., Davidson,N.E. & Poirier,G.G. Specific proteolytic cleavage of poly(ADP-ribose) polymerase: an early marker of chemotherapy-induced apoptosis. *Cancer Res.* **53**, 3976-3985 (1993).

58. Kaufmann,S.H. *et al.* Topoisomerase II levels and drug sensitivity in adult acute myelogenous leukemia. *Blood* **83**, 517-530 (1994).

59. Felix,C.A. *et al.* ALL-1 gene rearrangements in DNA topoisomerase II inhibitor-related leukemia in children. *Blood* **85**, 3250-3256 (1995).

60. Felix,C.A. Secondary leukemias induced by topoisomerase-targeted drugs. *Biochim. Biophys. Acta* **1400**, 233-255 (1998).

61. Felix,C.A., Kolaris,C.P. & Osheroff,N. Topoisomerase II and the etiology of chromosomal translocations. *DNA Repair (Amst)* **5**, 1093-1108 (2006).

62. Meyer,C. *et al.* Diagnostic tool for the identification of MLL rearrangements including unknown partner genes. *Proc. Natl. Acad. Sci. U. S. A* **102**, 449-454 (2005).

63. Nakada,S. *et al.* Early G2/M checkpoint failure as a molecular mechanism underlying etoposide-induced chromosomal aberrations. *J. Clin. Invest* **116**, 80-89 (2006).

64. Strissel,P.L., Strick,R., Rowley,J.D. & Zeleznik,L. An in vivo topoisomerase II cleavage site and a DNase I hypersensitive site colocalize near exon 9 in the MLL breakpoint cluster region. *Blood* **92**, 3793-3803 (1998).

65. Strissel,P.L. *et al.* DNA structural properties of AF9 are similar to MLL and could act as recombination hot spots resulting in MLL/AF9 translocations and leukemogenesis. *Hum. Mol. Genet.* **9**, 1671-1679 (2000).

66. Libura,J., Slater,D.J., Felix,C.A. & Richardson,C. Therapy-related acute myeloid leukemia-like MLL rearrangements are induced by etoposide in primary human CD34+ cells and remain stable after clonal expansion. *Blood* **105**, 2124-2131 (2005).

67. Szabo,G., Jr., Boldog,F. & Wikonkal,N. Disassembly of chromatin into approximately equal to 50 kb units by detergent. *Biochem. Biophys. Res. Commun.* **169**, 706-712 (1990).

68. Szabo,G., Jr. 50-kb chromatin fragmentation in the absence of apoptosis. *Exp. Cell Res.* **221**, 320-325 (1995).

69. Weintraub,H. Histone-H1-Dependent Chromatin Superstructures and the Suppression of Gene Activity. *Cell* **38**, 17-27 (1984).

70. Kokileva,L. Endogenous degradation of rat liver chromatin studied by agar gel electrophoresis of nuclei. *Mol. Biol. Rep.* **13**, 139-143 (1988).

71. Kokileva,L. Comparative study of induction of endogenous DNA degradation in rat liver nuclei and intact thymocytes. *Comp Biochem. Physiol B Biochem. Mol. Biol.* **111**, 35-43 (1995).

72. Tchurikov,N.A. & Ponomarenko,N.A. Detection of DNA domains in Drosophila, human, and plant chromosomes possessing mainly 50- to 150-kilobase stretches of DNA. *Proc. Natl. Acad. Sci. U. S. A* **89**, 6751-6755 (1992).

73. Szekvolgyi,L. *et al.* Nick-forming sequences may be involved in the organization of eukaryotic chromatin into approximately 50 kbp loops. *Histochem. Cell Biol.* 1-11 (2005).

74. Varga,T., Szilagyi,I. & Szabo,G., Jr. Single-strand breaks in agarose-embedded chromatin of nonapoptotic cells. *Biochem. Biophys. Res. Commun.* **264**, 388-394 (1999).

75. Szilagyi,I. *et al.* Non-random features of loop-size chromatin fragmentation. *J Cell Biochem.* **89**, 1193-1205 (2003).

76. Saluz,H. & Jost,J.P. A simple high-resolution procedure to study DNA methylation and in vivo DNA-protein interactions on a single-copy gene level in higher eukaryotes. *Proc. Natl. Acad. Sci. U. S. A* **86**, 2602-2606 (1989).

77. Parra,I. & Windle,B. High resolution visual mapping of stretched DNA by fluorescent hybridization. *Nat. Genet.* **5**, 17-21 (1993).

78. Bacso,Z., Everson,R.B. & Eliason,J.F. The DNA of annexin V-binding apoptotic cells is highly fragmented. *Cancer Res.* **60**, 4623-4628 (2000).

79. Bacso,Z. & Eliason,J.F. Measurement of DNA damage associated with apoptosis by laser scanning cytometry. *Cytometry* **45**, 180-186 (2001).

80. Kuo,M.H. & Allis,C.D. In vivo cross-linking and immunoprecipitation for studying dynamic Protein:DNA associations in a chromatin environment. *Methods* **19**, 425-433 (1999).

81. Balint,B.L. *et al.* Arginine methylation provides epigenetic transcription memory for retinoid-induced differentiation in myeloid cells. *Mol. Cell Biol.* **25**, 5648-5663 (2005).

82. Balazs,M., Mayall,B.H. & Waldman,F.M. Simultaneous analysis of chromosomal aneusomy and 5-bromodeoxyuridine incorporation in MCF-7 breast tumor cell line. *Cancer Genet. Cytogenet.* **57**, 93-102 (1991).

83. Gal,I. *et al.* Protease-elicited TUNEL positivity of non-apoptotic fixed cells. *J Histochem. Cytochem.* **48**, 963-970 (2000).

84. Gilbert,N. & Allan,J. Distinctive higher-order chromatin structure at mammalian centromeres. *Proc. Natl. Acad. Sci. U. S. A* **98**, 11949-11954 (2001).

85. Gilbert,N. *et al.* Chromatin architecture of the human genome: gene-rich domains are enriched in open chromatin fibers. *Cell* **118**, 555-566 (2004).

86. Rutledge,R.G. & Cote,C. Mathematics of quantitative kinetic PCR and the application of standard curves. *Nucleic Acids Res.* **31**, e93 (2003).

87. Bacolla,A. *et al.* Breakpoints of gross deletions coincide with non-B DNA conformations. *Proc. Natl. Acad. Sci. U. S. A* **101**, 14162-14167 (2004).

88. Bacolla,A. & Wells,R.D. Non-B DNA conformations, genomic rearrangements, and human disease. *J. Biol. Chem.* **279**, 47411-47414 (2004).

89. Bacolla,A., Wojciechowska,M., Kosmider,B., Larson,J.E. & Wells,R.D. The involvement of non-B DNA structures in gross chromosomal rearrangements. *DNA Repair (Amst)* **5**, 1161-1170 (2006).

90. Kolomietz,E., Meyn,M.S., Pandita,A. & Squire,J.A. The role of Alu repeat clusters as mediators of recurrent chromosomal aberrations in tumors. *Genes Chromosomes. Cancer* **35**, 97-112 (2002).

91. Rudiger,N.S., Gregersen,N. & Kielland-Brandt,M.C. One short well conserved region of Alu-sequences is involved in human gene rearrangements and has homology with prokaryotic chi. *Nucleic Acids Res.* **23**, 256-260 (1995).

92. Froelich-Ammon,S.J., Gale,K.C. & Osheroff,N. Site-specific cleavage of a DNA hairpin by topoisomerase II. DNA secondary structure as a determinant of enzyme recognition/cleavage. *J. Biol. Chem.* **269**, 7719-7725 (1994).

93. Wang,Y., Knudsen,B.R., Bjergbaek,L., Westergaard,O. & Andersen,A.H. Stimulated activity of human topoisomerases IIalpha and IIbeta on RNA-containing substrates. *J. Biol. Chem.* **274**, 22839-22846 (1999).

94. Wang,Y., Thyssen,A., Westergaard,O. & Andersen,A.H. Position-specific effect of ribonucleotides on the cleavage activity of human topoisomerase II. *Nucleic Acids Res.* **28**, 4815-4821 (2000).

95. Ju,B.G. *et al.* A topoisomerase IIbeta-mediated dsDNA break required for regulated transcription. *Science* **312**, 1798-1802 (2006).

96. Raffini,L.J. *et al.* Panhandle and reverse-panhandle PCR enable cloning of der(11) and der(other) genomic breakpoint junctions of MLL translocations and identify complex translocation of MLL, AF-4, and CDK6. *Proc. Natl. Acad. Sci. U. S. A* **99**, 4568-4573 (2002).

97. Downs,J.A. & Jackson,S.P. Cancer: protective packaging for DNA. *Nature* **424**, 732-734 (2003).

98. Hake,S.B., Xiao,A. & Allis,C.D. Linking the epigenetic 'language' of covalent histone modifications to cancer. *Br. J. Cancer* **90**, 761-769 (2004).

99. Seligson,D.B. *et al.* Global histone modification patterns predict risk of prostate cancer recurrence. *Nature* **435**, 1262-1266 (2005).

100. Spiro,A. & Lowe,M. Quantitation of DNA sequences in environmental PCR products by a multiplexed, bead-based method. *Appl. Environ. Microbiol.* **68**, 1010-1013 (2002).

101. Taylor,J.D. *et al.* Flow cytometric platform for high-throughput single nucleotide polymorphism analysis. *Biotechniques* **30**, 661-669 (2001).

102. Pataki,J. *et al.* Biological microbeads for flow-cytometric immunoassays, enzyme titrations, and quantitative PCR. *Cytometry A* (2005).

9. ACKNOWLEDGEMENTS

I am grateful to Professor Rezső Gáspár who made it possible to accomplish my Ph.D. project in an open academic atmosphere at the Department of Biophysics and Cell Biology, and obtain expertise both in teaching and research activities.

I would like to thank the continuous support and training I received from my supervisor, Professor Gábor Szabó, who has guided me towards becoming a scientist. His enthusiasm and our motivating, fruitful discussions helped me to find my own way and to overcome the difficulties during my experimental work.

I wish to thank the conscientious technical assistance for Gyöngyi Dajka and Anikó Szabó, and the practical contributions of the members of our research group: Katalin Goda, Éva Hegedüs, Zsolt Bacsó and László Imre.

I am also grateful to Elza Friedlander, Peter Nagy and György Vereb who have introduced me into several biophysical techniquies, as well as to Bálint L Bálint who has helped me to familiarize myself with numerous advanced molecular biological methods.

I would like to thank Professor Margit Balázs and Professor Viktor Dombrádi for their collaborative work in FISH and gel-chromatographic studies.

I am grateful to the Europian Molecular Biology Organization (EMBO) for supporting me to continue my studies abroad, by awarding a short term EMBO fellowship.

Finally, but most importantly, I would like to thank my beloved family for their permanent love and infinite patience.

10. PUBLICATIONS

THE THESIS IS BASED ON THE FOLLOWING IN EXTENSO PUBLICATIONS:

(1) Szekvolgyi L, Hegedus E, Molnar M, Szarka K, Beck Z, Dombradi V, Austin CA and Szabo G. Nick-forming sequences may be involved in the organization of eukaryotic chromatin into approximately 50 kbp loops. *Histochem. Cell Biol.* (2006) **125:** (1-2): 63-73, **IF: 2.594**

(2) Szekvolgyi L, Balint LB, Imre L, Goda K, Szabo M, Nagy L and Szabo G. ChIP-on-beads: flow-cytometric evaluation of chromatin immunoprecipitation. Accepted for publication in *Cytometry Part A*, **IF: 2.698**

SUBMITTED MANUSCRIPT THE THESIS IS BASED ON:

(3) **Szekvolgyi L**, Rakosy Zs, Balint LB, Bacso Zs, Goda K, Vereb Gy, Varga S, Balazs M, Nagy L and Szabo G. Preformed nicks mark the boundaries of interphase chromatin loops.

FURTHER IN EXTENSO PUBLICATIONS:

(4) Pataki J, Szabo M, Lantos E, **Szekvolgyi L**, Molnar M, Hegedus E, Bacso Zs, Kappelmayer J, Lustyik Gy and Szabo G. Biologycal microbeads for flow-cytometric immunoassays, enzyme titrations and quantitative PCR. *Cytometry Part A* (2005) **68A**: 45-52, **IF: 2.698**

(5) Szilagyi I, Varga T, **Szekvolgyi L**, Hegedus E, Goda K, Kaczur V, Bacso Zs, Nakayama J, Posfai J, Pongor S and Szabo G. Non-random features of loop-size chromatin fragmentation *J Cell Biochem.* (2003) **89:**1193-1200, **IF: 2.664**

POSTERS:

1. Regularly spaced nicks delimit chromatin loops

   Lóránt Székvölgyi, Zsuzsa Rákosy, Bálint L Bálint, Zsolt Bacsó, Katalin Goda, Margit Balázs, László Nagy and Gábor Szabó. New York, Cold Spring Harbor Laboratory conference on Dynamic Organization of Nuclear Function (2006)

2. ChIP-on-beads: kromatin immunprecipitáció áramlási citometriás kiértékelése

   Székvölgyi Lóránt, Imre László, Bálint L Bálint, Goda Katalin, Szabó Miklós, Nagy László és Szabó Gábor. Budapest, Sejtanalitikai konferencia (2006)

3. DNS-fehérje interakciók az MLL gén töréspont klaszter régiójában

   Székvölgyi Lóránt, Bálint L Bálint, Dombrádi Viktor és Szabó Gábor

   Eger, Sejt- és Fejlődésbiológiai Napok (2005)

4. Mikrogyöngyök áramlási citometriás analízisén alapuló diagnosztikai módszerek

   Pataki Judit, **Székvölgyi Lóránt**, Hegedűs Éva, Szabó Miklós, Lantos Erika, Lustyik György és Szabó Gábor. Budapest, Sejtanalitikai konferencia (2004)

5. Fixed cells as microbeads for various applications

   Szabo G, Lustyik G, Pataki J, Szabo M, **Szekvolgyi L**, Hegedus E, Fazekas F

   Cytometry Part A 59A (1): 154-154 May 2004. IDS Number: 819MV; ISSN: 0196-4763

6. Heteroduplex analysis by flow-cytometry

   Pataki Judit, **Székvölgyi Lóránt**, Lantos Erika, Szabó Gábor

   Predeal, Biophysical Congress (2003)

7. Hurok méretű DNS fragmentáció normál és apoptotikus sejtekben

   Székvölgyi Lóránt, Hegedűs Éva, Kaczur Viktória, Erdődi Ferenc és Szabó Gábor

   Siófok, Sejt- és Fejlődésbiológiai Napok (2002)

LECTURES:

1. 11q23 MLL bcr: hurok méretű kromatin fragmentáció vizsgálata egy rekombinogén lókuszon
   Székvölgyi Lóránt, Szarka Krisztina, Beck Zoltán és Szabó Gábor
   Pécs, Sejt- és Fejlődésbiológiai Napok (2004)

2. 11q23 MLL bcr: studying loop-size chromatin fragmentation at a recombinogenic locus
   Székvölgyi Lóránt and Szabó Gábor. Trieste, Theoritical course on genome dynamics and evolution (2004).

11. SUPPLEMENTARIES